The dendritic polymer DAB-Am16 as a novel tumoricidal compound

A dissertation submitted in partial fulfillment
of the requirements for the degree of
Doctor of Philosophy
at the
School of Pharmacy,
University College London

Anja Mirenska

August, 2012

Supervised by Dr Andreas G Schätzlein

Plagiarism statement

This thesis describes research conducted in the UCL School of Pharmacy between 1th October 2008 and 15th November 2011 under the supervision of Dr Andreas G Schätzlein. I certify that the research described is original and that any parts of the work that have been conducted by collaboration are clearly indicated. I also certify that I have written all the text herein and have clearly indicated by suitable citation any part of this dissertation that has already appeared in publication.

Signature: Date:

Abstract

In the 21st century, cancer is becoming the curse of the ageing population in developed countries. No satisfactory therapies are available for many tumour types, and application of existing therapies is limited by severe side effects. Thus, there is a great need of new approaches in cancer treatment. DAB-Am16 is a dendritic polymer with a globular structure, consisting of poly(propylene imine) branches that emerge from a diaminobutane core. Its intrinsic tumoricidal activity in mouse models was published in 2005, but no information on the mechanism of action was available. This thesis presents novel findings on the pathways underlying the anti-cancer activity of this dendrimer *in vitro* and *in vivo*.

Extensive chemical characterisation of DAB-Am16 confirmed its stability and purity. Severe time- and concentration-dependent cytotoxicity was observed for a panel of human tumour cell lines, while a small population of persisters was identified. Toxicity was accompanied by a delayed or abrogated cell cycle. There was an increased number of S phase cells, while the ability to synthesise DNA or to undergo mitosis was progressively lost with increasing DAB-Am16 concentration. The following cell death was found to be apoptotic and was biased in a cell cycle phase dependent manner. The order of apoptotic events upon DAB-Am16 exposure was determined.

Finally, an *in vivo* experiment confirmed that DAB-Am16 has a pronounced effect against human pancreatic cancer xenografts in mice, while being well tolerated by the animals. Post mortem examination of tumour tissue revealed cell cycle blockage of tumour cells from DAB-Am16-treated mice. However, disposition for further proliferation was not diminished, and no significant difference in tumour vascularisation was observed.

Acknowledgements

Foremost, I would like to show my gratitude to my principal supervisor Dr Andreas G Schätzlein for his support and advice throughout my thesis whilst still letting me the room to realise my own ideas. Without his guidance, this thesis would not have been written.

I also owe a debt of gratitude to my co-supervisors Prof Ijeoma F Uchegbu, Dr Anneliese Stell and Dr Brian Catchpole. They spared their time for regularly tracking my progress and contributing valuable ideas to this project.

This thesis wouldn't have become what it is without the friendly, warm and supportive atmosphere in our research group. The exchange and discussion of scientific ideas with the other laboratory members promoted the creation of this thesis. In particular, a very special thanks goes to Dr M Victoria Lozano and Dr Manuel J Santander-Ortega for their great help and continuous encouragement. Without Dr Lozano's contribution, the *in vivo* experiments would not have been conducted.

I would also like to thank Dr Kersti Karu for sharing her knowledge and experience in mass spectrometry and elemental analysis, and for the time she spent patiently teaching and guiding me in this area.

Dr Ayad Eddaoudi helped me to get acquainted with flow cytometry and offered advice on planning new experiments.

My fellow students and the staff made the time at the School a very special experience during the whole period I spent working on this thesis in London.

This project was enabled by a studentship of Bloomsbury Colleges and the use of the facilities of the School of Pharmacy.

I am deeply grateful to Matthias for his continuous personal support as well as for our scientific conversations. His encouragement, patience and care contributed greatly to the creation of this thesis, while undoubtedly the

time he spent proof-reading the manuscript and his advices on it improved its quality.

Finally, throughout my educational career, my family always believed in me and offered support whenever I needed it. It is impossible to express my deep gratitude for their encouragement and help during all the ups and downs. Despite the large geographical distance, I always felt the great support and the confidence in me from my grandmother, who was a great role model for being eager to gain new knowledge throughout the whole life. Sadly, she will not experience the completion of my PhD. This thesis is dedicated to her.

Contents

List of Figures

List of Tables

List of Abbreviations

AFM ..... Atomic Force Microscopy
AO ..... Acridine Orange
ATM ..... Ataxia telangiectasia mutated
ATP ..... Adenosine triphosphate
ATR ..... ATM and Rad3-related
BAD ..... Bcl-2 antagonist of cell death
BrdU ..... 5-bromo-2'-deoxyuridine
BSA ..... Bovine serum albumine
CFA ..... Colony formation assay
CSC ..... Cancer stem cell
DAB ..... Diaminobutane
DAPI ..... 4',6-diamidino-2-phenylindole
DEAE-DEX ..... Diethylaminoethyl-dextran
DM ..... Dichroic mirror
DMPC ..... Dimyristoylphosphatidylcholine
DMSO ..... Dimethyl sulfoxide
DNA ..... Deoxyribonucleic acid
dNTP ..... Deoxyribonucleoside triphosphates
DSB ..... Double-strand break
DTC ..... Drug-tolerant cell
EC50 ..... Half maximal effective concentration
EdU ..... 5-ethynyl-2'-deoxyuridine
EPR ..... Enhanced permeability and retention effect
ESI ..... Electrospray ionisation
FITC ..... Fluorescein isothiocyanate
i.v. ..... Intravenious(ly)
Ig ..... Immunoglobulin
INT . 2-(4-iodophenyl)-3-(4-nitrophenyl)-5-phenyl tetrazolium chloride
IR ..... Ionizing radiation
LDH ..... Lactate dehydrogenase
LL ..... Lower left
LP ..... Long pass
LR ..... Lower right
LSC ..... Light scatter
LUC ..... Luciferase
MALDI ..... Matrix-assisted laser desorption/ionisation
MGMT ..... Methylguanine methyltransferase

MMP, $\Delta\Psi_m$ ..... Mitochondrial membrane potential
MRP-5 ..... Multidrug resistance-associated protein 5
MS ..... Mass spectrometry
MTT .... 3-(4,5-Dimethylthiazol-2-yl)-2,5-diphenyltetrazolium bromide
MW ..... Molecular weight
NADH ..... Nicotinamide adenine dinucleotide (reduced form)
NADPH .. Nicotinamide adenine dinucleotide phosphate (reduced form)
NMR ..... Nuclear magnetic resonance
O^6BG ..... O^6-benzylguanine
OWLS ..... Optical Waveguide Lightmode Spectroscopy
PAMAM ..... Polyamidoamine
PBS ..... Phosphate buffered saline
PEG ..... Polyethylene glycole
PEI ..... Polyethylene imine
PI ..... Propidium iodide
PLL ..... Poly-L-lysine
PPI ..... Poly(propylene imine)
PS ..... Phosphatidylserine
PVA ..... Polyvinyl acetate
Rb ..... Retinoblastoma protein
RDA ..... Radioresistant DNA synthesis
RNA ..... Ribonucleic acid
ROS ..... Reactive oxygen species
RT ..... Room temperature
s.c. ..... Subcutaneous(ly)
TIC ..... Tumour initiating cell
TMRE ..... Tetramethylrhodamine ethyl ester
TOF ..... Time of flight
UL ..... Upper left
UR ..... Upper right

1 Introduction

1.1 Relevance

Cancer is a collective name for a set of diseases characterised by abnormal growth of cells that can be derived virtually from any tissue of the body. This unregulated growth leads to the appearance of malignant tumours, often capable of spreading into other parts of the body by a process called metastasis (National Cancer Institute 2012). The incidence of cancer increases with the age. If untreated, cancer is usually fatal. Currently, the prognosis differs very much with the cancer type, ranging from more than 90 % 5-year survival for testicular cancer to less than 5 % for pancreatic cancer (W. C. Huang 2008; World Health Organization 2011). For the highly aggressive brain tumour glioblastoma multiforma the median survival time is approximately 12 months and the survival of more than 36 months is 3–5 % (Barbus et al. 2011; Krex et al. 2007), while cure of glioblastoma is not possible at all (Stupp et al. 2009). The most successful treatment of local tumours is surgical removal. However, cancer is often diagnosed at an advanced stage when it has already spread to remote sites of the body. In this case, chemotherapy and radiotherapy are used to treat the disease (Aktories et al. 2005). Besides the limited success of these treatment modalities, they are usually associated with severe acute as well as long-term side effects that can themselves lead to death or to secondary malignancies (Brydøy et al. 2007; Gleeson et al. 2004; Oeffinger et al. 2010; Travis et al. 2010). Thus, improvement of cancer therapy is a pressing need in order to improve long-term survival rates and to alleviate side effects. New approaches to cancer therapy are required to overcome the existing problems.

Nanomedicine is a new and promising area of medical research. It is characterised by application of nanotechnology in the medical context. So far, nanomedical research for cancer applications mostly focused on drug delivery (e.g. liposomal or nanopolymeric drug carriers) and cancer

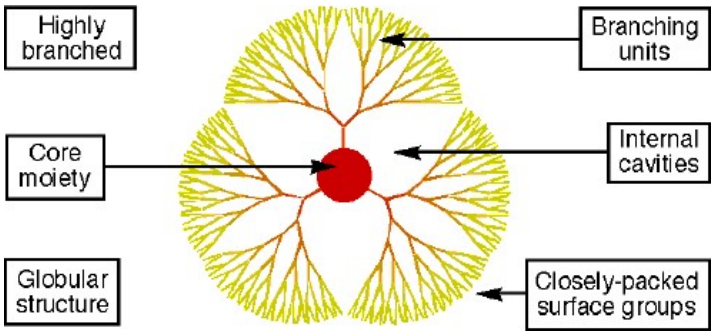

Fig. 1: The dendritic structure. A dendrimer consists of a core molecule with diverging branches. The branches are built of consecutive monomers. The outer shell consists of tightly packed functional groups, yielding the possibility of extensive surface modifications of these multivalent molecules. The highly symmetric hyperbranching results in a globular molecular shape. Modified from Shipway (1997).

diagnostics (K. K. Jain 2008; Namiki et al. 2011; Nie et al. 2007; Rawat et al. 2006; Zhang et al. 2008). The potential of nanoparticles to act as a new drug class themselves has not been exploited in a broad way. This thesis focuses on the investigation of the intrinsic anti-cancer effect of the dendritic nanopolymer DAB-Am16.

1.2 Dendrimers

1.2.1 Features and synthesis

Dendritic nanoparticles have been extensively investigated as drug carriers for targeted delivery of cancer therapeutics. They are globular synthetic polymers with a highly defined structure and pronounced monodispersity which accounts for the specific properties of this polymer class. The characteristic structural feature of a dendrimer is a core molecule with monomer units diverging from it. The branching units are arranged layer by layer in a concentric fashion (Fig. 1).

A dendrimer consists of a core molecule which becomes increasingly branched during each synthesis step. Fritz Vögtle and coworkers were the

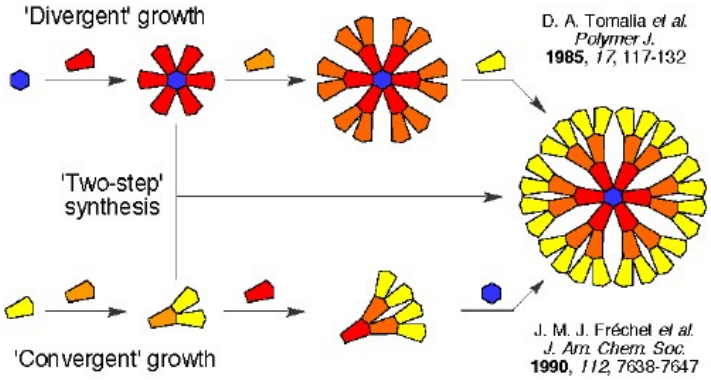

Fig. 2: Two different approaches to dendrimer synthesis. The divergent method implies the gradual addition of branches starting from the core molecule, while the convergent method follows the opposite direction, starting with peripheral branches and joining them together until they are ready to be attached to the core. Modified from Shipway (1997).

first to synthesise dendrimers, followed by the synthesis of the first family of dendrimers by Donald A Tomalia in 1985 (Buhleier et al. 1978; Tomalia et al. 1985). Tomalia and colleagues used a divergent synthesis approach, i.e., gradually adding new layers of the repeating unit to the reactive sites starting from the core molecule. Another synthesis method is the convergent approach, that has been introduced in 1990 by Jean MJ Fréchet. It starts with the molecular units that will eventually become the outer shell of the dendrimer and joins them step by step until attachment to the core molecule (Hawker et al. 1990). A schematic overview of these two methods is provided in Fig. 2. Dendrimers can be characterised by the number of branches added to the core. Generation 1 (G1) dendrimers have one layer of branches attached to the core moiety, while G2 dendrimers carry two layers and so on.

One type of dendrimers that has attracted much attention within the scientific community are the poly(propylene imine) (PPI) dendrimers. Most often, their core molecule is butanediamine. This core contains 4 sites that react with polypropylenimine during synthesis. The synthesis process is illustrated in Fig. 3. With increasing generation number, the density in the

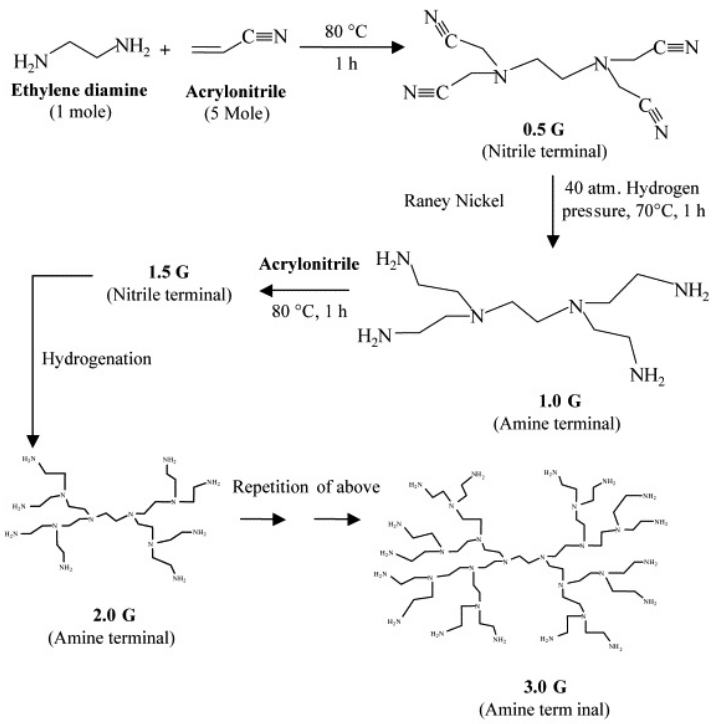

Fig. 3: The divergent synthesis of poly(propylene imine) dendrimers starts with a Michael addition between acrylonitrile and the diamine core molecule. This is followed by Raney nickel catalyzed hydrogenation under pressure to obtain the amino-terminated G1 PPI dendrimer. These steps are repeated until the desired generation number is obtained. Modified from Bhadra et al. (2005).

outer layer of the particle also increases up to the point when no further addition of functional groups to the outer shell is possible due to sterical limitations: a phenomenon that is referred to as “starburst”.

Another important group of dendrimers are poly(amidoamine) (PAMAM) dendrimers. Their synthesis also starts with Michael addition between a core diamine and methylacrylate. This is followed by a reaction with ethylenediamine. Subsequently, the two reactions are repeated for a defined number of times, thus creating different generations of dendrimers with an increasing positive charge density in the outer shell of the particle. According to the number of completed reaction cycles, these dendrimers are

referred to as G1 (generation 1), G2, G3 and so on. However, if one of the reaction cycles is halted after the addition of methylacrylate, the outer shell consists of carboxylate groups and is therefore negatively charged. These dendrimers are called G2.5, G3.5 etc.

An interesting application of dendrimers in nanomedicine is cancer treatment. Gene therapy targeting the abnormal gene expression observed in tumour cells is a novel approach. Gene delivery for gene therapy requires the usage of potent delivery agents. Viral vectors have been used with great success, especially due to their high transfection efficiency. However, immunogenicity is a major obstacle to the usage of viral vectors in human patients. Synthetic nanovectors have a number of features that make them superior to viral vectors. The major advantage is that nanoparticles can be designed to exert defined functions while avoiding risks associated with the use of viruses. For example, it is possible to create nanovectors for drugs that target specific cells and are not immunogenic. Apart from delivering genes, nanoparticles can also deliver drugs to tumour cells. Nanoparticles can be created to have a vast payload of drugs and to be able to release the drug in a controlled manner. Furthermore, there is evidence for a successful circumvention of P-glycoprotein induced multidrug resistance by using nanoparticles as vehicles for conventional drugs (for a review see Davis et al. 2008). Polycationic dendrimers can build complexes with DNA (so called dendriplexes) and transfect cells *in vitro* and *in vivo* (Merdan et al. 2002; Navarro et al. 2009). However, their transfection efficiency is lower than that of viral vectors, and cytotoxicity that could potentially damage healthy cells remains a problem (Mukherjee and Byrne 2012).

Dendrimers possess a number of interesting chemical and physical properties. Although drawings of the dendritic structure, e.g. in Fig. 1, generally imply perfect symmetry with all end groups pointing outward, this isn't necessarily the case in real life. A number of simulations as well as experimental studies have been performed to reveal the physical properties of dendrimers. Lescanec et al. (1990) developed a kinetic growth model to predict folding of dendritic branches and the distribution of end groups

throughout the entire dendrimer volume. Similar results were obtained by other research group using Monte Carlo simulations and a self-consistent mean field model (Boris et al. 1996; Mansfield et al. 1993). This model was empirically confirmed by the study of Mourey et al. (1992) who found a nearly linear increase of the intrinsic viscosity with the dedrimer generation, and a maximum in the intrinsic viscosity as a function of molecular weight. Importantly, a molecular dynamic study of Murat et al. (1996) points out that radius of gyration very much depends on the solvent quality and that the backfolding of dendritic end groups increases with generation number. These rather generic simulations on starburst molecules are complemented by specific simulations on the physical properties of PAMAM and PPI dendrimers (Cavallo et al. 1998; Naylor et al. 1989). Again, backfolding of end groups is predicted by several different computational approaches. Scherrenberg et al. (1998) performed experimental studies as well as molecular dynamics simulations on PPI dendrimers, showing that dendrimer dimension increases linearly with the generation number and that PPI dendrimers possess a fairly flexible overall structure with substantial backfolding in poor solvents which is in accordance with the more general predictions of Murat et al. (1996). Additionally, the computations of Welch et al. (1998) imply that backfolding would increase with increasing ionic strength of the solvent.

An important property of dendrimers is their low polydispersity. Hummelen et al. (1997) report the polydispersity of G5 PPI dendrimers to be 1.002, while Kallos et al. (1991) report a polydispersity of 1.0007 for G4 PAMAM. This is a considerable advantage compared to linear polymers that often possess a high polydispersity, making it difficult to use these structurally inhomogeneous polymer solutions in medical context. The high number of charged outer groups and thus the high surface charge accounts for the high solubility, miscibility and reactivity of dendrimers (Fréchet 1994). Furthermore, due to their globular structure dendrimers possess a high surface area compared to their volume allowing tight interactions with

other molecules or with biological structures, e.g. charged surfaces like cell membranes.

1.2.2 Medical applications

The first medical application of cationic dendrimers in general, and PAMAM and PPI dendrimers in particular, was their usage as gene transfection agents (Hollins et al. 2004; Navarro et al. 2009; Zinselmeyer et al. 2002) and drug delivery carriers (Esfand et al. 2001; Gillies et al. 2005). This is due to their high water solubility, high number of outer groups that can be modified for drug attachment, the internal cavities that can incorporate drug molecules, and their capability to bind nucleic acids and transfect cells. Dufes et al. (2005) showed that *in vivo* administration of complexes between the dendrimer and the mTNFα expression plasmid DNA to tumour-bearing mice lead to TNFα gene expression by tumour cells accompanied by tumour growth delay or regression. However, the authors also found that PPI dendrimers on their own have an intrinsic effect against cancer cells *in vivo* and are well tolerated by the mice. The first report about the anti-cancer effect of polycations reach as far as into early 1970s (Moroson 1971). Yet the mechanism that leads to tumour regression under dendrimer therapy remains unclear and it is important to focus further on the antitumour effect of dendrimers in order to be able to proceed to clinics one day.

One concern about the use of dendrimers as therapeutic compounds is that toxicity of positively charged dendrimers is a well-known problem (Malik et al. 2000). For example, high concentrated anionic nanoparticles as well as even low concentrated positively charged nanoparticles influence the integrity of the blood-brain barrier. Lockman et al. (2004) observed an increased accumulation of labelled sucrose in all brain compartments after treatment of *in situ* rat brains with cationic emulsifying wax nanoparticles at 10 and 20 $\mu g\,ml^{-1}$ (size: $97.2 \pm 68.9\,nm$). This raises concern about possible leakage of the content of luminal plasma into the endothelial tight junctions of the blood-brain barrier, subsequent swelling and eventually

endothelial cell death. On the other hand, it is important to notice that low concentrated anionic nanoparticles seem to be able to cross the blood-brain barrier without causing its damage (Lockman et al. 2004) which could have consequences for the development of new therapeutic applications for the treatment of brain diseases, e.g. brain tumours.

PAMAM dendrimers up to generation G5 do not seem to have noteworthy adverse effects when applied *in vivo* in Swiss-Webster mice at concentrations 5×10^{-6}, 5×10^{-5} and 5×10^{-4} mmol/kg even after 6 months lasting weekly injection as indicated by lack of significant weight difference and behavioural abnormalities compared to control mice and lack of microscopic or macroscopic tissue abnormalities. However, *in vitro* studies with V79 cells (Chinese hamster fibroblast cell line) suggest considerable biotoxicity (Roberts et al. 1996). The *in vitro* toxicity is very much generation dependent, resulting in cell death at 1 mM for G3, 10 µM for G5 and less than 100 nM for G7, without significant differences between 4 and 24 h exposure. Notably, the toxicity measurement *in vitro* occurred not until 6 or 7 days after dendrimer withdrawal and thus reflects not only immediate cell death, but also impaired long-term proliferation ability. This might explain the lack of significant differences between the two timepoints. Furthermore, PAMAM dendrimers have been reported to be non-immunogenic in mice. The biodistribution of these radioactively labelled dendrimers is generation-dependent. While G3 PAMAM dendrimers preferentially accumulate in liver, kidney and spleen (up to 15 ID/g(percent injected dose per gram)), G5 and G7 dendrimers are mostly found in pancreatic tissue (peak at 32 ID/g at 24 h for G5 and 20 ID/g at 2 h for G7). Additionally, according to radioactive labelling experiments, G7 is excreted urinary in a large amount (peak at 74 ID/g after 4 h). However, the authors argue that the high radioactivity in the urine might be due to metabolic demethylation rather than glomerular filtration.

To test if surface modifications of dendrimers with free amino groups would alleviate dendrimer toxicity *in vivo*, Dutta et al. (2008) examined haematological, histopathological and biochemical parameters in Wistar

rats that were treated with functionalised G5 PPI dendrimers. Surprisingly, although coupling of the tetrapeptide tuftsin (Thr-Lys-Pro-Arg) to the dendrimer amino groups increased the number of free amino groups on the surface of the particle, the toxicity of this construct was significantly lower than that of parental PPI dendrimers. This is thought to be due to masking of the amino groups by the bulky oligopeptide. Conjugation of *t*-BOC and mannose also dramatically decreased toxicity of the particles, probably by disguising the positively charged functional groups.

As for DAB-Am16, Dufes et al. (2005) could not observe considerable side effects upon its administration into mice. Results of cytotoxicity investigations *in vitro* are presented in the following section.

1.2.3 Cytotoxicity

A range of *in vitro* cytotoxicity testing methods based on different surrogate markers for viability or death is available. A comparably high throughput can be achieved with the MTT, Neutral Red (NR) and Alamar Blue (AB) assays. The MTT assay is based on the conversion of a yellow tetrazolium salt to purple, water-insoluble formazan by the mitochondrial succinic dehydrogenase in metabolically active cells (Berridge, Herst et al. 2005; Berridge and A. S. Tan 1993; Berridge, A. S. Tan et al. 1996; Mosmann 1983). AB is a oxidation-reduction indicator that changes its colour upon reduction by mitochondrial enzymes (Anoopkumar-Dukie et al. 2005; Uzunoglu et al. 2010). However, it has been reported that MTT and AB reduction could be partly carried out by cytoplasmic or microsomal enzymes. NR is a supravital dye that accumulates in the lysosomes of living cells (Borenfreund et al. 1985; Hamid et al. 2004; Weyermann et al. 2005). A more detailed insight into the mechanism of cell death can be achieved by the application of various probes for flow cytometric analysis.

Mukherjee, Davoren et al. (2010); Mukherjee, Lyng et al. (2010) applied the MTT, NR and AB assays on HaCaT and SW480 cells after treatment of the cells with PAMAM G4, G5 and G6. The overall tendency of the three

assays was in agreement with each other: the EC50 (Effective Concentration with a 50 % toxicity effect) decreased with increasing PAMAM generation number. However, the EC50 values varied considerably, and the same is true for the curve progression when the cytotoxicity was plotted against dendrimer concentration. Treatment time was another factor that led to a variation in the results of the three assays. In general, the MTT assay was found to be the most sensitive of the three assays. The NR assay exhibited a stimulatory effect of the dendrimer on the cells upon exposure to low dendrimer concentrations. The peak of the stimulatory effect corresponded to the EC50 of the MTT assay. The transition from non-toxic to toxic effect in the NR assay curve occurred at the EC50 of the AB assay. Measurements with Lysosensor confirmed an increased lysosomal activity below and up to EC50 from MTT assay. This increase in the lysosomal activity was not visible for up to the first 6 h after dendrimer addition (in fact there was a decrease of the lysosomal activity below the control during the first 6 h), but was clearly measurable after 24 h. Mitotracker staining intensity and thus mitochondrial activity decreased with increasing PAMAM concentration, thus following the results of the MTT assay. There was no clear, consistent trend in production of reactive oxygen species (ROS). In HaCaT cells, ROS production increased up to 1–3 h (dependent on the PAMAM generation) and decreased afterwards, until it fell below the control level after 4 h, but it rose again after 24 h. For SW480, ROS production rose during the first 6 h, but fell below the control level after 24 h. The authors explain the difference in ROS production between the cell lines in the different natural antioxidant levels. Most ROS production occurs at EC50 of the MTT assay or below. Apoptotic cell death was confirmed by flow cytometry (Yo-Pro/PI staining) and with the TUNEL assay. Based on these results, Mukherjee, Lyng et al. (2010) suggest a mechanism of action that includes cell entrance either via endocytosis (for high dendrimer concentrations) or hole formation (for low dendrimer concentrations). The absence of lysosomal activation during the first 6 h is explained by a lack of lysosomal involvement in early PAMAM effects as dendrimers taken up by endocytosis

could escape the endosomes due to the low pK of the amines (3.9 and 6.9) that can buffer the endosomal pH (proton-sponge hypothesis) (Haensler et al. 1993). Mitochondrial damage by the dendrimer is suggested to induce ROS production and to disrupt the mitochondrial activity, eventually leading to apoptosis. This would explain the fact that the MTT assay is the most sensitive cytotoxicity assay for PAMAM-treated cells. As HaCaT cells contain significantly more antioxidants than SW480 cells, they can more efficiently counteract the ROS increase that follows mitochondrial damage at the first time and at low PAMAM concentrations. At longer exposure times, the ROS defence mechanism collapses and lysosomal activity increases as a mechanism to neutralize the dendrimers and to remove damaged mitochondria (mitophagy).

Due to the high positive charge of cationic dendrimers, interaction with (negatively charged) cell membranes can potentially lead to cell membrane damage and cellular toxicity. The following section provides an overview on how dendrimers are known to interact with synthetic and cellular membranes.

1.2.4 Interactions with lipid membranes

Hong, Leroueil et al. (2006) compared the effect of different polymers on lipid bilayer and cellular membrane. For this purpose, poly-L-lysine (PLL), branched polyethylenimine (PEI), diethylaminoethyl-dextran (DEAE-DEX) as well as G5 PAMAM dendrimers were used. They also tested PEG and PVA, two neutral polymers. Hong, Leroueil et al. found that while polycationic polymers are all able to disrupt supported dimyristoylphosphatidylcholine (DMPC) lipid bilayers, neutral polymers are not. However, there are differences in the effects of exposure of the bilayer to different polymers. According to Hong, Leroueil et al., PLL induces the formation of new 4.0–4.8 nm deep defects, while PEI only extends naturally pre-existing depressions with a depth that corresponds to the removal of a full bilayer (4–5 nm). In contrast, DEAE-DEX causes membrane thinning (2–3 nm),

probably either by changing the orientation of lipids or by their removal. All three cationic polymers also cause enzyme leakage (LDH 140 kDa and LUC 61 kDa) from the cytoplasm when intact cells are exposed to nontoxic polymer concentrations (6 and 12 $\mu g\,ml^{-1}$ resulting in >80 % cell viability) for 1 h. Three different experiments show that PEI induces most enzyme leakage and most small molecule diffusion across the cell membrane. This might be due to the fact that PEI possesses the greatest charge density of all tested polymers. The authors also suggest from their data that linear polymers might be less capable of inducing membrane permeability than sphere-like (PAMAM), branched (PEI) or ring-containing (DEAE-DEX) particles.

Mecke, Uppuluri et al. (2004) examined the difference of the influence of positively and negatively charged G7 PAMAM dendrimers and G7-G5 core-shell tectodendrimers (i.e., higher molecular structures consisting of G5 dendrimers covalently attached to the outer shell of a G7 core dendrimer) on DMPC lipid bilayer on mica. As phospholipids are an integral part of cell membranes, this bilayer composition is a good choice to investigate dendrimer effect on biological membranes. The authors observed that G7 PAMAM dendrimers are capable of creating new holes in the bilayer as well as expanding pre-existing defects regardless of being positively or negatively charged, or even destruct the bilayer when applied at a high concentration. In contrast, tectodendrimers did not induce the formation of new holes, but attached to the edges of existing defects, moved into the holes and adsorbed to the mica filling out the entire hole. As a mechanism of hole formation induced by the dendrimers the authors suggest that due to strong interaction between the lipids and the dendrimers lipids detach from the mica and enclose the dendrimers to form dendrimer-filled vesicles.

Studies with Atomic Force Microscopy (AFM) and Optical Waveguide Lightmode Spectroscopy (OWLS) reveal details about the process of dendrimer absorption to the lipid surface and hole creation and extension. Parimi et al. (2008) scrutinised the interaction of PAMAM dendrimers of different generations (G2, G4 and G6) with supported DMPC lipid bilayers. They

found that the dendrimer concentration affects hole formation as well as the general mode of dendrimer-bilayer interaction. Exposure to 1 and 100 nM dendrimers leads to a mass loss of the bilayer, which indicates lipid bilayer destruction at these concentrations. At higher concentration and with increasing dendrimer generation the bilayer removal effect becomes more pronounced. However, at 10 nM, OWLS shows an increase of the net mass. This was true for all tested dendrimer generations. Parimi et al. conclude that dendrimer absorption outweighs hole formation at this concentration. AFM experiments visualise the dendrimer-bilayer interactions and due to specific software also allows quantification of hole formation. At 1 and 100 nM hole formation and lipid bilayer defects extension are observed. The authors surmise that the formation of lipid-dendrimer aggregates (similar to dendrisomes) and their removal from the bilayer are responsible for this effect. While G6 PAMAM dendrimers cause the formation of a bigger amount of holes, G4 dendrimers form less holes of a bigger size, probably carrying out more defect extension than *de novo* hole formation. In general, G2 dendrimers have a significantly lesser effect on lipid bilayer removal. At a 10 nM concentration, hole formation as well as dendrimer absorption to the lipid bilayer are detected. However, the hole formation is decreased compared to 1 and 100 nM dendrimer concentrations. Again, G2 PAMAM was less efficient in hole formation than the higher generation dendrimers. Altogether, the authors deduce from the results that at a concentration of 1 and 100 nM, hole formation is the prevalent way of action of the dendrimers on the bilayer, while at 10 nM predominantly an adsorption of the dendrimers takes place.

A number of studies have been conducted in order to investigate the efficacy and safety of the use of dendrimers as drug and DNA delivery vehicles. Toxicity studies revealed that cells remain viable after an exposure to dendrimers up to a concentration of 500 nM for up to 3 h (Hong, Bielinska et al. 2004). However, an interaction of positively charged late generation (e.g. G7) dendrimers with the cell membrane has been observed, eventually leading to the formation of 15–40 nm holes and leakage of cytosolic enzymes.

The net negative charge of cell membranes might facilitate the dendrimer-membrane contact. According to Hong, Bielinska et al., this hole formation is reversible as cells recover after withdrawal of dendrimers from the growth medium.

In contrast, uncharged dendrimers do not show interaction with the cell membrane. This and the fact that higher generations of cationic dendrimers are more effective than lower generations suggests that a high cationic charge density (charge/monomer ratio) favours polymer interaction with cell membrane phospholipids. Nonetheless, an uptake not only of cationic, but also of uncharged and anionic dendrimers via endocytosis can be observed. It has been shown that inhibition of different endocytotic processes with different inhibitors (Brefeldin A, colchicine, filipin, sucrose) in each case leads to a significantly reduced uptake of positively charged G4 PAMAM dendrimers (Kitchens, Kolhatkar et al. 2008). The following section presents an overview of experimental results pointing to endocytotic uptake of dendrimers.

1.2.5 Evidence for endocytotic mechanism of cell entry

PAMAM G4 dendrimers conjugated with the fluorophore Alexa647 associate with the cell membrane of HeLa cells within 1 h. However, internalization partly occurs only after 2 h. After 4 h, no membrane fluorescence is detectable any more and the dendrimer accumulates in the perinuclear area. This process is completed after 12 h, and there is no change in PAMAM dendrimer localisation within 48 h (Albertazzi et al. 2010). PAMAM G4-Alexa488 conjugate colocalises with control molecules for clathrin-dependent endocytosis (transferrin) and macropinocytosis (FITC-dextran), but does not colocalise with EGFP-marked caveolin. After cell entry, it accumulates in the perinuclear region, colocalising with lysosomal markers (lysosensor), but not with Golgi apparatus marker (Giantin)(Albertazzi et al. 2010). Furthermore, colocalisation with TAT (a peptide taken up rapidly by macropinocytosis and clathrin-dependent endocytosis) also can be observed,

although TAT enters the cell much quicker than PAMAM G4: already within 1 h. The speed of PAMAM G4 internalisation was found to be dependent on the cell line.

Seib et al. (2007) studied the internalisation of linear and branched PEIs as well as of cationic PAMAM dendrimers (G2–4) in B16f10 mouse melanoma cells. All polymers were used at 140 nM, and measurement was performed for 2 h. The above mentioned polymers were conjugated with Oregon Green (OG). The authors propose a cholesterol-dependent internalisation of PAMAM G4 as they observed 44 % reduction in PAMAM internalisation when cells were treated with MβCD, a putative inhibitor of pinocytosis. The same was true for branched PEI. However, a markedly increased uptake of linear PEI was detected under the same conditions, which the authors explain by a putative existence of different binding sites for branched and linear PEI on the cell membrane. These experiments were performed at significantly lower concentrations than those reported to induce enzyme leakage from cells by Hong, Bielinska et al. (2004) (200 and 400 nM for KBpLuc and Rat2pLuc cells, respectively) or membrane damage by Hong, Leroueil et al. (2006) who used PAMAM G5 at 6 and 12 µg ml^{-1} which corresponds to a concentration of $\sim$200 and 400 nM, respectively. In contrast, Parimi et al. (2008) observed membrane damage at as low concentrations as 1 and 100 nM. However, supported DMPC membranes are models that reflect some, but not all properties of plasma membrane, so comparison between the above-mentioned cellular experiments can be carefully interpreted as a hint that endocytosis might occur at lower concentrations than membrane damage. Precise comparison of minimal concentrations at which endocytosis and hole formation occur at the same treatment conditions of the same cell lines are necessary to test this supposition. It is also important to keep in mind that the dendrimers used in studies of Albertazzi et al. and Seib et al. are conjugated with fluorescent probes that might themselves enhance endocytosis to a large extent. For instance, OG is known to enhance transfection activity of

PAMAM dendrimers, presumably through hydrophobic interactions leading to disruption of endosomal membrane (Yoo et al. 2000).

Perumal et al. (2008) found that PAMAM dendrimer uptake (∼690 nM, 1 h) into A549 lung epithelial cells was significantly reduced upon reduction of the incubation temperature from 37 °C to 10 °C by 80–90 % for positively and negatively charged as well as neutral G4 dendrimers. Inhibition of cellular metabolism by treatment with deoxyglucose and sodium azide decreased the cellular uptake of the dendrimers by 40–50 % for charged and by 70 % for neutral dendrimers. Thus, the uptake of PAMAM dendrimers seems to include an energy-dependent as well as an energy-independent mechanism. These authors also found that upon inhibition of fluid-phase endocytosis by sucrose, dendrimer internalisation was also markedly decreased, most prominantly for G4-NH2 dendrimer (80 %). In contrast to the findings of Albertazzi et al., Perumal et al. (2008) propose a non-clathrin-mediated endocytosis pathway for PAMAM uptake, as chlorpromazine (a specific inhibitor of clathrin-mediated endocytosis) was able to reduce the internalisation of transferrin but not of PAMAM G4. Interestingly, filipin (an inhibitor of caveolae/cholesterol dependent endocytosis) had different effects on the three dendrimers used in this study: while G4-COOH uptake was decreased to the same extent as the uptake of lactosylceramide (marker for caveolae-dependent endocytosis), no effect on the neutral dendrimer and a significant increase of G4-NH2 uptake were observed. These results contradict the observations of Kitchens, Kolhatkar et al. (2008) who observed a significant inhibition of G4-NH2 uptake by Caco-2 cells in the presence of filipin. This might be due to the difference in cell features, as Perumal et al. used A549 lung epithelial cells. Inhibition of macropinocytosis and phagocytosis by cytochalasin did not have any effect on the uptake of all three dendrimers (positive control: FITC-dextran) by A549 cells. Nocodazole (an inhibitor of microtubules and thus of vesicular movement) only reduced the uptake of the anionic dendrimer (by 50 %), but not of the cationic and the neutral ones. An increase of the pH of intracellular organelles by ammonium chloride treatment decreased the uptake of the

anionic dendrimer, and slightly increased the uptake of G4-NH2. Uptake of the neutral dendrimer was not altered. Intracellularly, the cationic dendrimer was found not to colocalise with lysotracker, while the other two dendrimers did. G4-NH2 accumulated in the cell periphery. Perumal et al. suggest a caveolae-mediated uptake of anionic dendrimers, and a non-clathrin and non-caveolae dependent uptake mechanism for cationic and neutral dendrimers. However, all three dendrimer types seem to be taken up by endocytosis according to their results.

Kitchens, Foraker et al. (2007) investigated the mechanism of entrance of differently charged PAMAM dendrimers into Caco-2 intestinal epithelial cells. They found that at 100 nM, low (G2) as well as higher generation dendrimers (G4) colocalise with clathrin, with the lysosome-associated protein 1 (LAMP-1) and the early endosomal antigen 1 (EEA-1). Notably, when comparing the results of colocalisation experiments after 20 min and after 60 min, they observed an increased colocalisation of G2-NH2 dendrimers with LAMP-1. When Kitchens, Foraker et al. investigated the appearance of microvilli layer of the cells with TEM after 2 h treatment with dendrimers, they noticed that G2-NH2 dendrimers did not damage the microvilli, while G4-NH2 had a destructive effect on them. This effect increased with the concentration. These findings of Kitchens, Foraker et al. correspond with reports on hole formation in cell membrane by positively charged dendrimers (Hong, Bielinska et al. 2004; Hong, Leroueil et al. 2006; Mecke, Majoros et al. 2005; Mecke, Uppuluri et al. 2004; Parimi et al. 2008). On the other hand, Akesson et al. (2010) investigated the effect of PAMAM G6 on lipid vesicles and their results suggest that PAMAM G6 binds to the lipid membrane and at higher concentrations leads to aggregation of larger vesicles by electrostatically bridging the lipids, thereby deforming but not damaging the vesicles. The authors conclude that at physiological concentrations, PAMAM G6 would not permeate phosphatidylcholine/phosphoglycerol membranes, however they do not exclude the possibility of another nature of interaction between PAMAM G6 and negatively charged phosphatidylcholine in cell membranes,

as well as defect propagation in imperfect membranes. Evidence for an endocytotic uptake mechanism of PAMAM dendrimers as well as lysosomal colocalisation was also found by Saovapakhiran et al. (2009).

The cell entrance mechanism of SuperFect, a commercially available fractured G4 PAMAM dendrimer often used as transfection agent (Merkel 2009), was investigated by Manunta, P. H. Tan et al. (2004). By depletion of cellular cholesterol with MβCD, filipin III and nystatin as well as reconstitution of cholesterol content while or after this treatment in EA.hy 926 (human endothelial hybridoma), HEK293 (human embryonic kidney) and CHO (Chinese hamster ovary) cells, they found dendrimer binding to the cell membrane and entrance into the cell being cholesterol dependent. Because of colocalisation of dendriplexes (complexes of dendrimer with nucleic acid) with glycosphingolipid GM1 the authors conclude that lipid rafts are involved in the endocytotic uptake of dendriplexes by cells. In contrast, depletion of plasma membrane cholesterol by filipin III in HepG2 and HeLa cells that usually contain only little cholesterol, even increased the transfection efficiency with lipofectamine (significantly only in HepG2) (Manunta, Nichols et al. 2006). Inhibitors of clathrin-dependent endocytosis (chlorpromazine), phagocytosis and macropinocytosis (cytochalasin D), and macropinocytosis (wortmannin and LY294002) also did not decrease transfection efficiency, while a significant increase in transfection efficiency was observed in EA.hy 926 and HepG2 cells. Overexpression of AP180 (a dominant negative mutant of the clathrin accessory protein) and caveolin 1 led to increased uptake and transfection efficiency. Colocalisation of dendriplexes with caveolin 1 as observed with confocal microscopy further confirms the involvement of the caveolae-dependent endocytosis pathway in dendriplex uptake (Manunta, Nichols et al. 2006).

In summary, all of these studies confirm the uptake of PAMAM dendrimers via endocytosis. However, more detailed studies of the type of endocytosis yield contradictory results. Focusing specifically on cationic PAMAM dendrimers, involvement of clathrin-mediated endocytosis was suggested by Albertazzi et al. (2010); Kitchens, Foraker et al. (2007), involvement

of caveolae-dependent endocytosis was observed in studies of Kitchens, Kolhatkar et al. (2008); Manunta, Nichols et al. (2006); Seib et al. (2007), and macropinocytosis was suggested by Albertazzi et al. (2010). On the other hand, no involvement of neither clathrin- nor caveolae-mediated endocytosis nor macropinocytosis was found by Perumal et al. (2008), and no involvement of caveolae-dependent endocytosis was observed by Albertazzi et al. (2010). However, all of these studies used different generations of PAMAM dendrimers as well as different cell lines. Cell lines differ with respect to their plasma membrane lipid composition which might highly influence the endocytotic mechanisms used by the cells. Furthermore, given the observations that the capability to insert holes into artificial and biological cell membranes changes with the generation number, the endocytotic mechanism might be altered as well. For instance, it is conceivable that higher generation dendrimers exert a tighter interaction with negatively charged phospholipids within plasma membrane rafts, while being less prone to cholesterol-dependent internalization due to their bulkier size.

Although the studies listed above refer to PAMAM dendrimers, it can be assumed that their implications are also important for PPI dendrimers due to the very similar structure and physico-chemical properties.

1.2.6 Chemical characterisation

Safe application of dendrimers as human therapeutics requires a precise structural characterisation including quantification of possible impurities (e.g. dendrimers with structural defects or presence of other compounds in the sample). Analysis of structure-activity-relationships and thus future modification of the chemical structure in order to improve activity and safety require the knowledge of the precise chemical structure of the administered agent. Furthermore, stability of the pharmaceutical compound over time can only be monitored if methods for structural characterisation are available. The structure and purity of PPI dendrimers have been characterised by mass spectrometry (MS) and nuclear magnetic resonance (NMR) (Chai

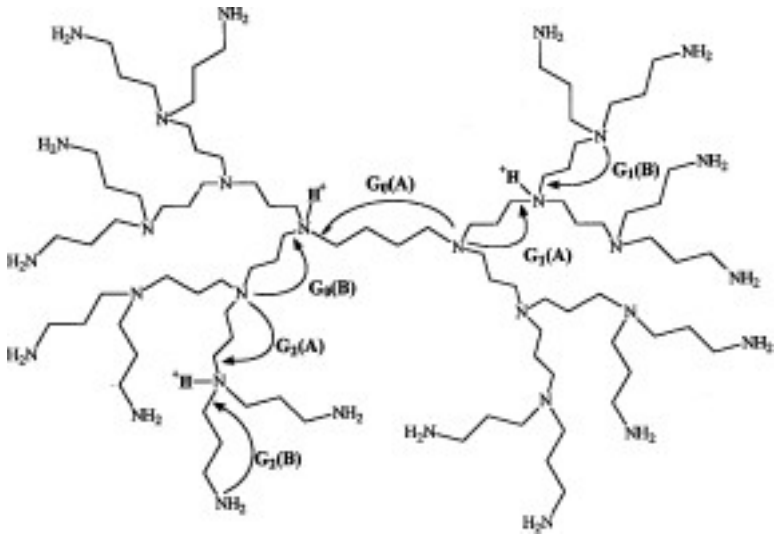

Fig. 4: Scheme of possible decomposition reactions of DAB-Am16 during MS/MS according to McLuckey et al. (2000).

et al. 2001). These techniques allow to reveal the molecular composition a sample in a quantiative way.

A generalised scheme for the various possible reactions that PPI dendrimers might undergo during the MS/MS measurements has been proposed by McLuckey et al. (2000). According to this scheme, a nucleophilic substitution occurs whereby a tertiary nitrogen situated in one of the inner shells serves as a nucleophile. This nitrogen atom attacks an α-carbon atom adjacent to the next nitrogen. If this carbon atom is further in the interior of the dendrimer (i.e., closer to the core than the nucleophile), the reaction is called "process A". If the attack occurs into the opposite direction, the reaction is designated "process B". The layer in which the protonated nitrogen atom is situated, is termed G_n, whereby n refers to the generation number. Herein, $n = 0$ represents an attack onto one of the core /*alpha*-carbon atoms (Fig. 4).

Based on this scheme, various charged fragments can be predicted to be seen in the spectrum. After fragmentation of the molecular ion (M +

H)$^+$ of the DAB-Am16 dendrimer 6 charged fragments should be observed (Fig. 5).

The experimental results support the theoretical predictions. McLuckey et al. applied electrospray ionisation (ESI) onto DAB-Am16 molecules and subsequently recorded the spectrum of the molecular ion in ion trap tandem mass spectrometry. All of the predicted peaks were observed in the mass spectrum except of G_2(B) that fell below the cutoff m/z value. Additionally, a peak at m/z 269 appeared that can be explained by dissociation of a fragment structurally correspondng to G_2(A) product from $G_0(B)_q$. The authors argue that similar dissociation reactions might have contributed to the peaks assigned to products of fragmentation reactions in Fig. 5.

To investigate the influence of different solvents on PPI G3 dendrimer conformation, Adhiya et al. (2002) applied matrix-assisted laser desorption ionisation (MALDI) or electrospray ionisation (ESI) to the dendrimer using solvents with different properties for sample preparation or spraying process. The molecular ion was subsequently subjected to post-source decay (PSD) and collisionally activated dissociation (CAD) measurements. The authors found a clear dependence of MS/MS spectra from the solvent used during ionisation. G_1(A) and G_2(A) fragmentations do not seem to occur when DAB-Am16 was dissolved in a non-polar, poor solvent (benzene). This is explained by backfolding of outer dendrimer branches and formation of hydrogen bonds between outer and inner amines.

NMR studies by Chai et al. (2001) confirmed that PPI dendrimers mostly adopt an extended conformation in polar solvents and a folded conformation in non-polar solvents. Interestingly, while structural defects were found in G4 PPI dendrimers (DAB-Am32), no such defect were seen in DAB-Am16.

1.2.7 DAB-Am16 dendrimer

The present study focuses on generation 3 polypropylenimine (PPI) dendrimers with a diaminobutane (DAB) core and 16 amino groups in the outer shell. G3 PPI dendrimers are well tolerated in vivo while having a profound

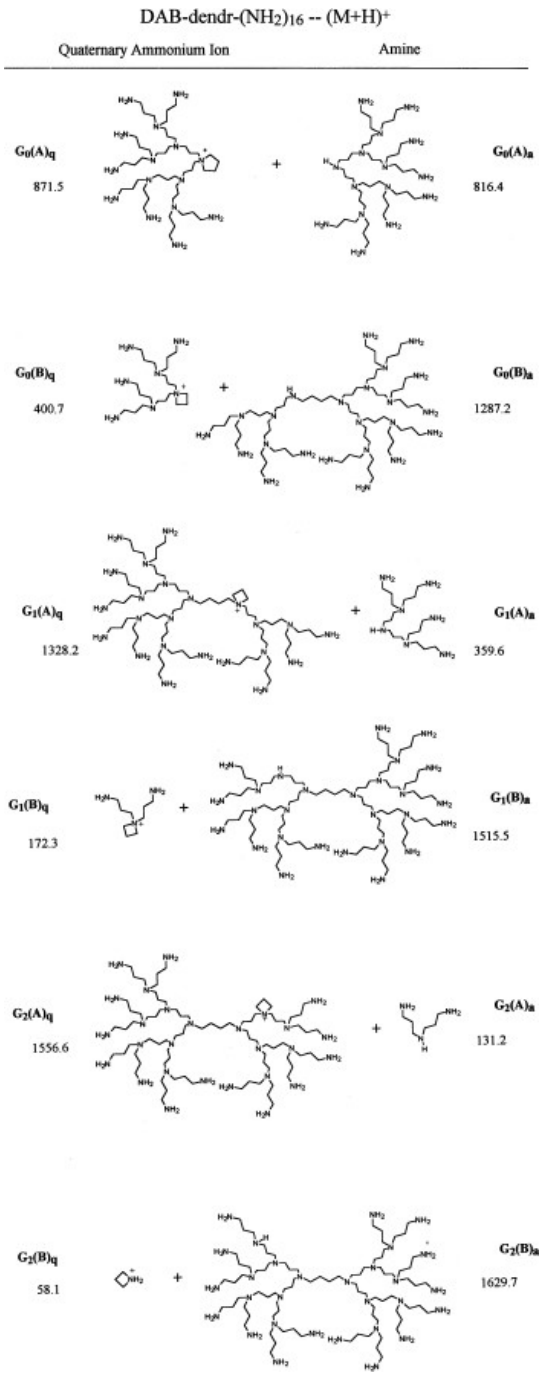

Fig. 5: Predicted fragments of DAB-Am16 due to mass spectrometric ionisation of the molecular ion (McLuckey et al. 2000).

anti-tumour effect (Dufes et al. 2005). Thus, this section gives an in depth introduction of this particular dendrimer.

DAB-Am16 has a molecular weight of 1.687 kDa and a hydrodynamic diameter of 1.9 nm (Voegtle 2000). Fig. 6 shows the chemical structure of DAB-Am16. The unique synthesis pathway leads to a polydispersity index of approximately 1 and a low number of defects compared to stochastically formed polymers (Hummelen et al. 1997). This implies that DAB-Am16 has a similarly well-defined chemical structure as conventional drugs. The molecular weight is also similar to conventional drugs (e.g. cyclosporine 1.2 kDa), but higher than that of standard anti-cancer agents (e.g. cisplatine 0.3 kDa, doxorubicin 0.5 kDa, etoposide 0.6 kDa).

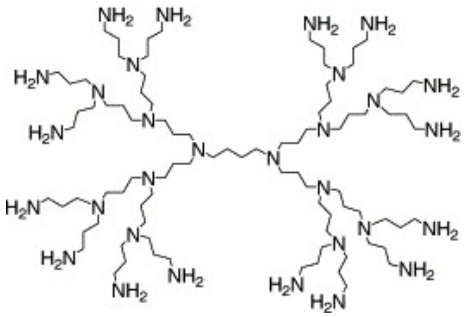

Fig. 6: The chemical structure of DAB-Am16.

It has previously been shown that upon exposure of cells to DAB-Am16, this dendrimer enters the cell nucleus within 30 min and binds to the DNA in a manner similar to doxorubicin. *In vivo* experiments on mice with tumour xenografts revealed that DAB-Am16 dendrimers as well as fractured G4 PAMAM and linear PEI have an intrinsic anticancer activity against colorectal, cervix and epidermoid carcinoma and leukemia (Dufes et al. 2005). The anti-cancer activity of DAB-Am16 in mice exceeds that of conventional antineoplastic drugs without having severe side effects. However, the mechanism of action of DAB-Am16 remains to be elucidated.

Omidi et al. (2005) reported that DAB-Am8 and DAB-Am16 dendrimers as well as their corresponding dendriplexes induce gene expression changes in human epidermoid carcinoma A431 and human adenocarcinomic alveolar basal epithelial A549 cells. The cells were exposed to 20 µg ml^{-1} dendrimer for 4 h, washed and allowed to recover for further 20 h. Changes following DAB-Am16 treatment with a non-toxic concentration were much more

profound than those after DAB-Am8 exposure, and dendriplexes induced less changes than the corresponding dendrimers alone. Furthermore, the profile of the gene expression changes was strongly cell line dependent. However, the authors derive from the data that mainly the expression of genes involved in cytokine signalling, apoptosis, cell cycle, DNA damage and DNA repair was altered. In particular, in both cell lines and after treatment with any of the dendrimers or dendriplexes proteasome $\alpha 4$ is upregulated (although not always significantly). Proteasome $\alpha 4$, also known as PA200, mediates repair of DNA double strand breaks and was found to facilitate tumour cell survival after IR-exposure (Blickwedehl et al. 2012; Ustrell et al. 2002). Several genes involved in G1 phase cell cycle progression are also affected, indicating that the observed effect of DAB-Am16 onto the cell cycle of cancer cells might be due to gene expression changes rather than to direct DNA damage. This is further confirmed by the fact that according to Omidi et al. the COMET assay did not show any DNA damage. They conclude that on the one hand, the observed alteration of cytokine signalling by PPI dendrimers supports the suggestion of Moroson that PPI dendrimers exert their anti-tumour activity via modulation of the immune system. On the other hand, Omidi et al. argue that a direct effect of the dendrimers against tumour cells by modification of apoptotic pathway as well as other genes that are necessary for cell growth and survival is conceivable. As it has been also shown that PAMAM dendrimers induce pore formation in the mitochondrial membrane and thus trigger the intrinsic apoptotic pathway (Lee et al. 2009), PPI dendrimers could elicit the same effect due to their similar molecular architecture and physico-chemical properties. As a matter of fact, Kuo et al. (2007) observed an effect of PPI dendrimers on reactive oxygen species generation and mitochondrial membrane potential of human U-937 macrophages and suggest the interaction of PPI dendrimers with the mitochondrial membrane of the cells.

Further investigation of the cytotoxic effect of DAB-Am16 requires a detailed elucidation of pathways that might contribute to DAB-Am16 mechanism of action. The following three sections give a short introduction

into the role of some key players of cell cycle regulation and apoptosis that have been investigated in the context of DAB-Am16 effect on cancer cells.

1.3 Key players of cell cycle progression, DNA damage and cell death

1.3.1 Role of cyclin D and of histone H3 phosphorylation within the cell cycle

The cell cycle is a sequence of events in the "life" of a cell that is roughly divided into four phases: G1, S, G2 and M. G1 and G2 are gap phases in which cell growth and control of genome integrity occur. DNA replication takes place within the S phase, while the M phase is the phase of cell division into two daughter cells. Regulation of the cell cycle is a complex process and a lot of questions remain unanswered on this issue. Mainly, the cell cycle is regulated by cyclins and cyclin-dependent kinases (Cdk) (Malumbres and Barbacid 2005; Malumbres, Harlow et al. 2009; Sánchez et al. 2005). Currently, 11 Cdk's (Cdk1–Cdk11) are known that can differentially associate with 9 cyclins (A, B, C, D, E, F, G, H and L). More Cdk-like and cyclin-box domain containing proteins have been identified, but the function of many of them remains obscure. Association of a particular Cdk with a particular cyclin promotes progression of the cell cycle at distinct times. Some of the functions of some Cdk/cyclin complexes are partly redundant, allowing cell cycle progression in the absence of the particular complex but with altered kinetics and with phenotypic changes (Malumbres and Barbacid 2005).

Cyclin D1 is an essential protein for cell cycle transition from G1 to S phase and is characterised as being a proto-oncogene (Bates et al. 1995). Cyclin D1 associates with Cdk4/6, enabling phosphorylation of retinoblastoma protein (Rb) (Fig. 7 on the following page). The phosphorylated Rb releases E2F transcription factors and allows the cell to proceed from G1 to S phase. Once the cell has entered the S phase, the level of Cyclin D1

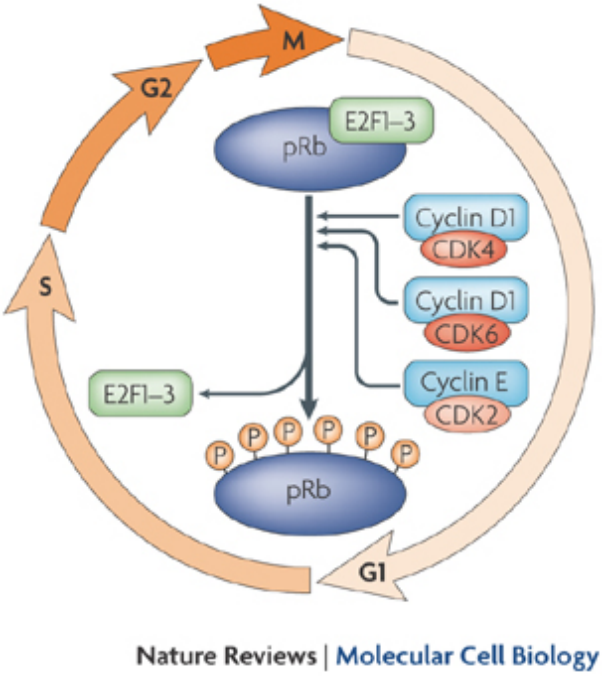

Fig. 7: The role of cyclin D1 in G1/S phase transition. Taken from Coller (2007).

drops and remains low until the beginning of G2 (Hitomi et al. 1999). However, cyclin D1 is deregulated in a range of cancers, facilitating uncontrolled growth and division of tumour cells (Alao 2007; Biliran et al. 2005; Chung 2004; Gautschi et al. 2007; S. Jain et al. 2004; E. S. Kim et al. 2011).

Having completed DNA replication in the S phase, cells pass into G2. Cell growth proceeds and genome integrity is verified before mitosis starts. At the beginning of mitosis, chromatin undergoes condensation. The G2/M checkpoint detects DNA damage and causes cell cycle arrest in G2 and DNA repair. It is regulated by the p38 kinase (Bulavin et al. 2001; Dmitrieva et al. 2002).

During mitosis, the nuclear chromosome condenses. This condensation is accompanied by phosphorylation of histone H3 at serine 10 (Hans et al. 2001). The phosphorylation starts at late G2, is completed in late prophase and is maintained until early anaphase. The dephosphorylation is completed

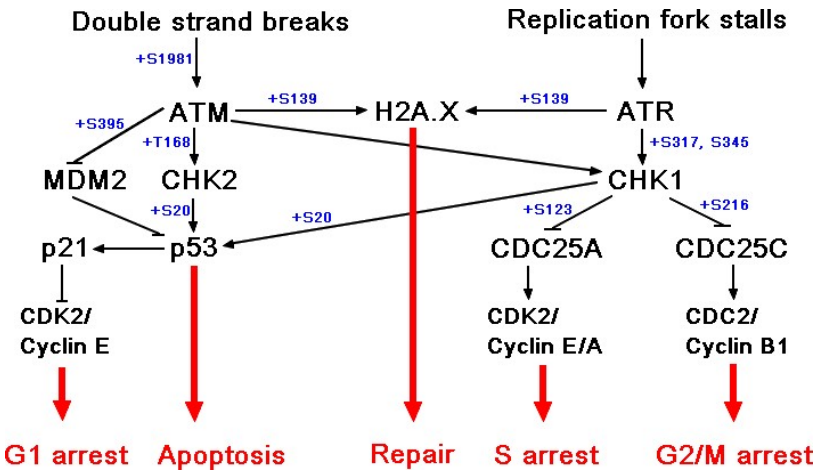

Fig. 8: The DNA damage pathway of mammalian cells. See text for details.

at early telophase (Hendzel et al. 1997). Thus, phosphorylation of histone H3 at serine 10 can serve as a specific marker for mitotic cells.

1.3.2 DNA damage sensing pathway

S phase arrest can be caused by triggering the S phase checkpoint of the cell. In fact, there are three different checkpoints within the S phase: the replication checkpoint, the S-M checkpoint and the intra-S-phase checkpoint (Bartek et al. 2004). While the intra-S-phase checkpoint is activated by DNA double-strand breaks (DSBs), the replication and the S-M checkpoint are elicited in response to problems with DNA replication, e.g. stalled replication forks. Unlike the G1 and G2 checkpoints, the S phase checkpoints do not arrest the cell cycle but slow down the progress through the S phase. Fig. 8 shows the main pathways that are involved in S phase checkpoints. The two serine/threonine kinases ataxia telangiectasia mutated (ATM) and ATM and Rad3-related (ATR) play a central role in slowing down DNA synthesis after exposure to genotoxic stress. Cells from ataxia telangiectasia patients lack ATM and show radioresistant DNA synthesis (RDA).

The classic conception of the cell response to DNA damaging agents distinguishes between double-strand breaks (e.g. due to ionizing radiation

or radiomimetic drugs) and DNA replication problems (e.g. due to dNTP-depletion after hydroxyurea treatment or DNA polymerase inhibition by aphidicolin). Double-strand breaks are thought to activate ATM, which in turn activates the serine/threonine kinase CHK2, p53 binding protein 1 (53BP1), Nijmegen breakage syndrome 1 (NBS1), breast cancer 1, early onset (BRCA1) and others. CHK2 then phosphorylates CDC25A at three sites (S123, S178 and S292) (Soerensen et al. 2003) which leads to ubiquitin-dependent degradation of this molecule. When unphosphorylated, CDC25A activates CDK2 interaction with Cyclin A and thus promotes S phase progression.

On the other hand, impairment of DNA replication is thought to activate ATR. This in turn activates the kinase CHK1 that phosphorylates the protein tyrosine phosphatase CDC25A at four different sites (S123, S178, S278 and S292). At this point, the ATM- and ATR-mediated pathways converge as these phosphorylations again lead to CDC25A degradation and S phase progression delay.

However, the discrimination between these two pathways is not as straightforward as it seems at first view. The finding that ATR-deficient but ATM-positive cells also display RDS suggests that ATR is also activated due to DSBs. This assumption is supported by the observation that although in ATR-deficient cells exposed to ionising radiation (IR) an immediate slowdown of DNA synthesis (fast response) occurs to the same extent as in wild-type cells, the maintenance of the DNA synthesis delay (slow response) is abolished in cells without ATR (X.-Y. Zhou et al. 2002). On the other hand, the slow response can be observed in ATM-deficient cells. X.-Y. Zhou et al. conclude that while ATM leads to increased CDC25A degradation via CHK2 immediately in response to IR and thus provides a fast response, ATR is also activated by IR and leads to a delayed CDC25A degradation via CHK1.

Interestingly, Soerensen et al. (2003) report that ATR is constantly activated in wild-type cells and induces CDC25A degradation at a basal

level. However, the IR-induced phosphorylation of CHK1 at S317 and S345 as well as the resulting CDC25A degradation are ATM-dependent.

1.3.3 Pathways of cell death

On the molecular level, two basic pathways of cell death can be distinguished: apoptosis and necrosis. Apoptosis is a tightly controlled sequence of events that occurs in response to intrinsic or extrinsic stimuli. The key players of this process are cysteine-aspartic acid proteases (caspases) that transmit the death signal, multiply it and activate other proteins that eventually lead to cell death (Hengartner 2000; Taylor et al. 2008). The caspases can be divided into initiator and effector caspases. Initiator caspases are activated via CARD (caspase activation and recruitment domain) or DED (death effector domain). The binding of these domains to their corresponding domains on other molecules causes clustering and transactivation of initiator caspases. Subsequently, they cleave the inactive pro-forms of effector caspases which in turn leads to activation of molecules that execute the apoptotic process. Different initiator caspases are activated in response to extracellular (e.g. binding to receptors of the TNF-R family) or intracellular (e.g. nutrient deprivation, cell cycle disturbance) stimuli. However, eventually both pathways converge. One of the most important effector caspases that is involved in both pathways is caspase-3 that cleaves a wide range of substrates that initiate the apoptotic cell death. Aside from and due to caspase activation, there are several other detectable hallmarks of apoptosis. One of the first events of the intrinsic apoptotic pathway cascade that leads to downstream initiator caspase (caspase-9) activation is pore formation in the mitochondrial membrane. This results in leakage of intermembrane content, particularly cytochrome c and different pro-apoptotic molecules. Cytochrome c together with Apaf-1 and pro-caspase 9 builds up the seven-fold symmetric apoptosome that leads to caspase-9 and subsequent caspase-3 activation. The loss of cytochrome c and decreased H^+ export after outer mitochondrial membrane disruption decrease ATP synthesis and also lead

to membrane depolarization. Thus, one of the early apoptotic events is the caspase-independent drop of mitochondrial membrane potential (Duessmann et al. 2003). After caspase-3 and other effector caspases are activated, they in turn cleave a range of cellular substrates to their active forms. Among others, this leads to the activation of the caspase-activated DNase (CAD) that fragments the nuclear DNA between nucleosomes into multiples of approx. 180 bp. Another indicator of apoptosis is the exposure of phosphatidylserine (PS) on the outer membrane leaflet of the cell. The mechanism of PS externalization is not well understood. While the general caspase inhibitor zVAD prevents PS exposure in several cell lines committed to the extrinsic apoptotic pathway (Martin et al. 1996; Vanags et al. 1996), PS exposure in primary T lymphocytes during apoptosis is caspase-independent and occurs simultaneously with the loss of mitochondrial potential (Ferraro-Peyret et al. 2002).

Besides apoptosis, another major type of cell death exists: necrosis. In the context of a multicellular organism, programmed cell death (e.g. sculpting of structures during development) occurs as apoptosis. Apoptotic cells do not cause inflammation as they do not burst and do not release the cell content. Instead, they are phagocytosed by macrophages or neighbouring cells. However, in response to certain toxins, cells can also undergo oncosis which is characterised by swelling, early cell membrane disruption and release of cytoplasmic content including factors that cause inflammation. Cells committed to apoptosis undergo secondary oncosis at a late stage.

However, some studies suggest that apoptosis and necrosis might share some important pathway members and that the choice of the cell death pathway does not solely depend on the character of the elicitor but also on its concentration and on the cell cycle phase of the treated cell at the moment of addition of the cytotoxic agent to the surrounding environment (Bonfoco et al. 1995; Hirsch et al. 1997; Yeung et al. 1999).

It has been suggested that autophagy is yet another form of (programmed) cell death (Tsujimoto et al. 2005). It is based on the engulfment of intracellular components into cytoplasmic vesicles, followed by their digestion

in lysosomes. Although the existence of this process is considered to be certain, the precise function of autophagy remains a matter of discussion. While clearly uncontrolled autophagy will eventually lead to cell death, it is unknown if regulated autophagy is not actually a survival mechanism in dying cells (Tsujimoto et al. 2005).

1.4 Problem statement and experimental strategy

After the discovery of the intrinsic anti-tumour effect and favourable toxicity profile of DAB-Am16 by Dufes et al. (2005), the question about the mechanism of action of DAB-Am16 became particularly important. Understanding of this mechanism is crucial for exploitation of the tumouricidal properties of this dendrimer in clinical settings. The aim of this thesis is to contribute to this understanding.

Two main *in vitro* effects of DAB-Am16 have been already known: tight binding to nucleic acids and formation of holes in lipid bilayers. Thus, three hypotheses arise from this knowledge. First, the dendrimer might damage the cell membrane in such a way that the cell loses the capability to retain its cytoplasmic content and to fix the holes, resulting in a necrotic cell death. The second hypothesis is that once within the cell, DAB-Am16 might enter the nucleus, interact with the nuclear DNA and lead either to its damage or to the incapability of DNA replication in the course of cell cycling. This might eventually lead to apoptotic cell death if the cell fails to circumvent the problem. Yet another possibility is that DAB-Am16 damages the mitochondrial membrane or membranes of other cellular organelles. However, this last possibility was not investigated within this project.

To investigate the first two hypotheses, DAB-Am16 was first chemically characterised to ensure its purity and stability. Then, overall cytotoxic and cytostatic effects were examined (Fig. 9 on the next page). This allowed to determine the concentration ranges and incubation times for further, more detailed experiments. It also led to first observations on how the dendrimer acts on a range of cancer cell lines. Once concentrations and time

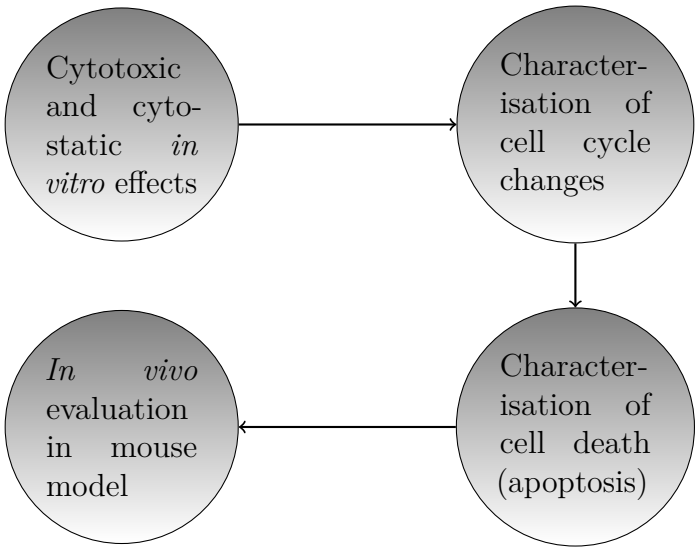

Fig. 9: Experimental approach to investigation of the mechanism of action of DAB-Am16.

frames were determined, the hypothesis that DAB-Am16 might derange the cell cycle was tested by observing the cell cycle profiles upon DAB-Am16 treatment. Subsequently, the mode of cell death was investigated, which allowed to draw conclusions on its mechanism, since hole formation in the cell membrane as cause of cell death would be expected to trigger necrosis, while DNA damage more probably would lead to apoptosis. Finally, effect on growth of MiaPaCa-2 xenografts in mice, on cell cycle and proliferation of the tumour cells *in vivo* was examined and the results were compared with the *in vitro* observations.

2 Materials and Methods

2.1 DAB-Am16 dendrimer

The dendrimer was purchased from SyMO-Chem BV (Eindhoven, The Netherlands). Three different vials ("batches") are available. Batch 1 has been opened for approx. 2 years and used for a number of experiments. Batch 2 was purchased together with batch 1, but was opened only in January 2010. Batch 3 was purchased in December 2009. All three batches have the same lot number 16AM-915651. The dendrimer was stored at 4 °C in opaque screw-topped glass bottles with a capacity enough for storage of approx. 30 g of DAB-Am16 each.

2.2 Analytical characterisation

2.2.1 NMR spectroscopy for structure determination and purity analysis of DAB-Am16

NMR spectra were acquired using Bruker Avance spectrometer equipped with 5 mm BBO probe including Z-axis pulse field gradients operating at nominal ^{1}H frequency of 400 MHz and ^{13}C frequency at 100 MHz. All spectra were processed using Spinworks 3. Chemical shifts were referenced to the residual $CHCl_3$ signal at 7.26 ppm (^{1}H). The parameters of the experiment setup were: acquisition time 3.95, 128 K time domain and relaxation delay of 2 s, sweep width of 20 ppm for ^{1}H and 220 ppm for ^{13}C, number of scans of 32 for ^{1}H, 8 for ^{1}H COSY and 1024 for ^{13}C. The dendrimer was measured in $CDCl_3$ at a concentration of 50 mg/ml.

2.2.2 Mass spectrometry and tandem mass spectrometry analysis of DAB-Am16 with electrospray ionisation

Further to NMR analysis, samples of the dendrimer from all three batches have been analysed by mass spectrometry (MS). Samples were dissolved at a concentration of 5 ng/µl in acetonitrile:water (1:1, v/v) with 0.1 % formic

acid. The spectrum was recorded with a quadrupole ion trap mass spectrometer (Thermo LCQ Finnigan) equipped with a nano-electrospray ion source and a Harvard Apparatus syringe pump. Sample was injected manually through the syringe pump and automatically by a direct injection using an Ultimate autosampler (Dionex, UK) coupled to the mass spectrometer. The flow rate of 0.8 µl/min was used in both experiments. The positive nano-electrospray mass spectra were acquired. The instrument operated using the following settings: spray voltage 1.9 kV, capillary temperature 200 °C, no sheath or auxiliary gas used. The m/z range from m/z 50–2000 was scanned, centroid data was collected. Other conditions were optimised automatically using the autotune function on DAB-Am16 at a concentration of 1 ng/µl. Data were collected either manually or automatically. Manual acquisition was performed to record MS and MS^2 spectra. MS^2 experiment was performed on a precursor ion, $[M]^+$. For acquisition of MS^2 spectra, the collision energy was set at 35 %. The MS^2 isolation width was set at 2.00, so as to allow the selection of precursor ion. MS, MS^2 scans consisted of three averaged "microscans" each with a maximum injection time of 200 ms. An automated program was set-up based on these acquisitions. Data was collected with the Xcalibur software (ThermoFinnigan).

2.2.3 Matrix-assisted laser desorption/ionisation-time of flight spectrometry for purity analysis

Spectra recorded with electrospray ionisation revealed some loss of dendrimer branches (section 3.1.2). This might occur due to in-source fragmentation of the molecule during the ionisation procedure as well as being present in the original sample. To scrutinise this issue further, matrix-assisted laser desorption/ionisation (MALDI)-time of flight (TOF) spectrometry was used as another technique of mass spectrometry analysis as this method provides a softer ionisation procedure and thus is preferred for molecules that can fragment easily with other techniques, particularly large molecules such as polymers and particularly dendrimers.

Additionally, this technique allows detection of possible high molecular contaminants. Briefly, the dendrimer was dissolved at a concentration of 0.25 µg/ml in methanol. One microlitre of sample was diluted in 20 µl of matrix solution (α-cyano-4-hydroxycinnamic acid 20 mg/ml in methanol). Sample (0.5 µl) was spotted on to the MALDI target plate. The samples were allowed to dry in air. MALDI spectra were recorded on an Applied Biosystems (Framingham, MA, USA) Voyager TOF mass spectrometer equipped with a nitrogen laser (337 nm). MALDI spectra were acquired in the positive-ion mode and were averages of 50 individual laser shots. The accelerating voltage was set at 20 kV, the focusing guide wire was at 0.01 % and the extraction delay time was 250 ns. Spectra were externally calibrated using a manufacture calibration mixture containing Angiotensin I (1.5 pmol/µl), ACTH (1-17 clip) (1.5 pmol µl), ACTH (18-39 clip) (2.0 pmol/µl), ACTH (7-38 clip) (3.0 pmol/µl), and bovine insulin (3.5 pmol/µl).

2.2.4 Elemental analysis of DAB-Am16 dendrimer

To further confirm the purity of the dendrimer, the weight percent of carbon, hydrogen and nitrogen in the sample was measured (CHN analysis). This is accomplished by dynamic flash combustion of the sample in presence of excess oxygen and determination of the amount of water, carbon dioxide and molecular nitrogen that arise from the combustion (Harris 1995). CHN analysis was done with the Carlo-Erba EA 1108 device with PC based data system Eager 200 for Windows, and a Sartorius Ultra Micro Balance 4504MP8.

2.3 Stability studies of DAB-Am16

To test the short term stability of dendrimer solutions stored under various conditions, DAB-Am16 was dissolved in 1 ml purified water at a concentration of 3 mg/ml by vigorously vortexing it until it was completely dissolved and stored either at –50 °C, at 4 °C, at room temperature (RT) or at 37 °C

in 2 ml microtubes (Eppendorf). MALDI-TOF analysis was performed after 24 h and after 6 days according to the procedure described in section 2.2.3.

2.4 Assessment of anti-proliferative effects of DAB-Am16

Several methods were applied to investigate the cytotoxic and cytostatic properties of DAB-Am16.

2.4.1 MTT assay

The MTT (3-(4,5-Dimethylthiazol-2-yl)-2,5-diphenyltetrazolium bromide) assay is a colorimetric cytotoxicity assay. MTT is a yellow, water-soluble tetrazole salt that is reduced to purple, water-insoluble formazan crystals by metabolically active cells. The absorbance of the formazan produced by the cells can be measured with a spectrophotometer at 500–600 nm after dissolving the formazan crystals in DMSO (Mosmann 1983). The conversion of the tetrazole to formazan was originally supposed to be confined to mitochondria, being carried out by the enzyme succinate dehydrogenase in mitochondrial Complex II. However, newer research suggests that the largest part of MTT reduction is NADH- and NADPH-dependent and involves enzymes of the endoplasmic reticulum (Bernas et al. 2002; Berridge and A. S. Tan 1993). In particular, MTT reduction is thought to be correlated with the glycolysis rate of the cells (Berridge, A. S. Tan et al. 1996).

The MTT reagent (Thiazolyl Blue tetrazolium bromide) was purchased from Alfa Aesar (Ward Hill, MA, USA). Cells were seeded at 500 cells per well in 96-well plates. They were allowed to grow for three days and then treated with DAB-Am16 (Sigma Aldrich) at indicated concentrations (200 µl per well) for either 4 or 24 h. Subsequently, cells were washed with Dulbecco's phosphate-buffered saline (DPBS, Invitrogen) and incubated for another 48 h with normal medium. Medium was discarded, cells washed with DPBS and 100 µl MTT solution (50 µg ml^{-1}) added. Cells were incubated

with the MTT solution for 2 h at 37°C, medium was removed accurately, 100 µl DMSO (Sigma Aldrich) added. After an incubation for 10 min at 37°C the absorbance at 570 nm was measured.

For analysis, background values were substracted. The cytotoxicity was determined as the ratio between the measured absorbance value of treated and untreated cells. Lysed cells (with Triton X-100 (Sigma Aldrich)) were used as a control for 100 % effect. All experiments were performed thrice, with six repeats per experiment. The 18 values were pooled and the overall mean was calculated.

2.4.2 LDH assay

Rapid onset of severe cytotoxicity can be monitored by detection of the release of cytoplasmic enzymes into the surrounding medium. This principle underlies the lactate dehydrogenase (LDH) assay that is based on colorimetric detection of LDH release (Korzeniewski et al. 1983). Within the cell, LDH converts lactate to pyruvate and thus is an essential component of glycolysis that is present in the cytosol of all mammalian cells. If the cell membrane becomes severely disrupted during necrosis or late stage apoptosis, LDH leaks out of the cell. For detection, the supernatant of treated cells is removed and the reaction mix is added. Within the reaction mix, lactate is oxidised to pyruvate by LDH upon reduction of NAD^+ to NADH. This NADH in turn is necessary for conversion of the tetrazole INT (2-(4-iodophenyl)-3-(4-nitrophenyl)-5-phenyl tetrazolium chloride) to formazan by the enzyme diaphorase, as illustrated in Fig. 10 on the following page. The absorption of the solution at 490 nm can be used to quantify the formazan and thus to assess plasma membrane integrity of the cells.

The CytoTox® 96 nonradioactive cytotoxicity assay (Promega Corporation, Madison, WI, USA) was used to quantitatively measure LDH. Cells were seeded at 500 cells per well in 96-well plates, grown for three days, treated with DAB-Am16 at indicated concentrations for the indicated periods of time and LDH released into the surrounding medium was determined

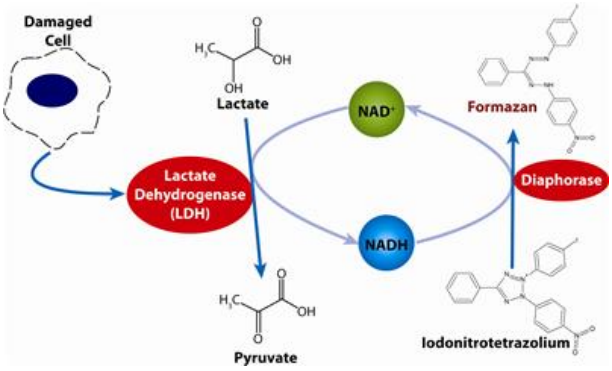

Fig. 10: Scheme of the LDH assay (*CytoScan™ LDH Cytotoxicity Assay*).

according to the manufacturer's instructions. Briefly, 50 µl supernatant were collected from each well, 50 µl reconstituted substrate mix were added, the samples were incubated for 30 min at room temperature before addition of stop solution (50 µl per well) and absorbance measurement at 490 nm.

For analysis, background values were substracted from the measured values and cell viability expressed as the ratio between the LDH release of treated cells and the LDH release of untreated control cells that were lysed 45 min before sampling (maximum LDH release). Experiments were performed in triplicates.

2.4.3 Colony formation assay

The colony formation or clonogenic cell survival assay tests the ability of single cells to divide and build colonies (Munshi et al. 2005). Formation of clonogenic colonies from single cells was investigated as early as in the 1950's with the minimum cell number per colony that allows further propagation being 25–50 cells (Puck et al. 1955). Since then, the ability to form colonies has been used as a method to test the loss of unlimited proliferative ability in cancer cells upon treatment with different cytotoxic drugs or irradiation *in vitro* (Bird et al. 1987; Franken et al. 2006; Roper et al. 1976; Twentyman et al. 1984). After the desired treatment, cells were collected, counted and 200 viable cells were seeded per well of 6-well plates in supplemented cell

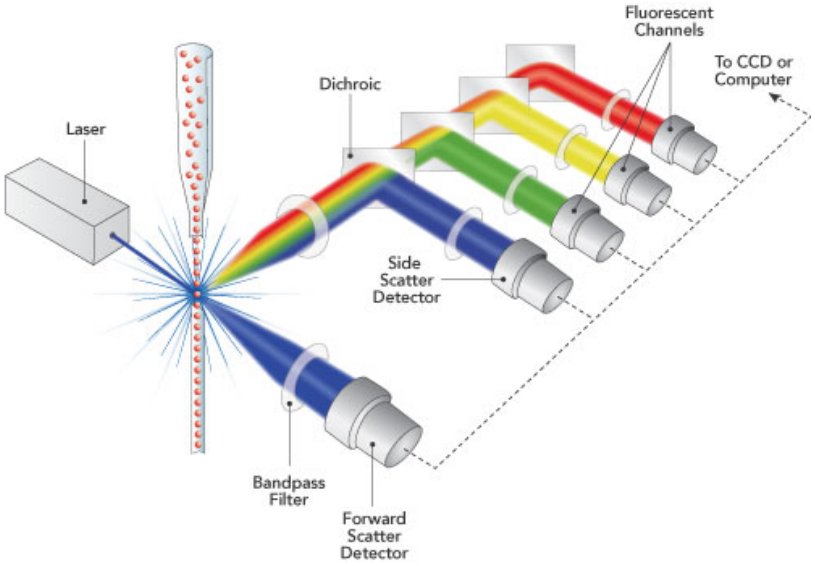

Fig. 11: General operating principle of a flow cytometer. As single cells pass through a laser beam, their fluorescence emission and the extent of light diffraction are recorded. Source: Semrock. Inc. (*Filters for Flow Cytometry*)

culture medium. After 7–10 days distinct colonies became visible under the microscope. Medium was removed, cells were carefully washed with PBS and the colonies were fixed and stained by 5 min incubation with 2 ml per well staining solution (0.5 % crystal violet in methanol). The solution was removed and the wells carefully washed with water. The plates were air-dried over night, pictures were taken of the wells and quantification was performed with ImageJ using a size-cutoff that corresponds approximately to a minimum of 50 cells per colony.

2.5 Flow cytometry

Flow cytometry is a method that has been widely used within the experimental work presented in this dissertation. For a better understanding of the figures that depict the results of flow cytometric experiments, a brief

Table 1: Excitation and detection channels of MACSQuant Analyzer.

Excitation wavelength	Channel	Emission filters	Detection range (nm)	Fluorochromes
405 nm	FL1	450/50	425–475	DAPI, MMC
488 nm	FL2	525/50	500–550	FITC, PhiPhiLux
	FL3	585/40	565–605	TMRE
	FL4	655 (LP) + 730 (LP DM)	655–730	PI
	FL5	750 (LP)	750–	
635 nm	FL6	655 (LP) + 730 (LP DM)	655–730	
	FL7	750 (LP)	750–	
488 nm	FSC/SSC	488/10	483–493	Light scatter

introduction into this method and data analysis techniques follows. This summary is based on Ormerod (2009); Shapiro (2003); Watson (1992).

A flow cytometer measures the light scatter and the fluorescence of single cells within a cell sample (Fig. 11 on the previous page). The flow cytometer that this work was performed with is the MACSQuant Analyzer from Miltenyi Biotec (Bergisch Gladbach, Germany) equipped with three lasers emitting light with 405, 488 and 635 nm wavelength, respectively. MACSQuant allows the simultenous measurement of up to 7 colours emitted by fluorescent probes by providing 7 emission filters. Additionally, the forward and the right angle (side) scatter can be measured. Table 1 summarizes the features of the channels within the MACSQuant Analyzer and lists the fluorochromes that were used for this thesis according to the channel they were measured in. Long pass (LP) filters only let pass higher wavelength, while a long pass dichroic mirror (LP DM) reflects all wavelengths that are higher than its specified wavelength.

There are several ways to present data obtained by flow cytometry. A *histogram* reflects the distribution of the recorded fluorescence intensity of the cell population for a single parameter, i.e. within one fluorescence channel. The fluorescence intensity is shown on the x-axis, while the number of cells emitting this fluorescence intensity is represented on the y-axis.

Examples of histograms can be seen in Figure 24 on page 84. When several samples (e.g. differently treated cells) are to be compared, their fluorescence intensity distributions can be overlayed within one histogram. However, if different cell numbers were recorded for these samples, the histogram has to be normalised to the area of the curve to allow accurate comparison. For an example see Figure 26 on page 86.

One of the main strengths of flow cytometry is the ability for multicolour detection, i.e. for every single cells up to 7 colours can be simultaneously detected with MACSQuant (and even more with some other machines), thus allowing to distinguish populations according to several parameters. The MACSQuantify software allows data presentation as two-dimensional plots where each axis corresponds to another fluorescence channel. Every single cell is depicted as a dot within a two-dimensional *dot plot* so that the correlation of two different parameters can be characterised (e.g. Figure 29 on page 91 right plot in the top row and both plots in the bottom row). Such two-parameter plots are also called *cytograms*.

A *density plot* is another form of a cytogram and can be a more intuitive way for identification of separate subpopulations. Areas with the highest density of cells are depicted red, those with less cells yellow, less dense areas are green and within areas with a low cell density each cell is represented by a blue dot. For an example see Figure 27 on page 88.

For data analysis, it can be desirable to focus on one particular subpopulation, e.g. to quantify the apoptotic cell subpopulation within the measured sample. If more than two parameters were measured, the subpopulations from one cytogram or histogram can be plotted on new cytograms/histograms with other parameters on the axes. For this purpose, the user can draw a region around the population of interest. This drawing is called a *gate* (e.g. the red gate in Figure 27 on page 88). An unlimited number of gates can be set for each sample, and each gate is designated a name and a colour. Statistical analysis can be performed separately on populations within different gates. It is also possible to plot a population within a gate on a new plot or histogram and to set further subgates which

leads to a nested gate hierarchy. To find out where a gated subpopulation is located on a plot of the whole population or another subpopulation regarding its parameters, it can be depicted on a dot plot in a distinct colour (e.g. the violet subpopulation in Figure 35 on page 96 in the right column against the background of the whole population depicted in black).

In addition to the detection of fluorescence intensities, a measurement with a flow cytometry also gives information about the light scattering properties of the cells. The *forward scatter (FSC)* is a measure for how much light is scattered in the forward direction while the *side scatter (SSC)* detects the scattering of light to the right angle of the laser beam (e.g. left column in Figure 33 on page 95). Generally speaking, forward scatter is regarded as a mean to estimate the size of a cell relative to the other cells within the sample, while side scatter correlates with the granularity and shape of the cell.

In a usual flow cytometry experiment, at least 10,000 events are recorded. A large limitation of conventional flow cytometry is the limited number of fluorophores that can be detected per cell. This is due to the overlap of emission spectra of the fluorophores. Although the amount of the overlap can be measured with single-stained control samples and then automatically substracted from the measured values by the machine, the emission spectra of simultaneously measured dyes should still be reasonably separated. Another disadvantage of flow cytometry is the inability to simultaneously visualise cell morphology and the fluorescence distribution within the cell. Despite these limitations, flow cytometry is a very powerful and versatile tool for elucidation of cellular pathways.

2.6 DNA quantification

To assess the effect of DAB-Am16 on the cell cycle, quantitative staining of DNA was performed with propidium iodide.

2.6.1 Propidium iodide staining

Propidium iodide (PI) is a DNA intercalating dye that has been extensively used for cell cycle profiling since the late sixties of the previous century (Crissman, Orlicky et al. 1979; Crissman and Steinkamp 1973; Dengler et al. 1995; Fried et al. 1976; Hudson et al. 1969; Krishan 1975; Mazzini et al. 1983; Waring 1970). It has an excitation range of approximately 450–600 nm and a broad emission spectrum of about 550 to more than 700 nm (*Product Spectra - Propidium iodide/DNA*). In this project, the excitation wavelength 488 nm and an emission filter of 655–730 nm (655 (LP) + 730 (LP DM)) was used. Cells were harvested by trypsinization keeping the original medium, as apoptotic cells become especially buoyant and might be discarded with the medium. Subsequently, cells were washed with phosphate buffered saline (PBS), the pellet was loosened by gently tapping the vial, ice-cold 70 % ethanol was added while vortexing to prevent cell clumping and cells were incubated with the ethanol for at least 30 min at 4 °C. Cells were then washed with PBS and RNA was digested by 15 min incubation with 50 µl RNase A (100 µg/ml) at room temperature. PI (50 µg/ml, 250 µl) was added to the sample for an incubation time of 30 min at room temperature prior to measurement with the MACSQuant flow cytometer. Fluorescence was recorded on a linear scale and the cell cycle profile was displayed as a fluorescence histogram.

2.6.2 BrdU staining

5-bromo-2'-deoxyuridine (BrdU) is a thymidine analogue that can be incorporated into DNA during its synthesis. After incorporation, BrdU can be detected with an antibody by flow cytometry (Dean et al. 1984; Dolbeare et al. 1983; Gratzner 1982; Gratzner and Leif 1981; Gratzner, Leif et al. 1975). In this experiment, 10 µM BrdU in PBS was added to the cell culture 30 min before harvesting and washing the cells. After 30 min fixation with 70 % ethanol at 4 °C, cells were washed twice with PBS and resuspended in 500 µl hydrochloric acid for 30 min at room temperature. Acid was then

spinned off and the cells washed twice with PBS and once with PBS-T (PBS + 0.1 % BSA + 0.2 % Tween 20). 20 µl mouse monoclonal anti-BrdU antibody (BD Biosciences, 347580) were added directly to the cell pellet for 20 min at room temperature. Cells were washed once with PBS-T and incubated with 5 µl polyclonal FITC-conjugated goat anti-mouse antibody (BD Biosciences, 554001) for 20 min at room tempreature in the dark. Cells were washed once with PBS and stained with propidium iodide as described in section 2.6.1. For logarithmic FITC detection, FL2 was used at MACSQuant [excitation 488 nm, emission filter 525/50 (500–550 nm)]. Simultaneous detection of propidium iodide was performed as described in section 2.6.1. Compensation between channels FL2 and FL4 was performed manually.

2.7 Detection of apoptosis and cell proliferation

2.7.1 Mitochondrial potential, cell membrane permeabilisation and caspase activation

A multifaceted approach was chosen to investigate the mode of cell death caused by DAB-Am16. Characteristics of cells measured are (Donald Wlodkowic et al. 2011; D. Wlodkowic et al. 2010):

- Light scattering properties
  - Due to cell shrinkage and increased cell granularity apoptotic cells show a decrease in forward scatter and increase in side scatter.
- Mitochondrial membrane potential
  - The mitochondrial membrane potential drops as the mitochondrial permeability transition pore opens.
- Cell membrane integrity

  - Perforation of the cell membrane is the last step of apoptosis ("secondary necrosis") that is followed by complete cell disintegration and death.

- Caspase activation
  - Caspase-3 is a key molecule that is activated during apoptosis and leads to the characteristic apoptotic events within the cell.

- DNA fragmentation
  - Caspase-3 activates an endonuclease that cleaves the nuclear DNA, thus rendering DNA fragments to leave the cell and letting the cell with a decreased DNA amount that can be seen upon DNA staining.

The simultaneous measurement of several parameters for each single cell allows not only to determine the onset of apoptosis, but also the time course of events. Results showed that signs of apoptosis could be determined as early as 2 h after addition of DAB-Am16 to the cell culture medium, indicating a fast onset of cytotoxic effects of the dendrimer.

Cell death is associated with a drop in mitochondrial membrane potential ($\Delta\Psi_\mathrm{m}$) leading to the failure of adenosine triphosphate (ATP) production (Ly et al. 2003). During apoptosis, $\Delta\Psi_\mathrm{m}$ collapses and pro-apoptotic factors are released from mitochondria. There is a disagreement if these factors activate caspase-3, or if in turn caspase-3 activation leads to $\Delta\Psi_\mathrm{m}$ and pro-apoptotic factor release. Bossy-Wetzel et al. (1998) showed that cytochrome c release from mitochondria can occur without a drop of $\Delta\Psi_\mathrm{m}$, while this drop can take place after caspase-3 activation. Karpinich, Tafani, Rothman et al. (2002) showed that collapse of $\Delta\Psi_\mathrm{m}$ occurs late in the apoptotic cascade upon etoposide treatment of Jurkat cells. In Jurkat cells lacking p53 and Bax, Karpinich, Tafani, Schneider et al. (2006) found that at early time points, cytochrome c release from mitochondria is necessary for caspase-3 activation. However, at later time points in turn caspase-3

stimulates mitochondrial cytochrome c release. The pan-caspase inhibitor ZVAD decreases cytochrome c release as well as overall loss of cell viability at incubation times of more than 6 h. Thus, there is no generally applicable order of apoptotic events and $\Delta\Psi_m$ drop can appear both before and after caspase-3 activation. Ahsen et al. (2000) showed that mitochondrial cytochrome c release does not necessarily cause depolarisation of the inner mitochondrial membrane. Similarly, Arnoult et al. (2002) observed that cytochrome c release triggered by the pro-apoptotic Bcl2 family member Bax does not lead to the release of the apoptosis-inducing factor AIF. In some leukemic cell lines, partial reduction of $\Delta\Psi_m$ occurs before caspase-3 activation, but active caspase-3 initiates a feedback loop, triggering complete $\Delta\Psi_m$ collapse and cell death (Marzo et al. 2001). Lakhani et al. (2006) found that caspases 3 and 7 act upstream of the change of $\Delta\Psi_m$ in fibroblasts. These findings indicate the time series of caspase activation and mitochondrial membrane potential collapse is not unequivocal and might differ between cell lines as well as be dependent on the treatment applied.

To assess the mitochondrial membrane potential, the cationic, lipophilic, cell-permeant dye Tetramethylrhodamine ethyl ester (TMRE) (Invitrogen, Paisley) is used. It accumulates and fluoresces in mitochondria depending on the mitochondrial membrane potential $\Delta\Psi_m$, so TMRE-positive cells are those with an intact mitochondrial membrane potential, while cells with a collapsed $\Delta\Psi_m$ appear TMRE-negative (Scaduto et al. 1999).

For determination of cell membrane integrity, the capability of the non-cell permeant DNA dye DAPI (Sigma Aldrich, St. Louis) to enter the cell after DAB-Am16 treatment is measured. Those cells that have an intact cell membrane do not exhibit DAPI fluorescence, as DAPI cannot cross an unperforated cell membrane. On the other hand, cells with holes in the plasma membrane are readily entered by DAPI (Donnenberg et al. 2007). Within the cell, DAPI binds to DNA and exhibits blue fluorescence.

Caspase-3 activation was tested with the cell-permeant caspase-3 substrate PhiPhiLux G1D2 (OncoImmunin Inc., Gaithersburg). This fluorogenic substrate contains the amino acid sequence DEVDGI that is recognised

by active caspase-3. Upon clevage by the active caspase-3, the substrate emits green fluorescence which can be detected by flow cytometry (Telford et al. 2004).

After DAB-Am16-treatment cells were incubated with 100 nM (TMRE) for 30 min, harvested and centrifuged. Medium was removed completely and 40 µl PhiPhiLux G1D2 were added to the pellet. The pellet was carefully dissolved in this PhiPhiLux solution and cells were incubated for 1 h at 37 °C. Cells were then washed once with PBS and dissolved in 200 µl PBS with 5 µl DAPI (200 µg/ml) per sample. DAPI fluorescence was detected in FL1, PhiPhiLux G1D2 in FL2 and TMRE in FL3, all of them on logarithmic scale. Compensation was carried out with single-stained cells.

2.7.2 EdU and histone H3 detection

5-ethynyl-2'-deoxyuridine (EdU) is a thymidine analogue that is used for the same purpose as BrdU. The advantage of EdU compared to BrdU is its easy detection by click chemistry that leads to the copper-catalysed formation of a covalent bond between the alkyne EdU and the azide Alexa Fluor 647 that makes the acidic denaturation of the cellular DNA obsolete (Buck et al. 2008). This in turn allows to combine EdU-staining with the staining with different antibodies.

Cells were incubated with 10 µM EdU (Invitrogen, Paisley) for 30 min, harvested and washed once with PBS. 100 µl 4 % paraformaldehyde were added to the pellet and cells were fixed for 15 min at room temperature in the dark. Cells were then washed once with washing buffer (1 % BSA in PBS) and incubated with 0.1 % Triton-X 100 in PBS for 10 min at room temperature. Cells were then washed once with washing buffer and the supernatant was completely removed after centrifugation. The click reaction cocktail with Alexa Fluor 647 was freshly prepared according to the manufacturer's instruction. The pellet was dissolved in the click reaction mixture and incubated for 30 min at room temperature in the dark. Cells were washed twice with PBS-T (3 % BSA, 0.05 % Triton-X 100 in

PBS) and the supernatant was completely removed after the second wash. 1 µl phospho-Histone H3 (Ser10) (6G3) mouse monoclonal antibody (Cell Signaling, 9706) was added to the pellet for 1.5 h (room temperature in the dark). Cells were then washed again with PBS-T which was completely removed after centrifugation. 5 µl FITC polyclonal anti-mouse Ig antibody (BD Biosciences, 554001) were added for 20 min at room temperature in the dark. The cells were washed once with PBS, and DNA staining with PI was performed as described in section 2.6.1. FITC was measured in FL2 (logarithmic scale), PI in FL4 (linear scale) and Alexa Fluor 647 in FL6 (logarithmic scale). Compensation was performed with single-stained samples.

2.7.3 Detection of phosphorylated histone H2A.X

Histone 2A.X (H2A.X) is phosphorylated at serine 139 upon occurrence of stalled replication forks or DNA double-strand breaks (Ewald et al. 2007; Lowndes et al. 2005; Paull et al. 2000; Rogakou et al. 1998). The phosphorylated H2A.X is also called γ-H2A.X.

Cells were harvested and washed once with PBS. 100 µl 4 % paraformaldehyde were added to the pellet and cells were fixed for 15 min at room temperature in the dark. Paraformaldehyde was spun off and cells were permeabilised with 0.1 % Triton-X 100 for 10 min at room temperature. Cells were then washed twice with blocking buffer (3 % BSA, 0.05 % Triton-X 100 in PBS), spun off and the supernatant removed completely. 1 µl phospho-Histone H2A.X (Ser139) (20E3) rabbit monoclonal antibody Alexa Fluor 488 conjugate (Cell Signaling, 9719) was added to the pellet for 1 h (room temperature in the dark). The cells were washed once with PBS, and DNA staining with PI was performed as described in section 2.6.1. Alexa Fluor 488 was measured in FL2 (logarithmic scale) and PI in FL4 (linear scale). Compensation was performed with single-stained samples.

2.8 *In vivo* evaluation

Female mice (CD1-nu; initial mean weight 20 g) housed in groups of five at 19 °C to 23 °C with a 12-hour light-dark cycle were fed a conventional diet (Rat and Mouse Standard Expanded, B&K Universal, Grimston, United Kingdom) with mains water ad libitum. Experimental work was carried out in accordance with U.K. Home Office regulations and approved by the local ethics committee.

Tumour cell suspension [MiaPaCa-2 human pancreatic carcinoma (ATCC CRL-1420)] in exponential growth was injected s.c. (5×10^6 cells in 100 µl overall volume consisting of 50 µl DMEM cell culture medium (Invitrogen) supplemented with 10 % Foetal Bovine Serum (Biosera, Miami, USA) and 5 mM L-Glutamine (Invitrogen), and 50 µl Matrigel (BD Biosciences)) per flank. Tumours typically reached diameters of 5 mm or more within 13 days. Average animal weight was 24.4 ± 1.4 g across all groups and the whole experimental period. DAB-Am16 in 5 % dextrose was administered to 6 mice intraveneously via the tail vein on days 1, 3, 5, 8, 10, 12, 15 and 17 at 10 mg/kg. A negative control group of 6 mice did not receive any injections. A positive control group of 5 mice was injected with gemcitabine (Sigma-Aldrich, Dublin, Ireland) in physiological saline (1.7 mg per mouse) on days 1, 4, 7, 11, 14 and 16. Tumour size and weight were recorded by the same person on every day of DAB-Am16 injection. One day after the last injection the animals were sacrificed, the tumours removed and cut in several pieces. One piece was stored on ice in PBS-EDTA (PBS with 0.1 % (w/v) EDTA), another two pieces were fixed in 10 % formalin for 48 h at 4 °C and then transferred into 70 % ethanol for long-term storage at room temperature, and one piece was immediately frozen in liquid nitrogen and stored at –80 °C. The piece in PBS-EDTA was dissociated as described by Heinlein et al. (2010). The tumour tissue was cut in small pieces and consecutively filtered through a 100 µm cell strainer being in contact with PBS-EDTA in a petri dish and a 35 µm filter (BD Biosciences and Miltenyi Biotec, respectively). The filters were washed with PBS-EDTA

and the resulting solution was filled up to 10 ml. The cells were centrifuged, the supernatant removed, the pellet resuspended in 0.5 ml PBS-EDTA and fixation was carried out by slowly adding 5 ml ice-cold 70 % ethanol while gently vortexing. Cells were then stored at 4 °C for a week. The DNA staining with propidium iodide and the flow cytometric cell cycle measurement were performed as described in section 2.6.1.

2.9 Statistical analysis

Statistical analysis was performed with Microcal OriginPro 8. For *in vitro* experiments, the standard deviation was used for plotting error bars, while standard error of the mean was plotted for *in vivo* data. Significance testing was performed with One-Way ANOVA using Bonferroni Test for means comparisons. The significance level tested was 0.05 in all cases. Non-linear curve fitting for the MTT assay was conducted using a logistic dose-response model according to the following equation:

$$y = \frac{A_1 - A_2}{1 + (x/x_0)^p} + A_2$$

EC50 values were then calculated based on this curve fit.

3 Results

3.1 Analytical characterisation of DAB-Am16

For meaningful experimental results it is crucial to ensure that the dendrimer used is of highest quality and purity. Another important aspect is the stability of the dendrimer over time as well as after exposure to different environmental conditions. To address these issues, a number of analytical tests have been performed on all three batches described in section 2.1. The results were compared with data obtained by Chooi (2007) in our group as well as with published data (Adhiya et al. 2002; Chai et al. 2001; McLuckey et al. 2000).

Analytical characterisation of DAB-Am16 was performed by nuclear magnetic resonance (NMR), mass spectrometry (MS) and elemental analysis.

3.1.1 NMR spectroscopy for structure determination and purity analysis of DAB-Am16

^{1}H, ^{13}C and COSY NMR were performed for structure identification and for comparison of three different dendrimer vials that were purchased and opened at different time points. The latter comparison allows to make a statement on the stability of the dendrimer during long-term storage.

The ^{1}H NMR spectra obtained from all three samples are shown in Fig. 13 on page 67. The carbon atoms of the dendrimer have been assigned consecutive numbers, as illustrated in Fig. 12 on page 69. As the molecule is symmetric only the enumeration for one branch starting from the core and ending at one of the 16 outer carbon atoms is shown for a better overview. Therefore, carbon atoms exist with the same environment, i.e. two atoms have been assigned number 1, two carbon atoms have the environment corresponding to number 2, four carbon atoms should be included in the peak for number 3 and so on. As every carbon atom bears two hydrogen atoms, the area under the peak for hydrogen atoms at carbon number 1 corresponds to four hydrogen atoms and the same principle applies for all

Table 2: Expected and the mean measured ratios of peak areas in the ^{1}H NMR spectra.

			Experimental values		
Chemical shift [ppm]	Carbon atom numbers	Expected number of H atoms	Vial 1	Vial 2	Vial 3
1.483	1	4			
1.7	4, 7, 10	88	91	92	90
2.5	2, 3, 5, 6, 8, 9	88	91	92	90
2.677	11	32	33	33	31

the other peaks. The peak for the hydrogen atoms for the carbon atoms 4, 7 and 10 overlaps with the hydrogen atoms of the terminal amine groups that have to be taken into account as well. Using the peak for hydrogen atoms at carbon 1 as a reference point, the number of hydrogen atoms that build up the other peaks has been calculated and compared with the expected values. All these values are shown in table 2 for all three vials. It is evident that all peaks obtained could be assigned according to the dendrimer structure and that the difference between empiric and theoretical data is very small for all peaks which suggests a high purity of the dendrimer used for the manufacturing. Additionally, the NMR spectroscopy results correspond very well to the data of Dr Chooi (Fig. 13 on page 68) as well as to the spectra reported in the literature (Chai et al. 2001).

To further confirm the purity and identity of the dendrimer, ^{13}C and ^{1}H COSY spectra were also recorded. Again, all three vials yielded very similar results, so only one representative spectrum for each NMR type is shown in Fig. 14 on page 70. The ^{13}C spectrum corresponds very well to the literature data (Chai et al. 2001). Also, the quantification of the experimental data shows a good correlation with exception of C atom 4. The value for this atom is almost three times higher than the expected one. A closer look at the peak shape reveals that two peaks seem to have merged at this point. The identity of the second peak is not clear. However, it is

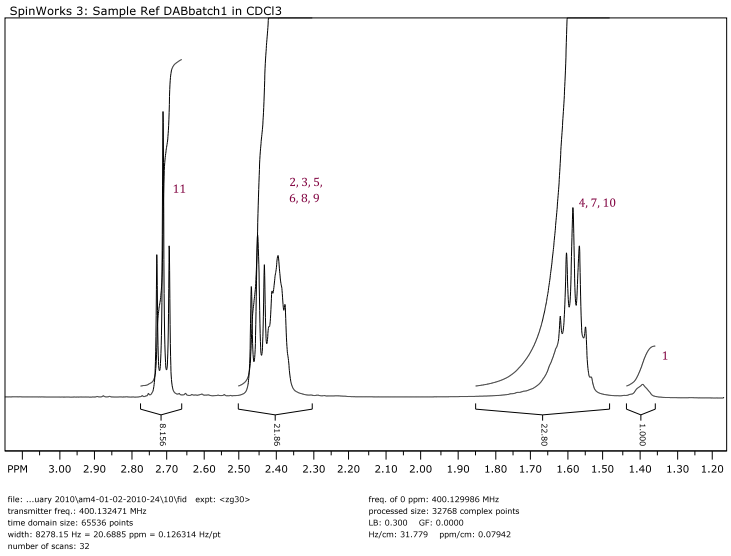

(a) Vial 1

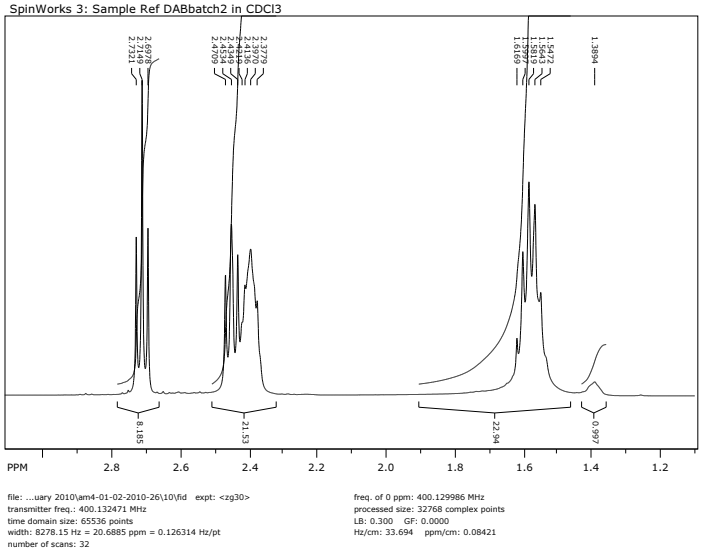

(b) Vial 2

Fig. 13: ^{1}H NMR of the three DAB-Am16 vials stored for different time ranges (continued on the following page)

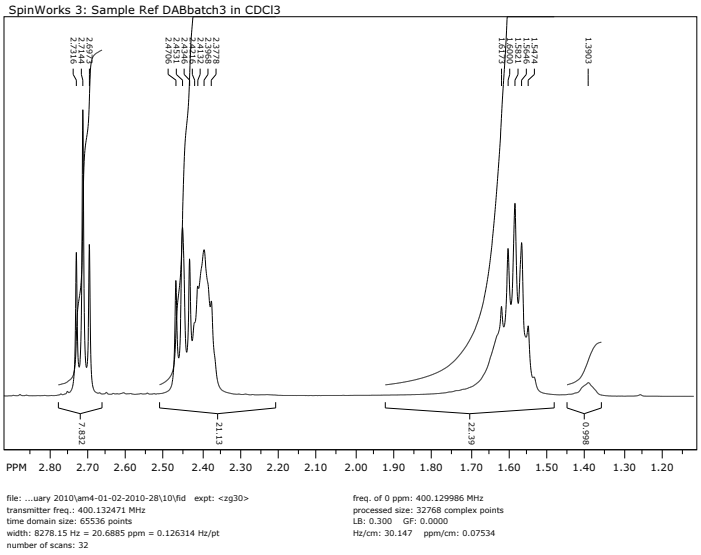

(c) Vial 3

Fig. 12: ^{1}H NMR of the three DAB-Am16 vials.

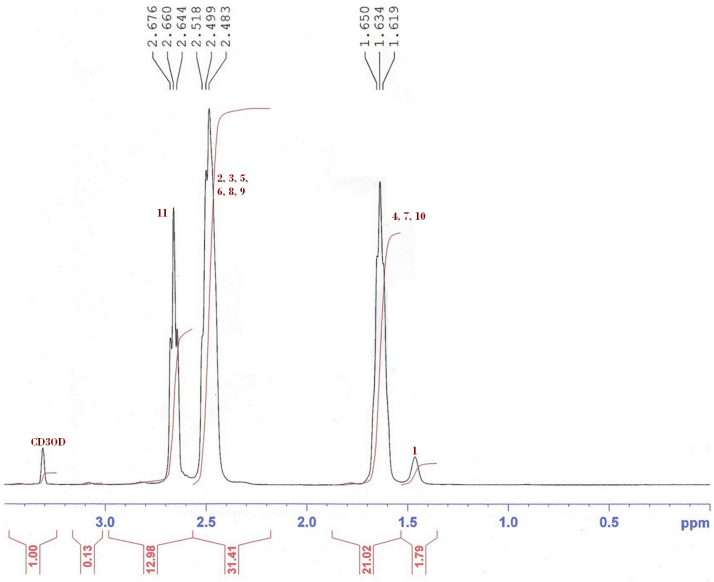

Fig. 13: NMR data from previous experiments, provided by Dr Kar Wai Chooi.

Table 3: Expected and the mean measured ratios of peak areas in the ^{13}C NMR spectrum.

Chemical shift [ppm]	Carbon atom numbers	Expected number of C atoms	Experimental values (vial 2)
25.090	1	2	2
24.561	4	4	11
30.940	10	16	15
40.740	11	16	16
51.935	9	16	15
52.300	6, 5, 8	20	19
52.563	3	4	4
54.373	2	2	3

conceivable that a small fraction of dendrimers in the sample might have minor defects and an additional peak arises from this altered structure.

The 2D COSY spectrum shows cross-peaks between the peaks corresponding to atoms (11) and (4, 7, 10), (9) and (4, 7, 10), (2, 3, 5, 6, 8) and (4, 7, 10). There is no coupling between (2, 3, 5, 6, 8) and (11), (9) and (11), (2, 3, 5, 6, 8) and (9). Considering the structure of the molecule (Fig. 12), the results completely match the expectations.

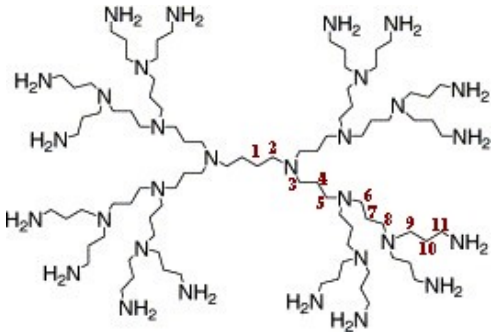

Fig. 12: The numbering scheme of C atoms for the peak assignment of the NMR spectra.

3.1.2 Mass spectrometry and tandem mass spectrometry analysis of DAB-Am16 with electrospray ionisation

Again, the spectra of the dendrimers from all three samples show an identical composition of the vial content. Only the spectrum for vial 2 is shown in Fig. 15a on page 72. The peak at m/z ratio 1686.6 corresponds to the molecular ion (precursor ion). The peak at m/z 1629.6 indicates the loss of

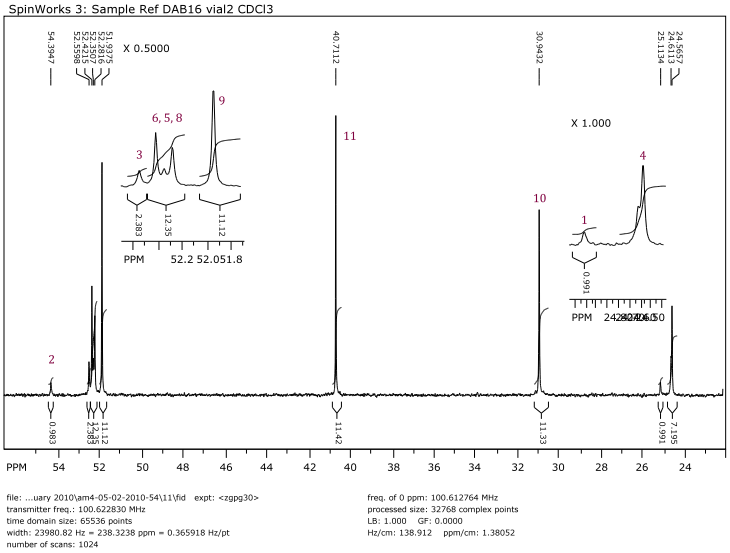

(a) ^{13}C NMR

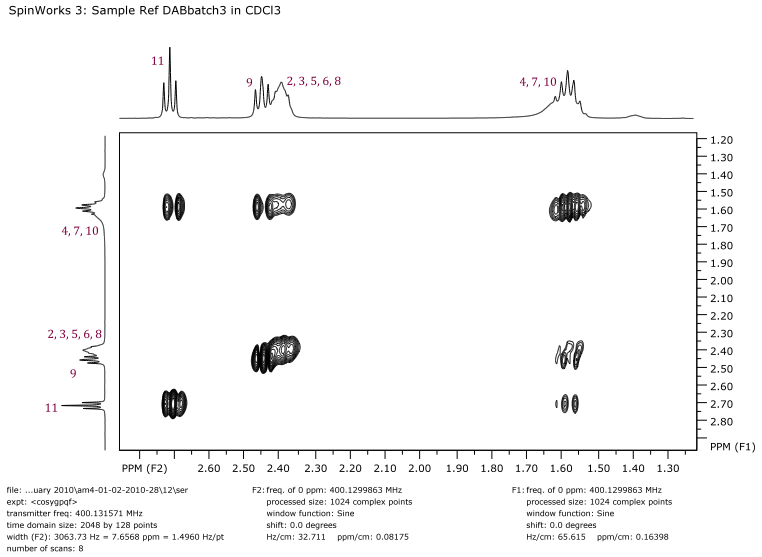

(b) COSY NMR

Fig. 14: Representative ^{13}C and COSY spectra.

a $(CH_2)_3NH_2$ group (a 3rd generation branch) at the outer shell. A loss of a second group of the same size explains the peak at *m/z* 1573.6. When a second generation branch is lost consisting of $(CH_2)_3N[(CH_2)_3NH_2]_2$, a peak at *m/z* 1515.4 can be seen. Finally, the loss of a whole branch emerging from a nitrogen atom of the core leads to a mass difference of approx. 400, which results in the peak at *m/z* 1287.4. The existence of a double-charged molecular ion leads to the peak at *m/z* 844.3, the triple-charged molecular ion corresponds to the peak at *m/z* 563.5 and the four times charged molecular ion is seen at *m/z* 422.9. Some other peaks with very low intensities are also present in the spectrogram that can be explained by further fragmentation and ionisation events. The peak at *m/z* 1748.5 might correspond to an adduct of DAB-Am16 with acetonitrile and sodium although there is a mass difference of 2 to the expected *m/z* value which might be due to proton loss.

Fig. 15b on the following page shows an MS/MS spectrum of the molecular ion of DAB-Am16. The three main peaks correspond to the results of intramolecular nucleophilic substitution reactions: from an attack of an amine group onto the adjacent α-C-atom a quaternary ammonium ion and a neutral amine arise (Adhiya et al. 2002; McLuckey et al. 2000). Dependent on the generation layer of the protonated nitrogen different sizes of fragments appear. The arising quaternary ammonium ions have *m/z* ratios of 1555.5, 1327.3 and 870.8 for generation 2, 1 and 0, respectively. This matches exactly the observed MS/MS spectrum and further confirms the identity of the sample.

3.1.3 Matrix-assisted laser desorption/ionisation-time of flight spectrometry for purity analysis

The previously mentioned loss of dendrimer branches in the MS spectra might occur due to in-source fragmentation of the molecule during the ionisation procedure as well as being present in the original sample. To scrutinise this issue further, matrix-assisted laser desorption/ionisation

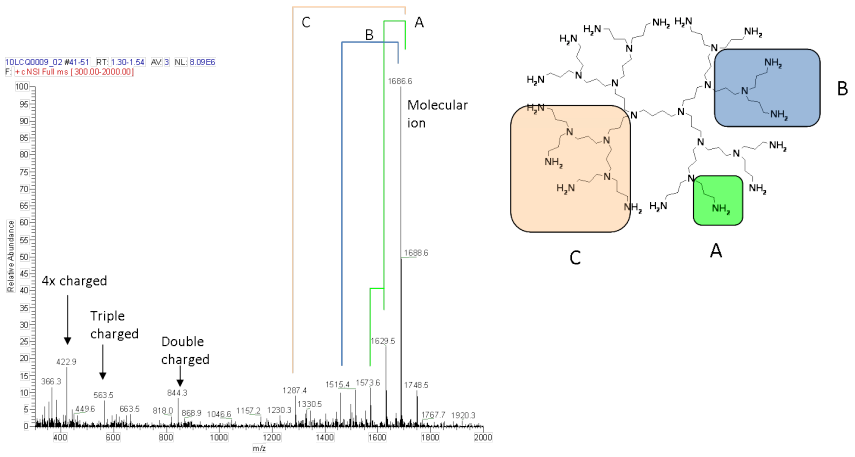

(a) Mass spectrometry measurements of a sample of DAB-Am16 from vial 2 with electrospray ionisation (ESI). The peaks are assigned according to the colour scheme provided on the right of the spectrum.

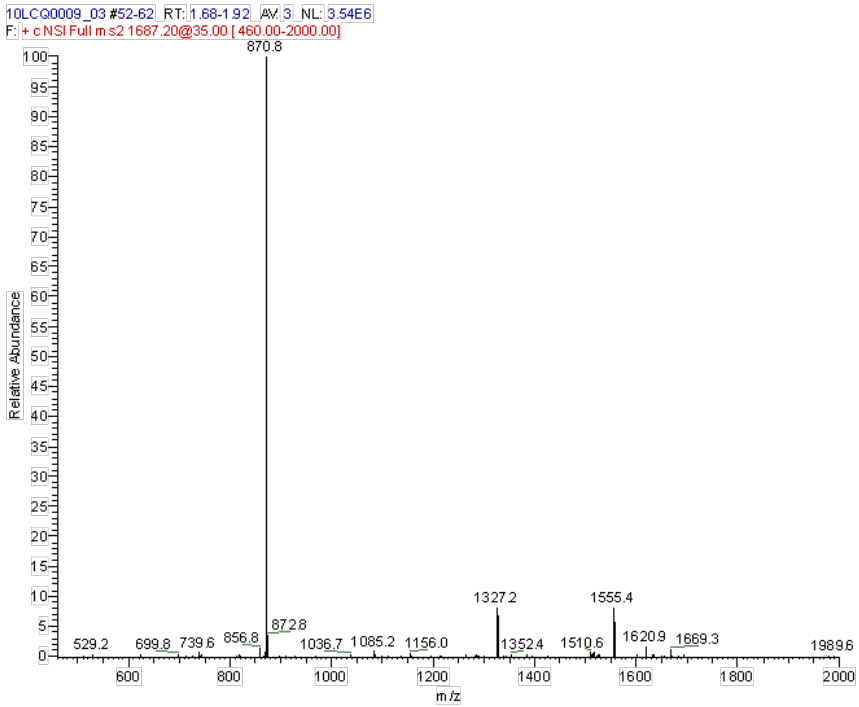

(b) MS/MS spectrum of the molecular ion of the DAB-Am16 dendrimer.

Fig. 15: Mass spectra of DAB-Am16.

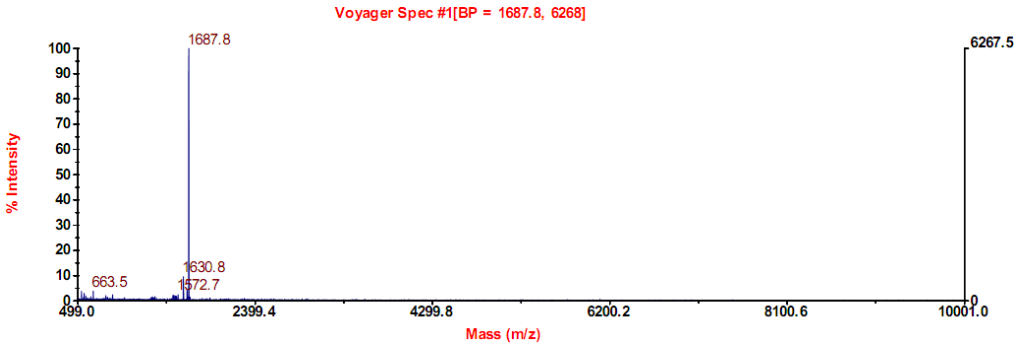

Fig. 16: MALDI-TOF analysis of the dendrimer from vial 2.

(MALDI)-time of flight (TOF) spectrometry was used as another technique of mass spectrometry analysis as this method provides a softer ionisation procedure and thus is preferred for molecules that can fragment easily with other techniques, particularly large molecules such as polymers and particularly dendrimers. Additionally, this technique allows detection of possible high molecular contaminants.

As can be seen in Fig. 16, no high molecular weight contaminants are observed. The prominent peak at m/z 1687.8 corresponds to the molecular ion of DAB-Am16, while the two small peaks at m/z 1630.8 and 1572.7 again can be assigned to the loss of one or two $(CH_2)_3NH_2$ branches. This can be attributed to the existence of a small percentage of minor defects that occur during the sequential procedure of dendrimer synthesis. The peak at m/z 663.5 was also seen after electrospray ionisation and cannot be explained at the moment. It could be either another fragment of the dendrimer or a contaminant. However, its intensity is very low, indicating the high purity of the sample. Similar results were obtained for samples from all three vials.

3.1.4 Elemental analysis of DAB-Am16 dendrimer

The results are shown in Table 4 on the following page. The minor deviance between the observed and the expected values especially for the relative amount of carbon in the sample can be explained by the minor defects that

Table 4: Elemental analysis of DAB-Am16 dendrimer samples from all three vials.

Element:	C			H			N		
Vial:	1	2	3	1	2	3	1	2	3
	59.80	60.84	60.39	11.30	12.33	12.63	22.58	23.94	24.01
	59.73	60.85	60.41	11.36	12.48	12.48	22.75	23.89	23.92
	60.72	60.74	60.52	12.69	12.48	12.63	24.48	23.81	24.93
	60.89	60.78	60.49	12.51	12.51	12.48	24.58	23.91	24.91
Mean:	60.29	60.8	60.45	11.97	12.45	12.56	23.6	23.89	24.44
Overall mean:	60.51			12.32			23.89		
Standard deviation:	0.26			0.31			0.43		
Expected:	62.66			12.43			24.91		

were also seen in the mass spectrum (loss of one or two branches of the 3rd generation layer).

3.2 Stability studies of DAB-Am16 with MALDI-TOF

Fig. 17 on the next page shows two representative spectra: at room temperature after 1 day and at 37 °C after 6 days. In both spectra, a high peak for the molecular ion at m/z 1686.7 is observed. The small peaks at m/z 1629.7 and m/z 1514.7 can be attributed to minor defects discussed in section 3.1.2. The peak at m/z 870.5 has been seen previously in the MS/MS spectrum as a quaternary ammonium ion emerging from a nucleophilic substitution reaction. A small peak for a contaminant or another dendrimer fragment is again seen at m/z 663.5–643.9.

Overall, it is evident from this data that no decomposition of DAB-Am16 dissolved in water occurred even after exposure to 37 °C for 6 days.

3.3 Characterisation of the growth properties of the cell lines

For the cell lines that have been used for *in vitro* experiments, growth curves were recorded in order to estimate the duration of exponential

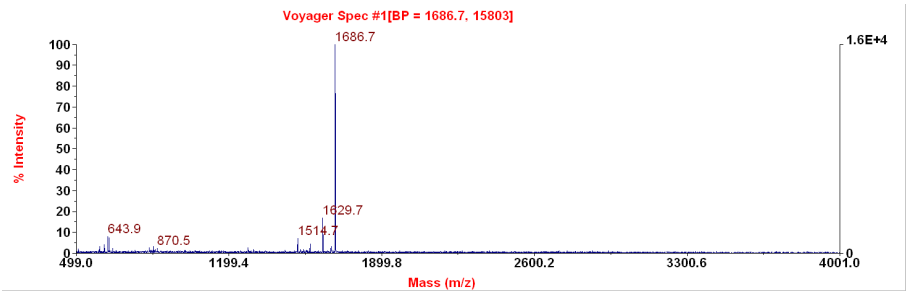

(a)

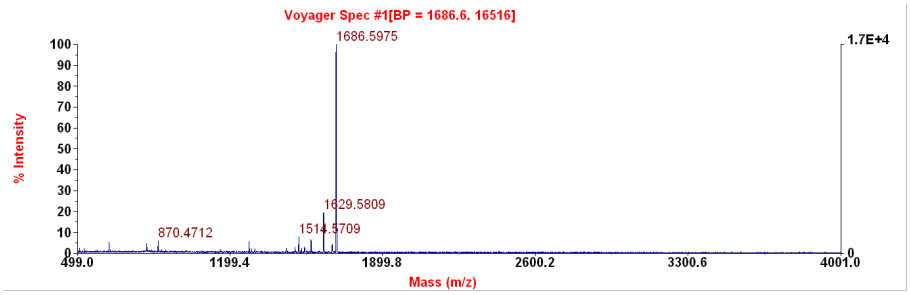

(b)

Fig. 17: MALDI-TOF spectra of DAB-Am16 dissolved in water and stored at (a) room temperature for one day and (b) 37 °C for 6 days.

growth and the doubling time of the cells. The results are shown in Fig. 18 on the following page. It can be seen from the growth curves that cells in general need approx. 3 days to adapt after having been seeded (lag-phase) before they start growing exponentially (log-phase). As a consequence, for experiments with DAB-Am16, cells were seeded 3 days prior to addition of the dendrimer to ensure that they were in the log-phase when the dendrimer started to take effect on them. This is important because a lot of anti-cancer agents act specifically against fast growing cells that are usually found in tumours. Assuming that DAB-Am16 might also act on cell growth and division, the investigation of the precise effects of DAB-Am16 was performed during the phase of fastest cell growth. The doubling time for the cell lines was calculated according to the following formula:

$$T(d) = (t_3 - t_1) \times \frac{log(2)}{log(Q_3/Q_1)}$$

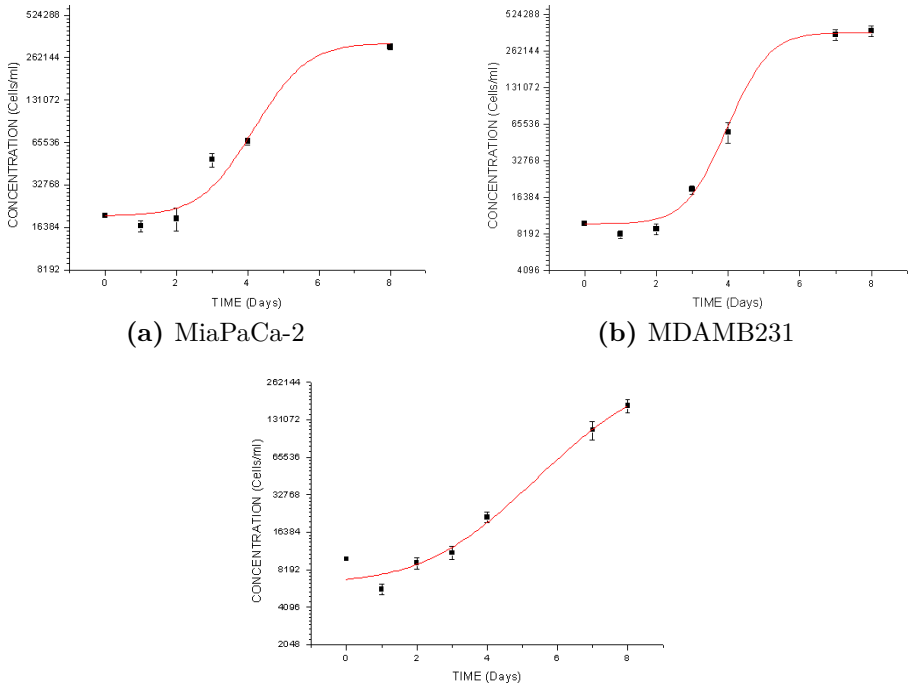

(a) MiaPaCa-2 **(b)** MDAMB231

(c) U87MG

Fig. 18: Growth curves for MiaPaCa-2, MDAMB231 and U87MG cell lines. The doubling times are 18 h, 17 h and 30 h, respectively.

3.4 DAB-Am16 exhibits a concentration- and time-dependent cytotoxic effect

Once the identity and purity of the dendrimer was established, the anti-proliferative effect of DAB-Am16 was scrutinised. The MTT and LDH assays were used for the evaluation of the cytotoxicity, while the colony-formation assay (CFA) was applied to examine the cytostatic effect.

3.4.1 Change of the glycolysis rate upon DAB-Am16 treatment

The results of the MTT assay for several cell lines is depicted in Fig. 19 on the next page and listed in Table 5 on the following page. The half maximal effective concentration (EC50) values differ between the cell lines and also clearly depend on the incubation time with the dendrimer. For 4 h, EC50 is

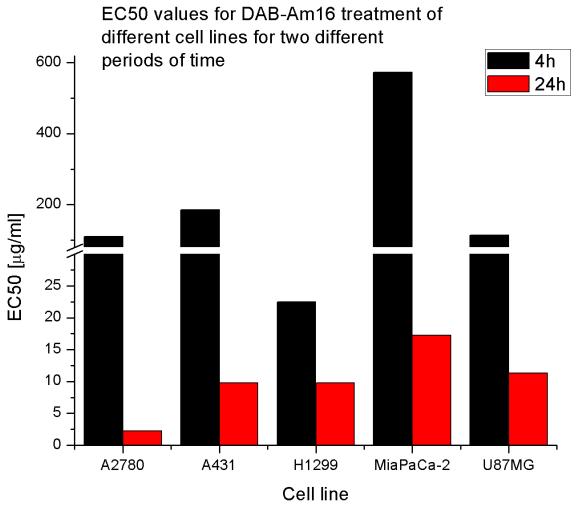

Fig. 19: EC50 values for several cancer cell lines according to the MTT assay.

Table 5: EC50 values of DAB-Am16 after 4 and 24 h lasting incubation of 5 different cell lines with the dendrimer.

	4 HOURS	24 HOURS
A2780	109.9 µg ml^{-1} (65.1 nM)	2.3 µg ml^{-1} (1.3 nM)
A431	184.8 µg ml^{-1} (109.6 nM)	9.8 µg ml^{-1} (5.8 nM)
H1299	22.5 µg ml^{-1} (13.3 nM)	9.7 µg ml^{-1} (5.8 nM)
MiaPaCa-2	572.2 µg ml^{-1} (339.2 nM)	17.2 µg ml^{-1} (10.2 nM)
U87MG	113.8 µg ml^{-1} (67.5 nM)	12.2 µg ml^{-1} (6.7 nM)

highest for MiaPaCa-2 (572 µg/ml) and lowest for H1299 (22 µg/ml), which means that upon short-term exposure MiaPaCa-2 is the most resistant and H1299 the most susceptible cell line among those that have been examined. For 24 h, again MiaPaCa-2 cells have the highest EC50 value (17 µg/ml), but this time A2780 cells have the lowest EC50 (2 µg/ml).

These results indicate that biological differences between the cell lines not only affect the overall response to DAB-Am16 treatment, but also influence the time that is necessary to reach a pronounced effect. However,

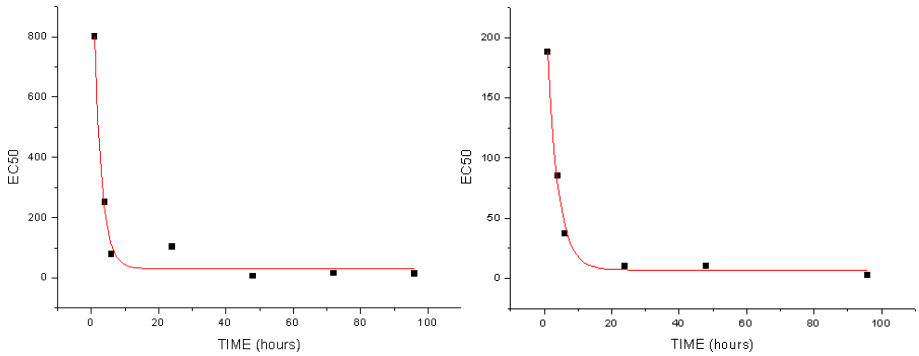

(a) MDAMB231 **(b)** MiaPaCa-2

Fig. 20: Change of EC50 values over time in MDAMB231 and MiaPaCa-2 cell lines.

all the cell lines that have been tested show a large decrease of the EC50 upon the increase of the incubation time from 4 to 24 h. Concentration-dependent cell death within the plates used for the MTT assay is confirmed by light microscopy. This observation raises the question if the decrease of EC50 with the time is linear and if it will reach 0 as cells treated at any concentration applied would be dead. This question was investigated by carrying out the MTT assay at more time points between 4 and 24 h as well as after longer time periods. The results are shown in Fig. 20. Surprisingly, after approx. 16–18 h incubation (estimated from an asymptotic curve fit), the EC50 does not further decrease, indicating that toxicity remains stable after one period of doubling time of these cell lines (17–18 h each). Before this time point, the slope of the falling EC50 curve was very steep. Thus, one can suspect that DAB-Am16 causes profound cytotoxicity during the first cell division after addition to the cell culture medium, however, it only has a cytostatic effect on the remaining cells. One possible explanation is that these cells might stop dividing and change to a metabolically dormant state that could be a protective mechanism to facilitate cell survival until the cellular environment becomes more favourable. This issue is discussed in more detail in section 4.2.1.

3.4.2 Cellular enzyme leakage upon DAB-Am16 treatment

To measure acute cytotoxicity, the LDH assay was applied to A2780 cells, the results are shown in Fig. 21 on the following page. Clearly, for 4 and 6 h time points an increase in LDH release and thus in cytotoxicity with the dendrimer concentration can be seen. The EC50 for 4 h is 250 µg/ml and thus more than twice as high as the one for the MTT assay (110 µg/ml). This is a very interesting observation since both assays measure cytotoxicity, but use different surrogate parameters. From these results, we can conclude that changes in cellular metabolism precede cell membrane damage. This is consistent with the apoptotic mode of cell death that is known to be linked with glycolysis by the pro-apoptotic molecule BAD (Bcl-2 antagonist of cell death). Danial et al. (2003) found that BAD and glucokinase (an essential constituent of the glycolysis pathway) are located together within a mitochondrial complex. Dephosphorylation of BAD upon glucose deprivation leads to apoptotic cell death. Due to this interconnection one can assume that MTT assay reveals early apoptotic changes as well as metabolic slow-down of surviving cells, while LDH assay detects the final cellular disintegration at a late stage of apoptosis.

3.4.3 Clonogenic cell survival after withdrawal of DAB-Am16

The results of the MTT assay led to the conclusion that cells that survived the time period equivalent to the doubling time of the particular cell line might enter a metabolically dormant state that they can leave upon dendrimer withdrawal. Thus, colony formation assay (CFA) was applied to test if surviving cells will recover and grow again after 24 h exposure to DAB-Am16. The number of colonies that grew out of 250 cells that had been seeded 5 days earlier is plotted in Fig. 22 on the next page for A431 and A2780 cells. Clearly, DAB-Am16 does have a long-term cytostatic effect on A2780 as the colony formation capability of surviving cells decreases significantly in a concentration-dependent manner. For A431 cells, there is no decrease compared to the untreated control for a concentration of

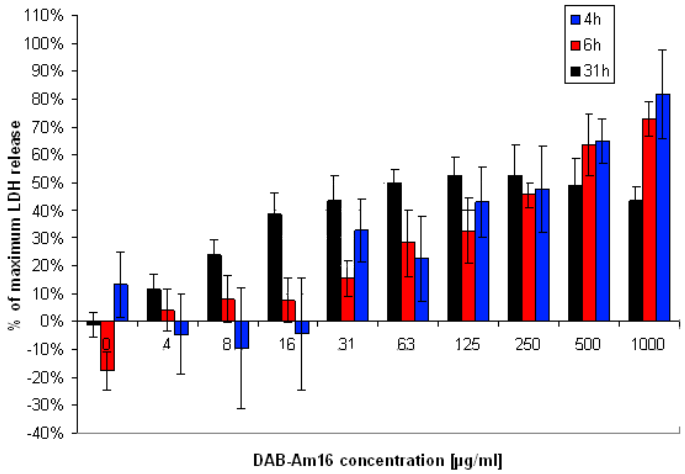

Fig. 21: Results of the LDH assay with A2780 cells. Error bars represent the standard deviation.

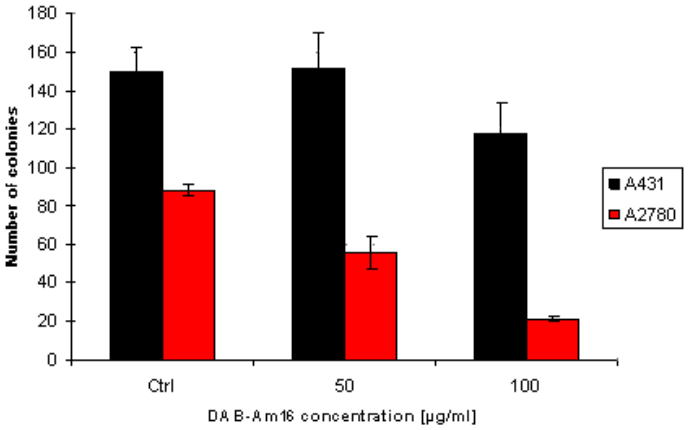

Fig. 22: Results of the colony formation assay with A2780 and A431 cells.

50 µg/ml and only a statistically insignificant decrease at 100 µg/ml. Again, these results highlight the importance of cell-specific features for the effect of DAB-Am16. All in all, one can see for both cell lines that cellular colony formation capacity is not completely abrogated after DAB-Am16 treatment, but it is decreased in a concentration- and cell line-dependent manner.

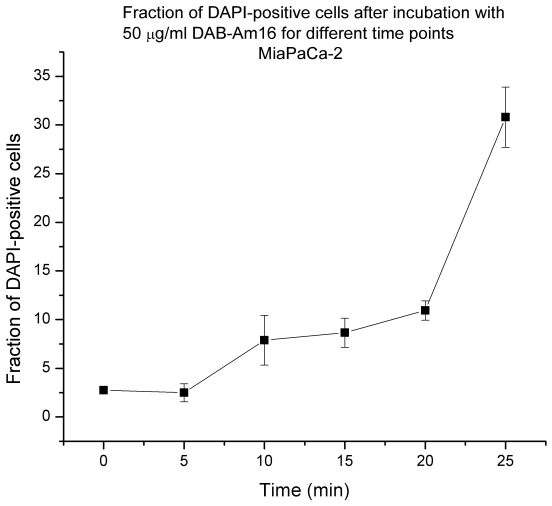

Fig. 23: DAPI entrance into DAB-Am16 treated MiaPaCa-2 cells over time.

3.4.4 Cell membrane permeabilisation occurs within 25 min after DAB-Am16 addition to MiaPaCa-2 cells

To further investigate the formation of cell membrane holes as a result of DAB-Am16 action, the ability of cell entrance of the DNA-binding fluorescent dye DAPI was determined. This dye cannot cross cell membrane at low concentrations and is used for live/dead cell distinction (Böck 2001; Doberstein et al. 1993). The fraction of cells that became DAPI-positive was measured every 5 min for a period of 25 min in order to determine the time point when DAB-Am16 action begins. Fig. 23 illustrates the change of DAPI permeability of MiaPaCa-2 cells at different time points after addition of 50 µg/ml DAB-Am16. The control cells were incubated with DAPI alone for the longest time period that was used for DAB-Am16 tests (25 min). 3 % of control cells were entered by DAPI after this time. After 10 min incubation of cells with DAPI and DAB-Am16 together, 8 % of cells were positive for DAPI, indicating that even after such a short incubation time DAB-Am16 exerts an effect on a subset of cells. Notably, a very steep

increase in DAPI permeability occurred between 20 and 25 min incubation time (from 11 % to 31 %). This seems to be the time needed for DAB-Am16 to gain entrance into the cell.

3.5 Changes in cell cycle progression caused by DAB-Am16

Dendrimers easily bind and condense nucleic acids, as well as enter the cell and deliver the nucleic acids (e.g. DNA) to the cell nucleus (Dufes et al. 2005). Consequently, as to the action of the dendrimer inside the cell, it is reasonable to assume that the dendrimer would enter the nucleus and interact with the cellular DNA. If this was the case, a disturbance of the cell cycle could be assumed. To test this assumption, cellular DNA was quantitatively stained with the intercalating fluorescent dye PI. Representative results are shown in Fig. 24 on page 84. The relative percentage of cells in all three cell cycle phases (from left to right G1/G0, S and G2/M) are shown in this figure. It is obvious that DAB-Am16 causes a massive disturbance of the cell cycle when applied to cells *in vitro*. In particular, the fraction of cells that are in the S phase increases with increasing concentration of the dendrimer. This means that DNA replication is halted or slowed down in the dendrimer treated cells. Possible reasons are stalled replication forks due to DAB-Am16 interaction with nuclear DNA, halted replication after dendrimer-induced DNA damage or as a consequence of the activation of intracellular molecular stress pathways that were triggered by the dendrimer but are not due to direct interaction of DAB-Am16 with the DNA. To test for the possibilities of stalled replication forks or DNA strand breaks, the presence of phosphorylated histone H2A.X (γ-H2A.X) within the cell was investigated. A fluorescently coupled antibody against γ-H2A.X was used for detection, and the fluorescence again was measured with a flow cytometer. Etoposide was used as positive control because this compound acts as a topoisomerase II inhibitor which eventually

leads to DNA strand breaks. Surprisingly, as can be seen in Fig. 25 on page 85, γ-H2A.X could not be detected in DAB-Am16 treated cells.

Fig. 26 on page 86 shows the change of the cell cycle profile of U87MG cells upon DAB-Am16 exposure. A clear change is detected even at a low concentration of 10 µg/ml DAB-Am16. It is obvious that DAB-Am16 causes an increase of the amount of cells in the S phase, predominantly within the beginning of the S phase, at the expense of the G1 phase.

In contrast to U87MG cells, an effect on the cell cycle profile of H1299 cells was only seen at high concentrations of the dendrimer (Fig. 26). At 100 µg/ml DAB-Am16, the change of the cell cycle profile is similar to that of U87MG cells. However, at 150 µg/ml DAB-Am16, the profile is shifted to the left, indicating a loss of DNA which is a clear sign of apoptotic processes. Thus, the effect of the dendrimer on H1299 cells is concentration-dependent - while at lower concentrations, it causes cell cycle arrest, with increasing concentration it leads to apoptosis.

To investigate the effect of DAB-Am16 on the cell cycle in more depth, bromodeoxyuridine (BrdU) was used along with DAPI, a DNA dye that similar to PI is applied for quantification of cellular DNA. When BrdU is present in the cell culture medium, cells incorporate it into their DNA during DNA replication in the S-phase. Cells that incorporated BrdU can then be detected with immunostaining, while simultaneously the overall cellular DNA can be quantified with PI or similar DNA dyes. This method can be applied for two different purposes:

1. Cells that are in the S-phase just before addition of DAB-Am16 can be marked by BrdU incorporation. For this purpose, cells are pulsed with BrdU for a short time (30 min), and DAB-Am16 is added immediately after BrdU withdrawal for the desired period of time (e.g. 24 h). After DAB-Am16-treatment, cells are immediately harvested, fixed and stained for BrdU and for DNA quantification. In this way, cells that were in the S-phase at the moment of DAB-Am16 addition

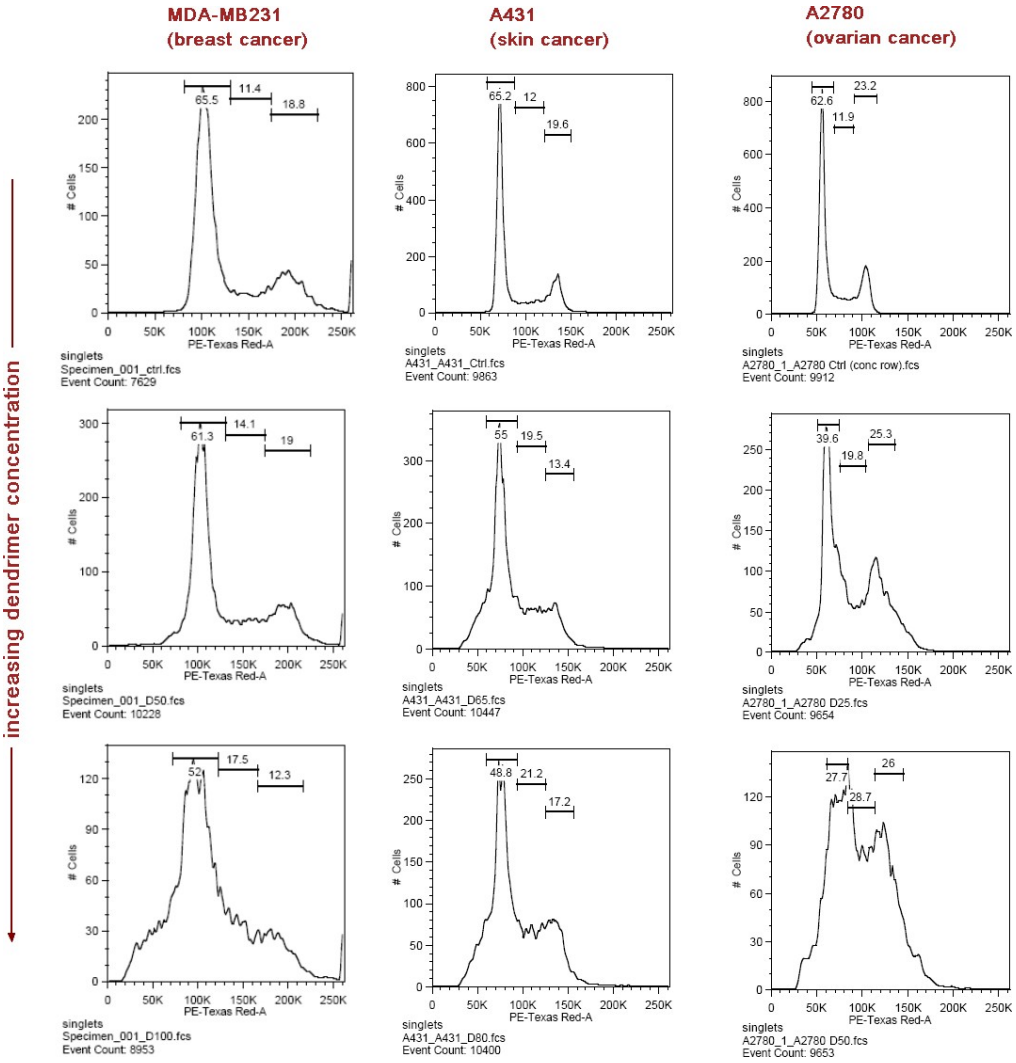

Fig. 24: Representative cell cycle profiles of three tumour cell lines. Cells were treated with different concentrations of DAB-Am16 for 24 h, harvested, stained with propidium iodide and analysed by flow cytometry. The upper row shows the untreated controls. The concentrations of DAB-Am16 used for the treatment of three cell lines, the profiles for which are depicted in the second and third rows are 50 µg/ml and 100 µg/ml (MDAMB231), 65 µg/ml and 80 µg/ml (A431) and 25 µg/ml and 50 µg/ml (A2780), respectively.

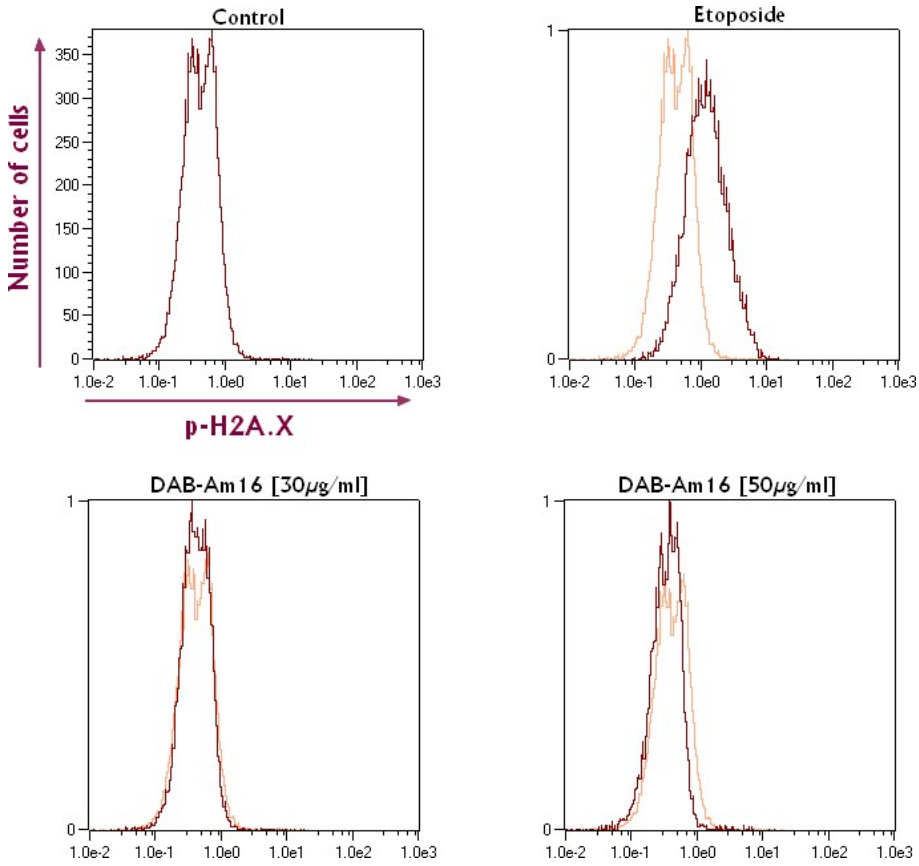

Fig. 25: Immunostaining of A2780 cells for γ-H2A.X upon DAB-Am16 treatment. Etoposide-treated cells are used as positive control. Cells were treated with either 30 µg/ml or 50 µg/ml DAB-Am16 for 3 h, stained and analysed with a flow cytometer. For easier comparison, the histograms of the positive control and the dendrimer treated samples have been overlayed with the histogram of the untreated control (orange).

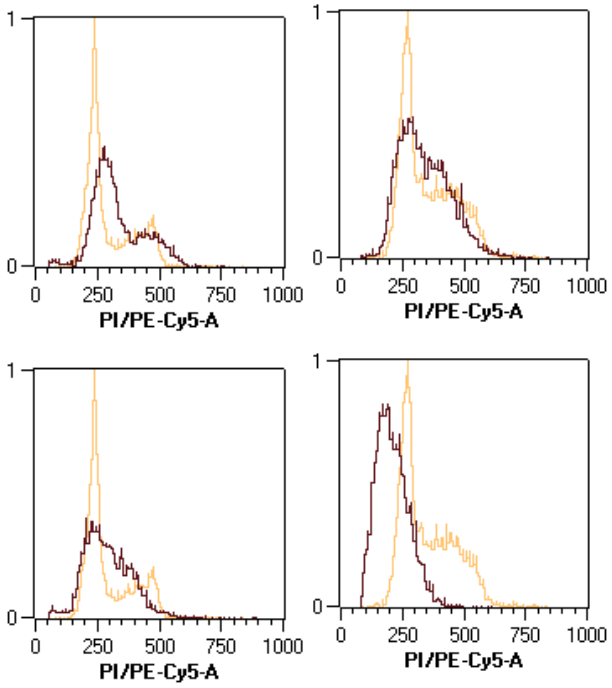

(a) U87MG **(b)** H1299

Fig. 26: Representative cell cycle profiles of the U87MG and H1299 cell line. The cells were treated, stained and measured as described in Fig. 24. This figure shows the cell cycle profile of U87MG cells treated with 10 µg/ml (upper histogram) and 20 µg/ml (bottom histogram), and H1299 cells treated with 100 µg/ml (upper histogram) and 150 µg/ml (bottom histogram), overlayed with the cell cycle profile of the untreated control cells (light orange) and normalised by area in order to exclude the influence of different numbers of measured events.

can be followed up regarding their cell cycle phase after DAB-Am16 treatment.

2. DAB-Am16 can be applied to the cells as usual, but after completion of the treatment cells are pulsed with BrdU. Immediately after this pulse, cells are harvested, fixed and stained as described above. This method allows the identification of the DNA synthesizing cells after DAB-Am16 treatment.

Fig. 27 on the following page shows the results of the analysis of cells pulsed before DAB-Am16 addition. In the untreated control sample, 88 % of all the cells have arisen from those that were in the S phase 24 h earlier as indicated by their positive BrdU staining. These BrdU-tagged cells can be found in any cell cycle phase, as can be seen from their DNA content (represented by DAPI fluorescence on the x-axis). When cells are treated with hydroxyurea, they accumulate at the beginning of the S phase as hydroxyurea arrests DNA replication by inhibiting the class I form of ribonucleotide reductase and thus depleting cellular deoxyribonucleoside triphosphates (dNTP) pool to the basal level (Bianchi et al. 1986; Hendricks et al. 1998; Koç et al. 2004). DAB-Am16 treatment does not force the S-phase cells to stop within the cell cycle, as similar to the control BrdU-tagged cells can be found in any cell cycle phase. However, the overall percentage of BrdU-tagged cells compared to non-tagged cells is smaller than in the control sample (66 % for 50 µg/ml DAB-Am16). Moreover, this percentage shows a decreasing tendency with increasing dendrimer concentration.

When cells are pulsed with BrdU immediately before being collected and stained, the fraction of BrdU-positive cells corresponds to those cells that are replicating DNA at that moment (primarily S-phase cells, but minor incorporation of BrdU can also occur during DNA repair). Fig. 28 shows that in the control population, approx. 45 % replicate their DNA at a given time point, while for the population treated with 50 µg/ml DAB-Am16 the fraction of DNA replicating cells makes up only 22 %. The drop in

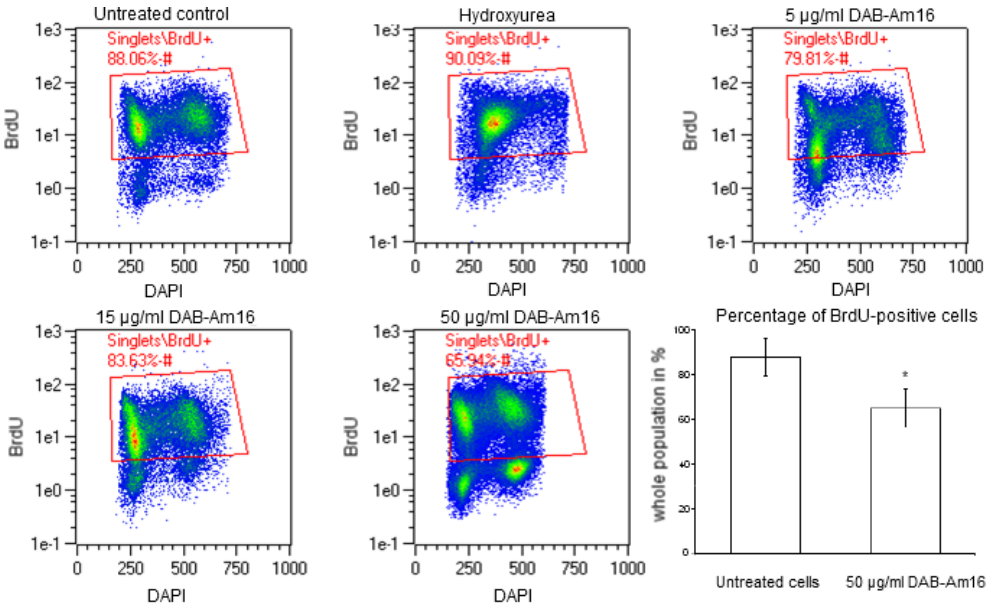

Fig. 27: MiaPaCa-2 cells pulsed with BrdU for 30 min before addition of DAB-Am16 for 24 h were harvested immediately after DAB-Am16 withdrawal, fixed and stained with anti-BrdU-antibody and with DAPI. The results are shown as a density plot. The amount of DAPI fluorescence corresponds to the DNA amount inside of the cell as is depicted on the x-axis. The fluorescence of the BrdU-detection is shown on the y-axis. The events shown only correspond to single cells, as cell doublets have been gated out before. The red gate shown on the plots corresponds to BrdU-positive cells. From upper left to bottom right corner: untreated control, positive control (hydroxyurea), 5 µg/ml, 15 µg/ml, 50 µg/ml DAB-Am16 and statistical comparison of the effect of 50 µg/ml DAB-Am16 with the control.

the number of DNA replicating cells depends on the concentration of the dendrimer, as an intermediate concentration results in an intermediate BrdU-positive cell number (34 % for 15 µg/ml), while the lowest tested DAB-Am16 concentration (5 µg/ml) seems not to have any effect on the proliferation rate of the cells. Additionally to the decrease of the fraction of BrdU-positive cells in samples treated with 15 µg/ml and 50 µg/ml DAB-Am16,

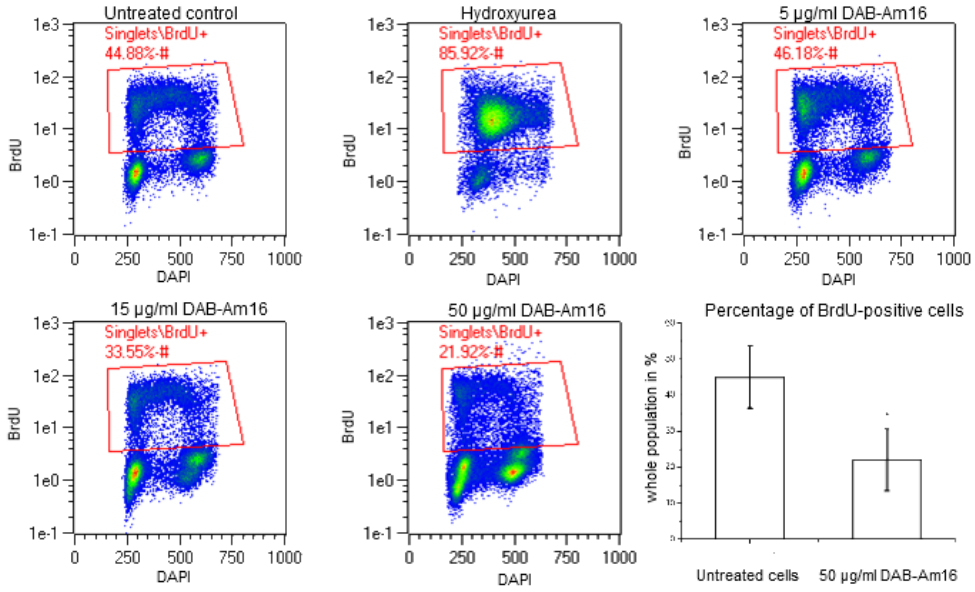

Fig. 28: MiaPaCa-2 cells pulsed with BrdU for 30 min after a 24 h treatment with DAB-Am16 were harvested immediately after BrdU withdrawal. The staining procedure, the method of illustration and the treatment conditions are the same as those described for Fig. 27.

there is a slight drop of fluorescence on the BrdU-channel even for cells that have been categorised as BrdU-negative in the control sample.

Considering the severe decrease of the DNA replication rate seen in Fig. 28 caused by DAB-Am16 treatment, the drop of the fraction of BrdU-positive cells in the DAB-Am16 treated samples in Fig. 27 can be explained by a decrease in cell proliferation, so that BrdU-tagged cells produce less daughter cells than untreated cells within the same time frame. However, the important conclusion to be drawn from these experiments is that cell cycle progression is not completely abrogated by DAB-Am16 but rather slowed down severely.

3.5.1 Cyclin D1 levels in A2780 cells change upon DAB-Am16 treatment in a concentration-dependent manner

A2780 cells were treated with different concentrations of DAB-Am16 for 24 h, fixed and stained with an antibody against cyclin D1 as well as with PI. The results are illustrated in Fig. 29 on the next page. Notably, the control cells do not show the expected pattern of cyclin D1 upregulation in G1 and G2, and downregulation during the S phase. M. Huang et al. (2000) found that A2780 cells have a low expression of cyclin D1, so that one can assume that under normal conditions, only a background level is detectable that remains stable in all cell cycle phases. However, upon exposure of A2780 cells to 10 µg/ml DAB-Am16, a clear upregulation of the cyclin D1 level is observed (Fig. 29) along with an accumulation of the cells at the beginning of the S phase. With elevated DAB-Am16 concentrations, a second population appears that has a lower cyclin D1 expression level than the control cells. These cells with a decreased cyclin D1 level are found across all the cell cycle levels, while those cells that remain with a high cyclin D1 level are localised within the beginning of the S phase.

3.5.2 Mitotic index and DNA synthesis are severely decreased after 48 h exposure to DAB-Am16

To test how DAB-Am16 affects the entrance into mitosis, U87MG and MDAMB231 cells were exposed to different concentrations of the dendrimer for 24 and 48 h. DNA-synthesizing cells were labelled by EdU incorporation. Cells were harvested, fixed and stained with an antibody against phosphorylated histone H3 as well as with a Click-reaction between EdU and Alexa-Fluor 647. Additionally, DNA was stained with PI. The results show that the effect of DAB-Am16 on the cell cycle is time- as well as concentration-dependent (Fig. 30 and Fig. 31). The change in the cell cycle profile was much more pronounced after 48 h than after 24 h and was more pronounced at higher dendrimer concentrations. The population of mitotic cells was virtually depleted after 48 h and the fraction of DNA-

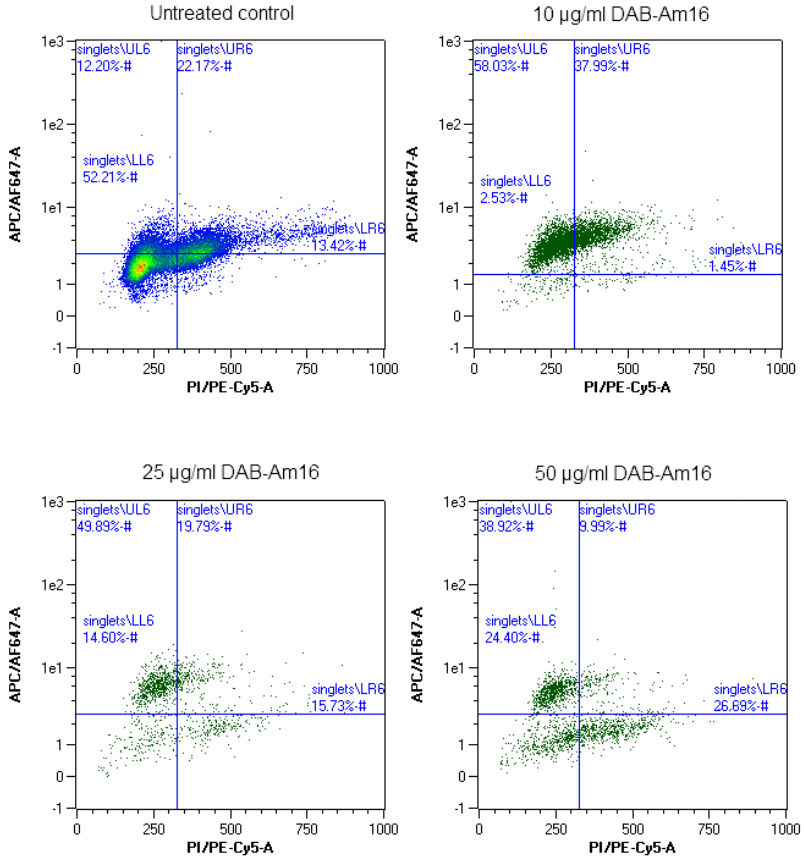

Fig. 29: A2780 cells treated with different concentrations of DAB-Am16 were stained for the level of cyclin D1. The y-axis shows the relative fluorescence on a hyperlogarithmic scale while the x-axis represents the DNA amount of the cells detected by PI staining.

synthesizing cells decreased dramatically. Strikingly, the number of cells with hyperdiploid PI signal increased strongly. This contravenes the drop of DNA synthesis, thus posing the question how cells with hyperploid DNA content can arise without synthesis of new DNA. A possible explanation of these observations is that the number of hyperploid cells does not increase, but instead propidium iodide intercalation with the DNA is promoted by changes of DNA conformation. This effect has been observed by other groups (Ferlini, Biselli et al. 1996; Ferlini, Di Cesare et al. 1996; Prosperi

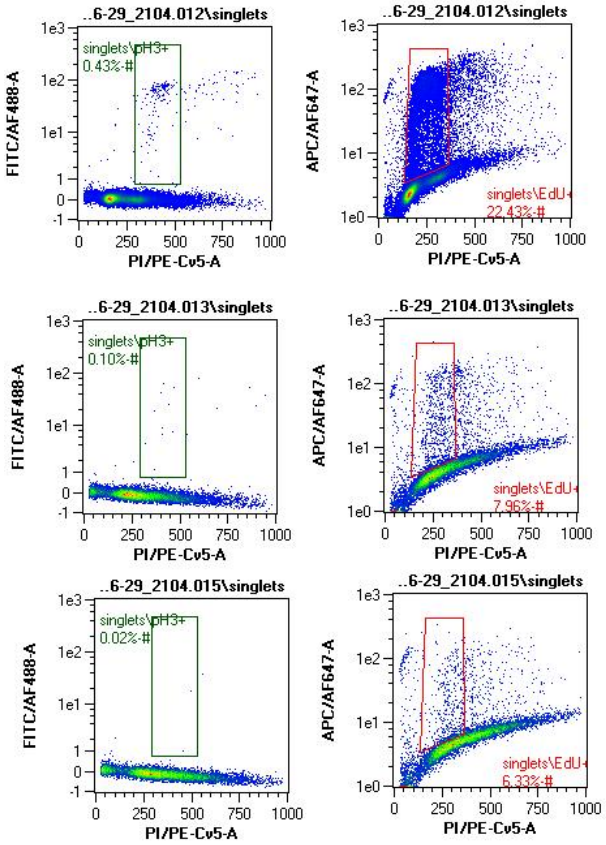

Fig. 30: U87MG cells were incubated with DAB-Am16 either at 10 or at 60 µg/ml for 48 h. Control cells were grown without DAB-Am16. Subsequently, the cells were incubated with the uridine analogue EdU which is incorporated into newly synthesised DNA similarly to BrdU. EdU was then fluorescently labelled to measure the fraction of DNA synthesizing cells. EdU fluorescence is shown on the y-axis of plots in the right column. To simultaneously identify mitotic cells, mitosis-specific phosphorylation of histone H3 was detected (y-axis of plots in the left column). Finally, cellular DNA was stained with PI which is shown on the x-axis on all plots.

et al. 1991) and also applies to several other DNA dyes (ethidium bromide, Hoechst33258), but is absent in cells stained with mithramycin or 7-AAD. This might be due to different sizes of these dyes (7-AAD: MW 1270; mithramycin: MW 1085; PI: MW 668) or different binding/intercalation properties. In fact, Prosperi et al. showed that PI fluorescence intensity increases upon

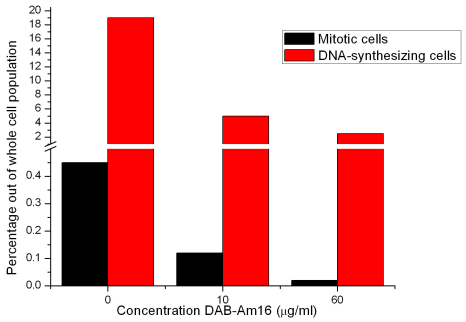

Fig. 31: Data from Fig. 30 as a histogram for better overview. Note the break within the y-axis due to large differences in the number of DNA synthesizing and mitotic cells.

partial digestion of DNA with conformation-specific endonucleases that preferentially cleave supercoiled active chromatin, but PI fluorescence does not increase after digestion of the DNA with sequence-specific nucleases. Ferlini, Di Cesare et al. found the pseudo-hyperploid population to be early apoptotic cells that share light scatter properties with cells within the sub-G1 peak and exhibit the uptake of the non-permeant DNA dye ethidium bromide before fixation. Another possible explanation is that DAB-Am16 itself interacts with the DNA and causes a conformational change, thus allowing more PI molecules to intercalate with the same amount of DNA.

3.6 DAB-Am16 triggers apoptotic cell death

Five characteristics that change during apoptosis were recorded for each cell: light scattering, mitochondrial membrane potential, cell membrane integrity, caspase activation and DNA fragmentation. Fig. 32a on the following page shows a schematic overview on the expected change in light scattering properties of apoptotic cells, while Fig. 32b shows a scheme of the 2D plot of mitochondrial membrane potential and cell membrane permeability.

3.6.1 Apoptosis in MiaPaCa-2 cells

To identify the order of cell death events due to DAB-Am16 exposure, gates were created around all distinguishable cell populations. The gates are explained in Fig. 33 on the next page and Fig. 34 on page 96.

It is possible to select a particular cell population on one plot with a gate, and highlight the selected cells within another plot. For example, one can draw a gate around the "healthy" cell population on the light scatter (LSC) cytogram and highlight all those cells that fall into this gate with the violet colour within the DAPI vs. TMRE dot plot. In this way, one gets the information about the TMRE and DAPI status of those cells that appear healthy on the LSC cytogram. The results are illustrated in Fig. 35 on page 96. On the right, the gating of distinct populations on the LSC plot is shown again. On the TMRE vs. DAPI plot, those cells that are within the P8 gate are highlighted violet. Clearly, the vast majority of these cells are TMRE-positive and DAPI-negative, thus showing all the features we would expect from healthy cells. While the untreated control sample

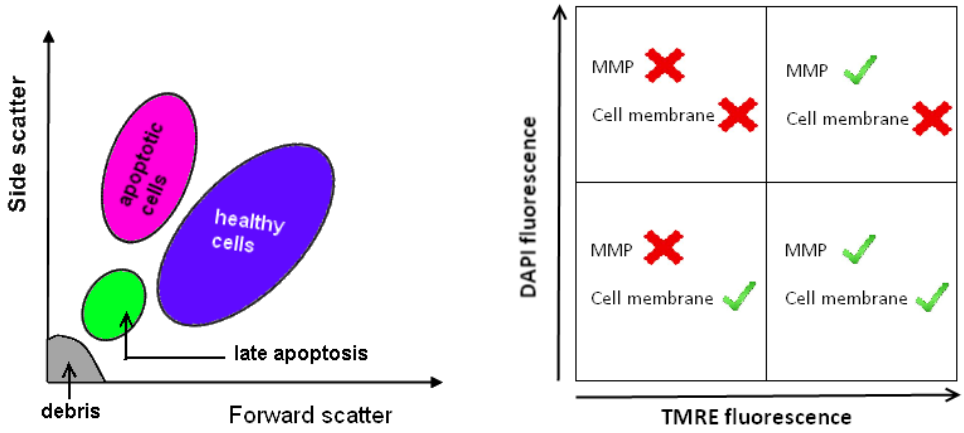

(a) Light scatter properties of apoptotic cells

(b) Mitochondrial potential and cell membrane integrity assay

Fig. 32: Schematic representation of the measurement of apoptotic characteristics of cells.

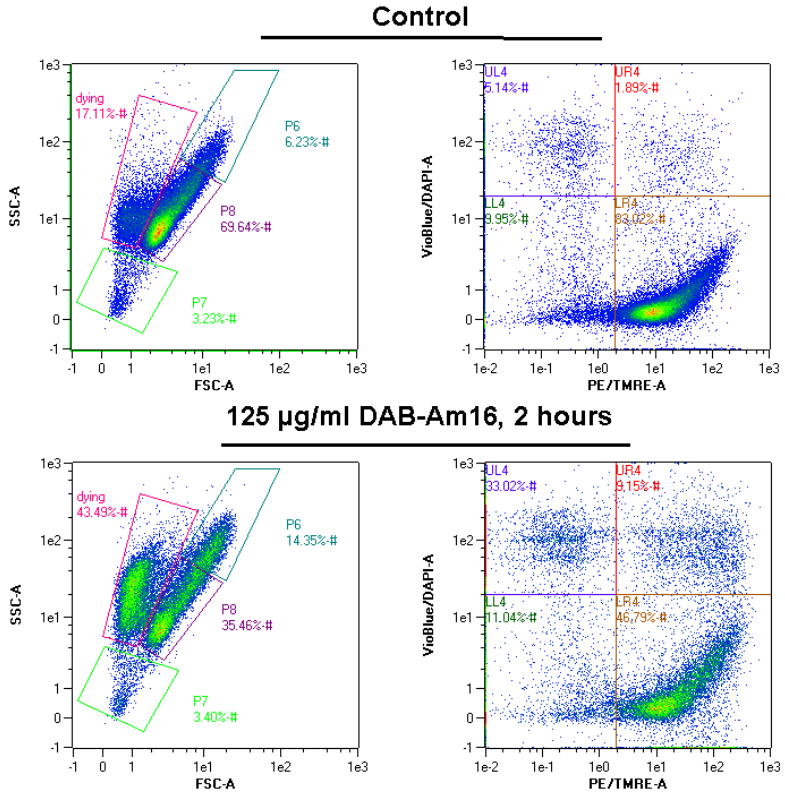

Fig. 33: The gate setting strategy for investigation of apoptosis with flow cytometry. MiaPaCa-2 cells were stained with TMRE, DAPI and PhiPhiLux. The upper row shows two representations of the control sample: Forward scatter (FSC) vs. Side scatter (SSC) on the left, and TMRE vs. DAPI on the right. The same two representations are applied on the sample treated with 125 µg/ml DAB-Am16 for 2 h which is shown in the bottom row. Four populations are distinguishable on the FSC vs. SSC plot: P8 (violet gate, "healthy cells" in Fig. 32a), P6 (darkcyan gate, part of the "healthy cells" in Fig. 32a), "dying" (pink gate, "apoptotic cells" in Fig. 32a) and P7 (lightgreen, "late apoptotic" in Fig. 32a). Debris as depicted in Fig. 32a is not shown in this figure. The TMRE vs. DAPI plot is divided into quadrants that are called LL4 (lower left, darkgreen), UL4 (upper left, violet), UR4 (upper right, red) and LR4 (lower right, brown). The percentages stated in each gate refer to the fraction of cells located within this gate out of the whole population that has been measured. Furthermore, caspase-3 positive cells are gated orange as shown on the histogram in Fig. 34.

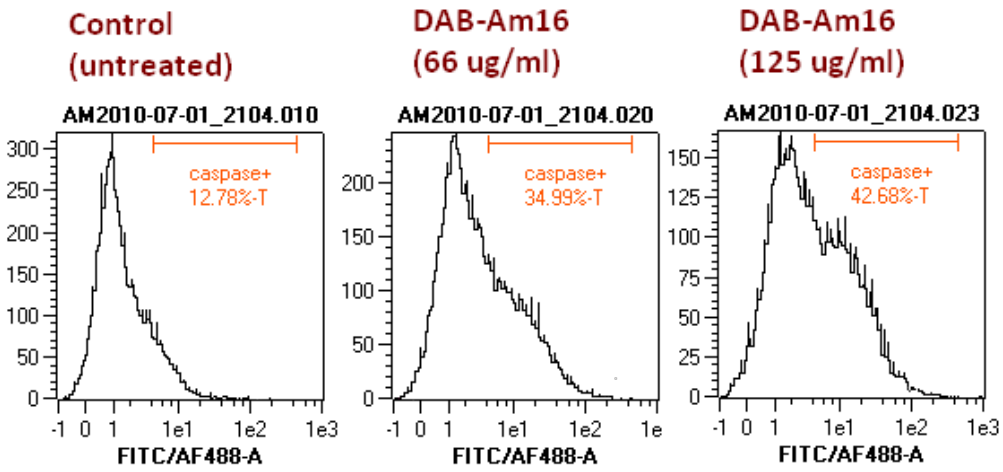

Fig. 34: Caspase-3 activation in MiaPaCa-2 cells. The x-axis shows the relative fluorescence of the cleaved caspase-3 substrate, while the y-axis corresponds to the number of cells. The orange gate quantifies the number of caspase-positive cells.

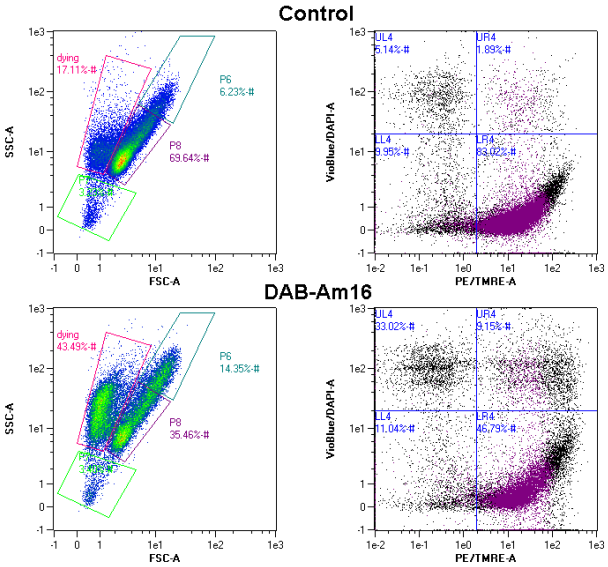

Fig. 35: Location of cells from the P8 gate (with normal light scattering) on the the LSC and the TMRE vs. DAPI plots. The gate was set on the LSC plot and the cells within the gate were then displayed on the TMRE vs. DAPI plot with the violet colour. The upper row shows the untreated control sample and the lower row shows MiaPaCa-2 cells after exposure to 125 µg/ml DAB-Am16 for 2 h.

contains 69.64 % of cells in the P8 gate on the LSC plot, only 35.46 % of cells treated with 125 µg/ml DAB-Am16 are within this gate, thus showing the drop in cell viability upon dendrimer treatment.

Once cells enter the apoptotic pathway, their side scatter usually increases and caspase-3 becomes activated. Cells with increased side scatter properties are gated with the P6 gate in Fig. 36a on the following page on the light scatter plots (left column). To check for the TMRE and DAPI status of these cells, we again apply the same strategy as described above, highlighting only those cells that were within the P6 gate on the TMRE vs. DAPI dot plot with the darkcyan colour (right column in Fig. 36a). In the untreated sample (upper row left), 6 % are found within the P6 gate, while this value rises to 14 % in the DAB-Am16 treated population (bottom row left). When visualised on the TMRE vs. DAPI plot, the vast majority (93 %) of these cells in the control sample are within the lower right corner (LR4), thus having an intact mitochondrial membrane potential and an intact cell membrane. Only 6 % are within the upper right quadrant (UR4). However, the situation is different for the dendrimer treated sample. A substantial number of P6-cells (33 %) is found to be DAPI- and TMRE-positive. The statistical data for the distribution of treated and untreated P6-cells between the quadrants is shown in Fig. 36b. These results indicate that the first step on the way to cell death upon DAB-Am16 treatment is hole formation within the plasma membrane as well as an increase of the side scatter of light.

Having analysed the first signs of apoptotic changes within the cells upon DAB-Am16 treatment, the question arises at which point caspase-3 is activated within the cells as this is often considered to be the point-of-no-return for the apoptotic process (Green 2000; Hengartner 2000; Kumar 1998). Moreover, as the reports on the order of caspase-3 activation and mitochondrial membrane potential drop are controversial, the order of these events in the case of DAB-Am16 treated MiaPaCa-2 cells is to be investigated. The location of caspase-positive cells on the LSC and the TMRE vs. DAPI plots is shown in Fig. 37a on page 99 and the statistical

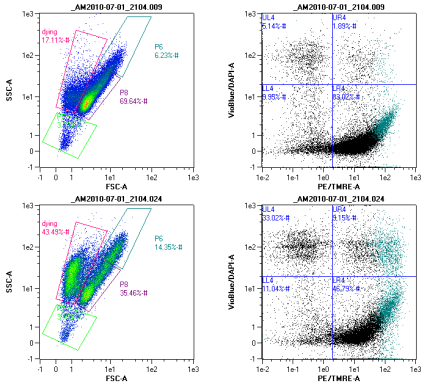

(a) Location of cells from gate P6 within the TMRE vs. DAPI plot

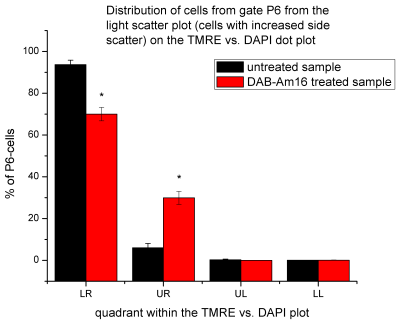

(b) Distribution of MiaPaCa-2 cells with increased side scatter within the TMRE/DAPI plot

Fig. 36: Location and distribution of MiaPaCa-2 cells with increased side scatter properties within untreated and dendrimer treated samples on the TMRE vs. DAPI plot. The stars indicate a significant ($p < 0.05$) difference between the untreated and the dendrimer-treated sample.

distribution of caspase-positive cells within the TMRE vs. DAPI plot is depicted in Fig. 37b. Clearly, the vast majority of caspase-positive cells within the dendrimer-treated sample is located either within the P6 gate (cells with elevated right angle light scatter) or within the "dying" cell population (cells with decreased forward light scatter), thus confirming the association of these light scatter properties with the commitment to apoptotic cell death. Within the TMRE vs. DAPI plot, far most of the caspase-positive cells are found within the lower right quadrant in the untreated sample, but this changes upon dendrimer treatment. In the treated sample, there is a significant decrease of the fraction of caspase-positive cells within the LR quadrant and a significant increase within the UL quadrant as well as an insignificate increase within the UR quadrant. However, almost no cells are found within the LL quadrant. This indicates that concurrent with caspase activation, the cells first acquire holes in the cell membrane (translocate from LR to UR on the plot in Fig. 37a) and then quickly lose the mitochondrial potential (translocation from UR to UL).

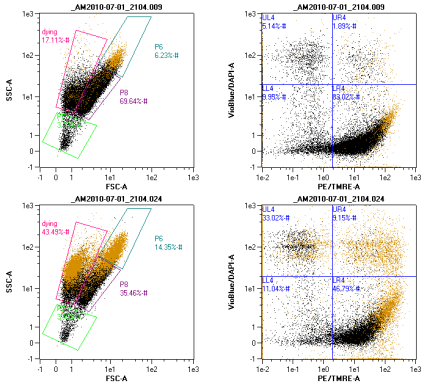

(a) Activation of caspase during MiaPaCa-2 apoptosis.

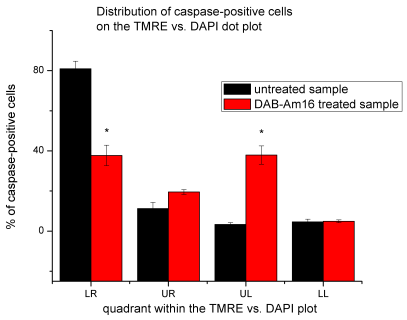

(b) Distribution of MiaPaCa-2 cells with activated caspase-3 within the TMRE/ DAPI plot

Fig. 37: Location and distribution of MiaPaCa-2 cells with activated caspase-3 (marked with the orange colour) within untreated and dendrimer treated samples on the TMRE vs. DAPI plot. The stars indicate a significant ($p < 0.05$) difference between the untreated and the dendrimer-treated sample.

However, caspase-positive cells are not found within the cell population that proceeded to the very last stage of cell death (LL quadrant).

Next, the mitochondrial and cell membrane status of cells designated as "dying" (having decreased forward light scatter values) within the LSC plot is to be analysed using the same strategy as above. Again, cells that are gated as "dying" on the LSC plot are highlighted within the TMRE vs. DAPI dot plot as pink dots and the fraction of these cells within the four quadrants is determined. As can be seen from Fig. 38, the number of these cells is again much lower within the control sample (17.11 %) than within the dendrimer-treated cell sample (43.49 %). Their distribution differs significantly as well. While most of these cells are within the lower right quadrant in the control population, the vast majority is within the upper left quadrant in the treated cell population, i.e., these are mostly cells with a permeabilised plasma membrane and collapsed mitochondrial membrane potential which previously was determined to be the ultimate

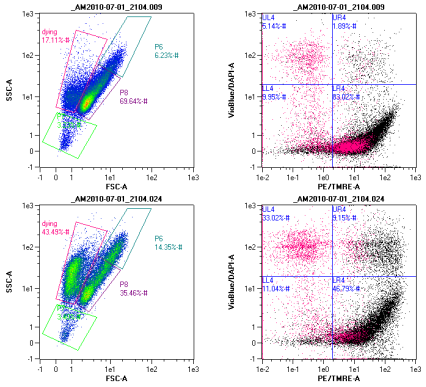

(a) Location of cells from gate "dying" within the TMRE vs. DAPI plot

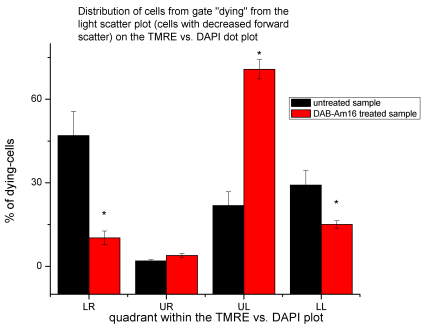

(b) Distribution of MiaPaCa-2 cells with decreased forward scatter within the TMRE/DAPI plot

Fig. 38: Location and distribution of MiaPaCa-2 cells with decreased forward light scatter properties within untreated and dendrimer treated samples on the TMRE vs. DAPI plot. The stars indicate a significant ($p < 0.05$) difference between the untreated and the dendrimer-treated sample.

state for caspase-positive cells. Thus, so far, the way to death of MiaPaCa-2 cells upon DAB-Am16 treatment was seen to lead through cell membrane permeabilisation, caspase-3 activation, increase of right angle light scatter, then decrease of both side and forward light scatter and collapse of $\Delta\Psi_m$.

The very last stage of apoptosis is characterised by cellular disintegration, which comes along with a large drop of light scattering, loss of DNA and finally only debris remains of the cell. In Fig. 39 on the following page, this is illustrated by setting gate P7 around cells that have extremely low light scattering properties and highlighting these cells with a green colour within the TMRE vs. DAPI plot. Evidently, these cells are located in the lower left quadrant, thus finally having lost DAPI fluorescence due to loss of DNA as DAPI is a DNA-binding dye, and also possessing a collapsed mitochondrial membrane potential.

In summary, the order of the events on the way to cell death after DAB-Am16 exposure is as follows:

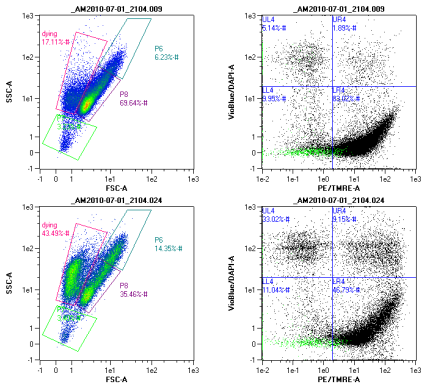

(a) Location of cells from gate P7 within the TMRE vs. DAPI plot

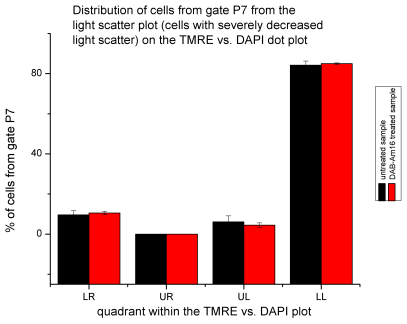

(b) Distribution of MiaPaCa-2 cells with severely decreased light scatter within the TMRE/DAPI plot

Fig. 39: Location and distribution of MiaPaCa-2 cells with severely decreased forward and right angle light scatter properties within untreated and dendrimer treated samples on the TMRE vs. DAPI plot. There is no significant difference between the untreated and the dendrimer-treated sample in any of the quadrants.

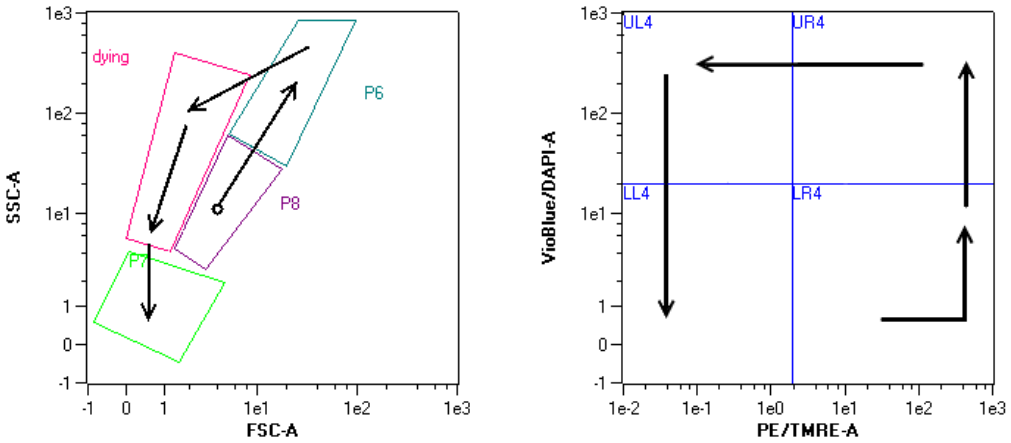

Fig. 40: Summary of the death path of MiaPaCa-2 cells upon DAB-Am16 treatment as represented by multicolour flow cytometry measurements.

1. Cell membrane permeabilisation, increase of right angle light scatter (side scatter) and caspase-3 activation

2. Loss of mitochondrial membrane potential, decrease of forward light scatter and finally loss of caspase-3 activity

3. Further decrease of both forward and side light scatter, loss of DAPI fluorescence, cellular disintegration

A graphical representation of the order of the events is shown in Fig. 40 on the previous page.

Considering the discussion in section 3.4.2 that according to the MTT and LDH assays metabolic changes precede leakage of large cytosolic enzymes out of the cell, the results of the TMRE/DAPI staining first seem to contradict those findings because here cell membrane permeabilisation is detected by DAPI influx prior to metabolic changes by collapse of $\Delta\Psi_m$. A plausible explanation is that DAB-Am16 first enters the cell via formation of cell membrane holes in the nanosize range, then exerts its cytotoxic effect and only at the last stage large holes in the cell membrane occur as a late apoptotic event. When DAB-Am16 (MW 1,687) forms nanoholes in the cell membrane, DAPI (MW 350) can enter the cell through these holes, while LDH (MW 140,000) is too big to leave the cell through these holes and is only released upon final cell membrane disintegration.

3.6.2 Apoptosis in A2780 cells

Fig. 41 on the following page shows the distribution of A2780 cells between the quadrants on the TMRE vs. DAPI plot after treatment with 70 µg/ml DAB-Am16 for 4 h compared to the untreated control. In the control sample, almost all cells are located within the LR quadrant, i.e. they have a normal mitochondrial membrane potential and an intact cell membrane. In contrast, less than 50 % of dendrimer-treated cells are located within this quadrant. Most of the remaining cells in this sample are found within the UL quadrant, indicating a collapsed mitochondrial membrane potential and

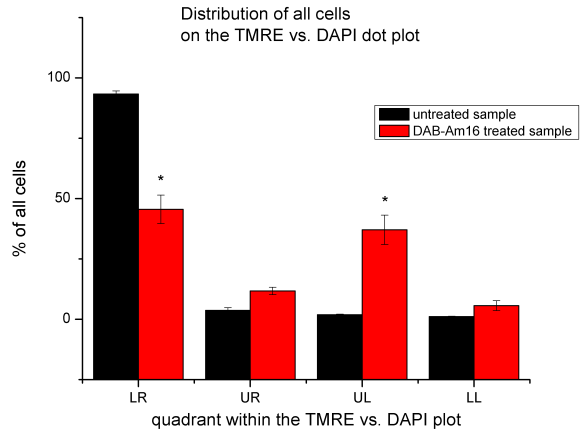

Fig. 41: Distribution of untreated and DAB-Am16 treated A2780 cells on the TMRE vs. DAPI plot. The treated population was exposed to 70 µg/ml DAB-Am16 for 4 h. The stars indicate a significant ($p < 0.05$) difference between the untreated and the dendrimer-treated sample.

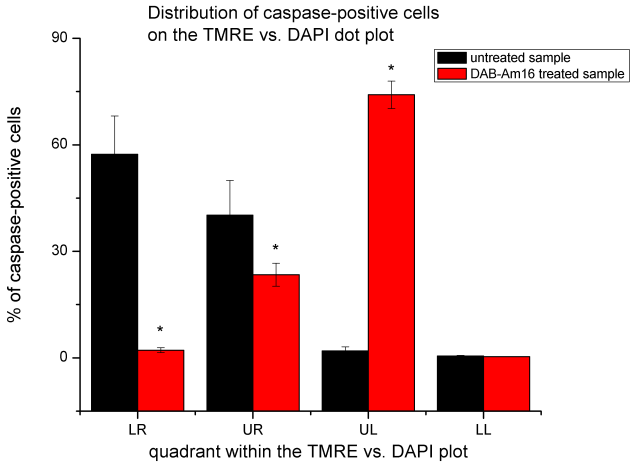

Fig. 42: Distribution of caspase-positive A2780 cells on the TMRE vs. DAPI plot. The treated population was exposed to 70 µg/ml DAB-Am16 for 4 h. The stars indicate a significant ($p<0.05$) difference between the untreated and the dendrimer-treated sample.

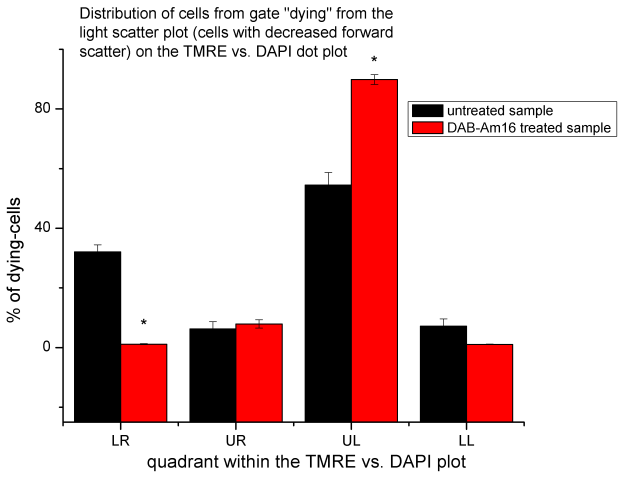

Fig. 43: Distribution of A2780 cells with decreased forward light scatter on the TMRE vs. DAPI plot. The treated population was exposed to 70 µg/ml DAB-Am16 for 4 h. The stars indicate a significant ($p < 0.05$) difference between the untreated and the dendrimer-treated sample.

a perforated plasma membrane. Moreover, 38 % of the dendrimer-treated cells were found to be caspase-positive (control sample: 6 %) and 35 % exhibit a decreased forward light scatter (control sample: 2 %). Thus, DAB-Am16 shows a clear cytotoxic effect on A2780 cells within a short time frame, triggering the apoptotic pathway.

The distribution of caspase-positive cells on the TMRE vs. DAPI plot is shown in Fig. 42 on the previous page. 60 % of caspase-positive cells in the control sample are within the LR quadrant, and almost all the other cells are found within the UR quadrant. Thus, the vast majority of caspase-positive cells within the control sample have an intact mitochondrial membrane potential, while some of them have a perforated cell membrane, presumably due to the mechanical stress caused by cell sample handling before the measurement. In contrast, 75 % of caspase-positive cells within the dendrimer-treated sample are in a much more advanced stage on the way to cell death, being located in the UL quadrant and thus having both, a collapsed $\Delta\Psi_m$ and holes in the cell membrane. Significantly

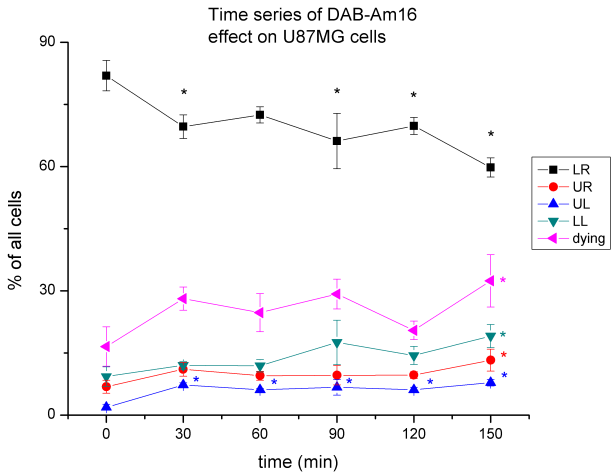

Fig. 44: The fraction of cells within particular gates is plotted against duration of exposure to 50 µg/ml DAB-Am16. The stars indicate a significant ($p < 0.05$) difference between the untreated and the dendrimer-treated sample.

less caspase-positive cells are located in LR and UR quadrants within the dendrimer-treated sample.

A similar difference in distribution is also seen for the population of cells that show a decreased forward scatter ("dying" cells on the LSC plot) as can be seen in Fig. 43 on the preceding page. More than 80 % of dendrimer-treated cells from this population are found within the UL quadrant as it is the case for 75 % of caspase-positive cells. In contrast to the control, almost none of the "dying" cells are located within the LR quadrant.

3.6.3 Apoptosis in U87MG cells

U87MG cells were used to characterise how the number of cells with apoptotic features changes with increasing duration of exposure to DAB-Am16. TMRE and DAPI fluorescence as well as the light scattering properties of cells were measured after exposure to the dendrimer for 30, 60, 90, 120 and 150 min and compared to the untreated control sample. The results

are shown in Fig. 44 on the previous page. Already after 30 min a significant drop of the number of cells within the LR quadrant and a significant increase of cells within the UL quadrant is observed. An increase of the "dying" cell population (according to the LSC plot) is also seen after 30 min, although this difference is not statistically significant. During the next time points up to 120 min, the percentages of cells within the designated gates do not change. However, after 150 min, all the gates show a significant difference compared to the control: the LR-quadrant population clearly decreases, while the percentage of cells within the other three quadrants and the percentage of cells with decreased forward light scatter ("dying") increases significantly. These results indicate that the cytotoxic effect of DAB-Am16 is observable already after 30 min. However, within the next 1.5 h (time point 120 min), there is no further change. Between 120 and 150 min, another clear change takes place, leading to a further rise of cells exhibiting apoptotic properties.

3.7 Cellular RNA content decreases upon DAB-Am16 exposure

Acridine Orange (AO) is a metachromatic dye that fluoresces in different wavelengths dependent on if it is bound to single-stranded or double-stranded nucleic acids. After selective denaturation of RNA it is possible to stain DNA and RNA with green and red colour, respectively. This allows to measure RNA content of cells and correlate it to their cell cycle phase.

Fig. 45 on page 108 shows the results of AO staining of U87MG cells. To exclude doublets, the area of the green fluorescence signal was plotted against its height and only the cells on the diagonal were selected as singlets. According to Fig. 45, less than 1 % of singlets are RNA_{low}, while RNA_{low} cells constitute 14 % of the treated cell population. The percentage of cells within the G2 phase is approximately the same in both samples (35 % in control and 37 % in treated sample), but while 76 % of G2 cells (27 % out of 35 % of overall singlets) are found in the upper right quadrant within

the control cell population, only 31 % of G2 cells in the dendrimer-treated sample are in this quadrant, indicating a significantly lower percentage of cells with a high RNA content. When the RNA_{low} cell population is overlayed with the whole cell population on the DNA histogram plot (upper panel in Fig. 45), a peak arises within the S-phase cells after DAB-Am16 treament, while most of RNA_{low} control cells are located within the G1 and G2 phases. Quantitatively, 33 % of the RNA_{low} cells of treated sample are located in the S-phase, while only 19 % of the RNA_{low} control sample cells are within the S-phase. Accordingly, less of RNA_{low} cells are in G1 and G2 phases in the treated sample (13 % and 20 %, respectively) than in the control (34 % and 27 %, respectively). Another difference is the high number of RNA_{low} cells within the cell population with a DNA content higher than that of G2 (possible hyperploid cells) in the treated cell sample. Thus, DAB-Am16 leads to a markedly decreased RNA content of cells, especially in the S-phase and the hyperploid cell populations.

Fig. 46 on page 109 shows the results of the AO staining for A431 cells either untreated or treated with 75 µg/ml DAB-Am16 for 24 h. A similar pattern is observed as for U87MG cells:

- There is a higher fraction of RNA_{low} cells within the dendrimer-treated sample than within the control (5.18 % vs. 0.87 %).
- In the control population, 68.6 % of G2 cells have a high RNA content compared to 20 % in the dendrimer-treated sample.
- More RNA_{low} cells are located within the S-phase in the treated sample compared to the control (41.49 % vs. 26.49 %), while less cells are found in G1 (26.00 % vs. 35.10 %) and approx. the same number is found in G2 (13 % vs. 9.93 %).

The only difference is the lack of RNA_{low} cells within the hyperploid cells that, however, make up only a small fraction of the overall cell population.

MiaPaCa-2 cells show a markedly different cell cycle change after treatment with DAB-Am16 compared to other cell lines. They do not show

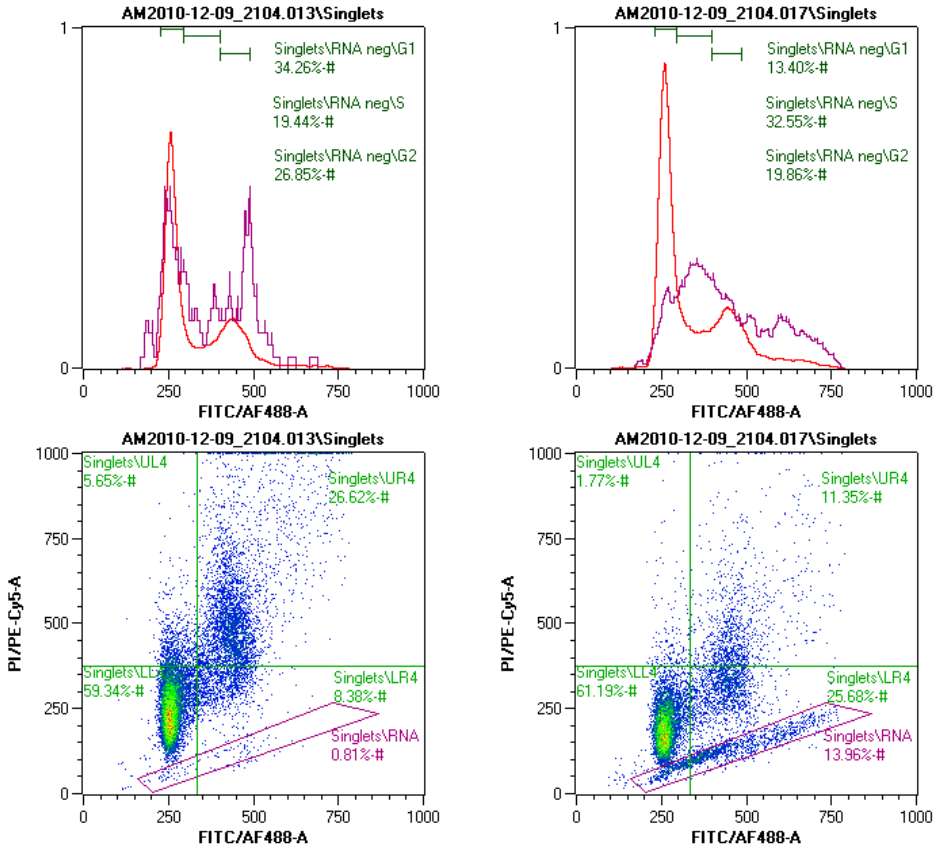

Fig. 45: Differential staining of DNA and RNA of U87MG cells: **(a)** non-treated control and **(b)** treated with 10 µg/ml DAB-Am16 for 24 h. Singlets have been selected by plotting Area vs. Height of the DNA staining colour (not shown). The bottom row shows a density plot of all singlets with green (DNA) fluorescence on the x-axis and red (RNA) fluorescence on the y-axis. Those cells that exhibit a particularly low RNA content are selected with a violet gate. The upper panel shows DNA histograms (red) and an overlay of the RNA_{low} cells (violet). The histograms are normalised to the area and are smoothed due to the very low number of RNA_{low} cells.

S-phase arrest, but exhibit G2-phase arrest instead. This poses the question how they behave in terms of the distribution of RNA_{low} cells compared to A431 and U87MG cell lines. Fig. 47 illustrates that again there is a higher percentage of RNA_{low} cells within the DAB-Am16 treated cell sample

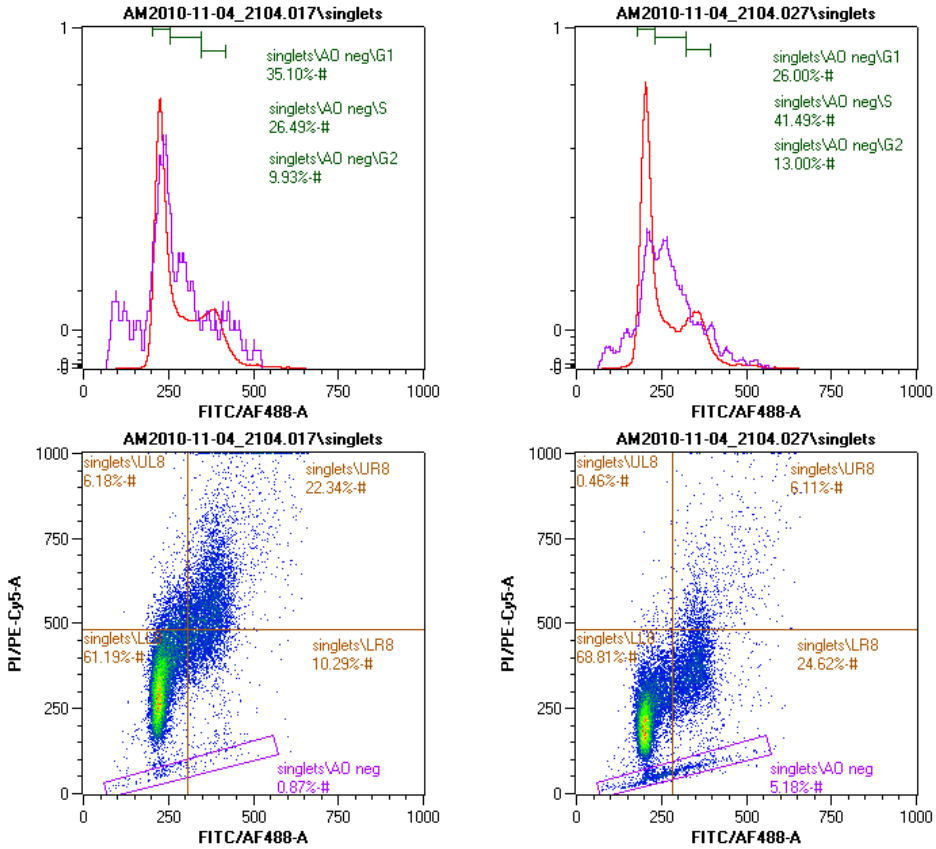

Fig. 46: Differential staining of DNA and RNA of A431 cells: **(a)** non-treated control and **(b)** treated with 75 µg/ml DAB-Am16 for 24 h. Analysis was performed in the same way as described for Fig. 45.

compared with the control (16 % vs. 3 %), but unlike the other cell lines, the more RNA_{low} MiaPaCa-2 cells in the treated sample accumulate in the G2 phase of the cell cycle than within the control sample (13 % vs. 5 %).

Fig. 48 on page 111 shows a plot of the fraction of RNA_{low} cells dependent on the DAB-Am16 concentration applied for all three cell lines that have been discussed above. For all three cell lines, there was an increase of the percentage of RNA_{low} cells with rising DAB-Am16 concentration. However, while for MiaPaCa-2 cells, this percentage rose only up to approx. 10 µg/ml and then remained stable at about 14 %, the increase for A431 cells was

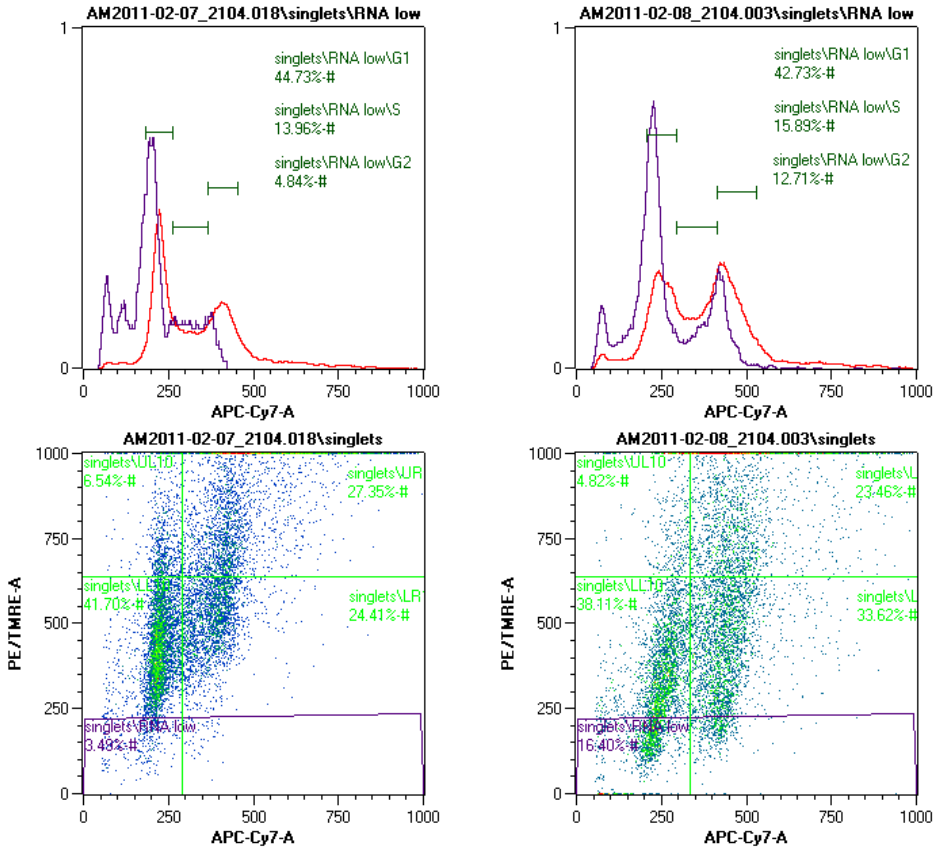

Fig. 47: Differential staining of DNA and RNA of MiaPaCa-2 cells: **(a)** non-treated control and **(b)** treated with 50 µg/ml DAB-Am16 for 24 h. Analysis was performed in the same way as described for Fig. 45.

linear over the whole range tested, but the values were lower (up to approx. 5 % at 75 µg/ml). For U87MG, the initial increase was similarly steep as for MiaPaCa-2, but no data is available for DAB-Am16 concentrations higher than 10 µg/ml.

3.8 Effect on tumour cells *in vivo*

The tumour size and the animal weight were first measured on day 7 after tumour implantation. On day 8 since the first measurement, the animals

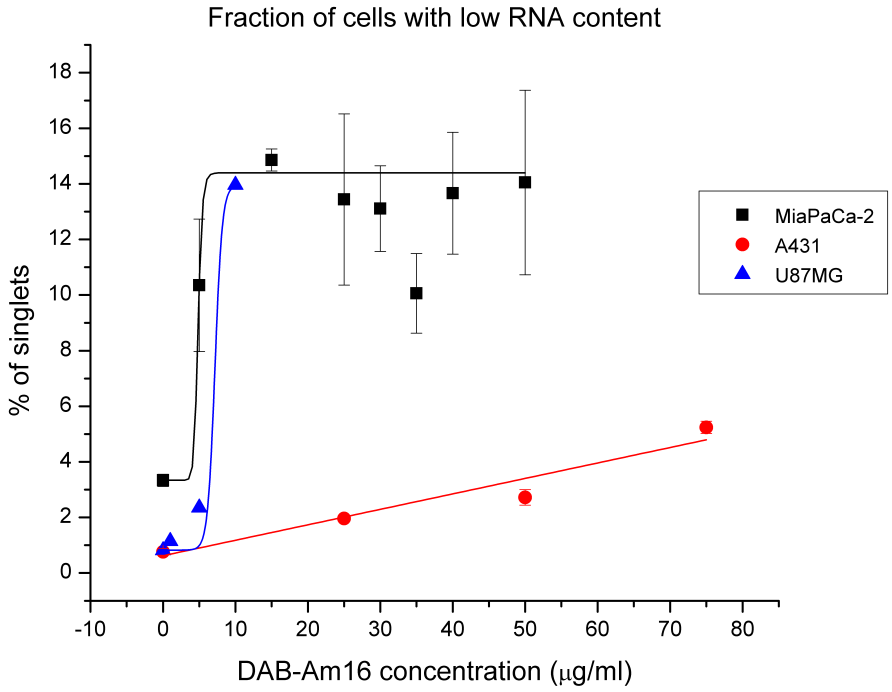

Fig. 48: Fraction of cells with a low RNA content within samples of MiaPaCa-2, A431 and U87MG cells dependent on the concentration of DAB-Am16 that the cells had been exposed to.

with growing tumours (17 out of 20 injected) were assigned to one of the three groups "control" (6 animals), "DAB-Am16-treated" (6 animals) and "gemcitabine" (5 animals) so that each of the groups contained a representative set of tumour growth kinetics and tumour sizes. The first injection of DAB-Am16 was carried out on the same day, while gemcitabine was injected one day later for the first time. Tumour size and animal weight were recorded three times a week. For data analysis, the tumour size of each animal on each day of measurement was normalised to the tumour size of this animal of the first day of measurement. The mean relative tumour growth for each group was plotted with error bars representing the standard error. Animals were culled on the day of the fourth consecutive

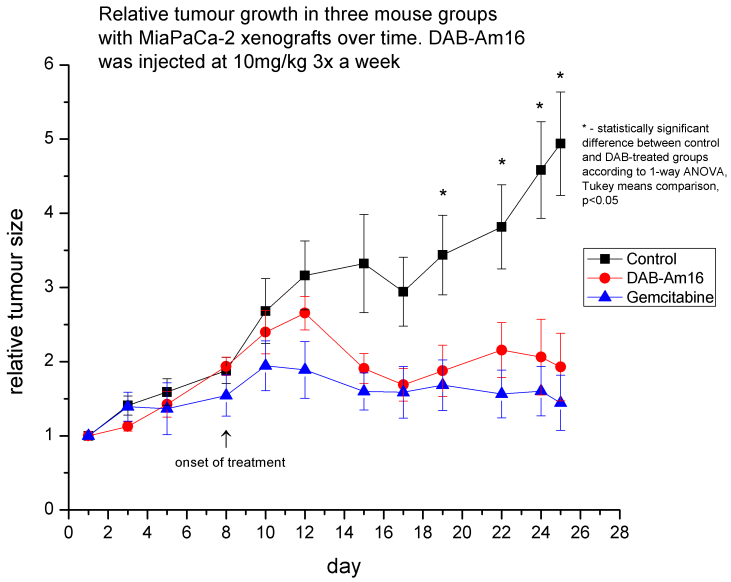

Fig. 49: The relative tumour size over time. The x-axis shows the number of days since the first size measurement (8 days after xenograft injection). Measurements were performed on each day of the injection of DAB-Am16 since treatment onset and on day 25 before culling the animals.

measurement at which the mean tumour size of the DAB-Am16-treated group was significantly ($p<0.05$) smaller than the mean tumour size of the control group. One animal of the DAB-Am16-treated group was found to be dead without any obvious reason on the next day after the 7^{th} injection. Fig. 49 shows that the control tumours grew fivefold within 25 days with a clear tendency to further growth, while the tumours within the DAB-Am16-treated group had on average approx. twofold larger volume than at the beginning, remaining stable in size since the 2^{nd} injection of DAB-Am16. There was no significant difference between DAB-Am16 and gemcitabine treatment with respect to tumour size. Fig. 50 on the following page shows that the weight of all animals dropped transiently after the first DAB-Am16 injection, but the animals recovered quickly and the weight remained stable after the second injection. This is in accordance with previous observations by Dufes et al. (private communication).

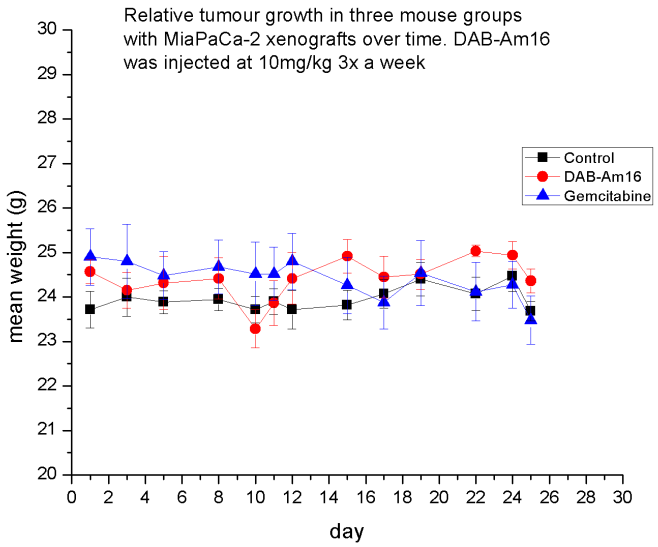

Fig. 50: The animal weight over time. Animals were weighed on the same days as tumour measurements (Fig. 49) and additionally on day 11 due to the severe weight drop detected on day 10.

As tumour growth was inhibited by DAB-Am16, one would assume that the proliferation capacity of the tumour cells was compromised. To test this hypothesis, immunohistochemical analysis of Ki-67 expression of tumour tissue was performed. Ki-67 is a proliferation marker that is expressed by proliferating cells during all cell cycle phases, but is not expressed in resting G0 cells (Scholzen et al. 2000). For each individual tumour, three pictures were made on random positions within the tissue sample, and all three pictures were used for visual assessment of Ki-67 expression for each tumour. An example of the grading of one tumour per rating value is shown in Fig. 51 on the next page. An overview of the absolute frequency and cumulative relative frequency of the rating values for each treatment group is shown in Table 6 on page 115. Unfortunately, due to the small amount of available tissue especially in the treated groups, not all tumours could

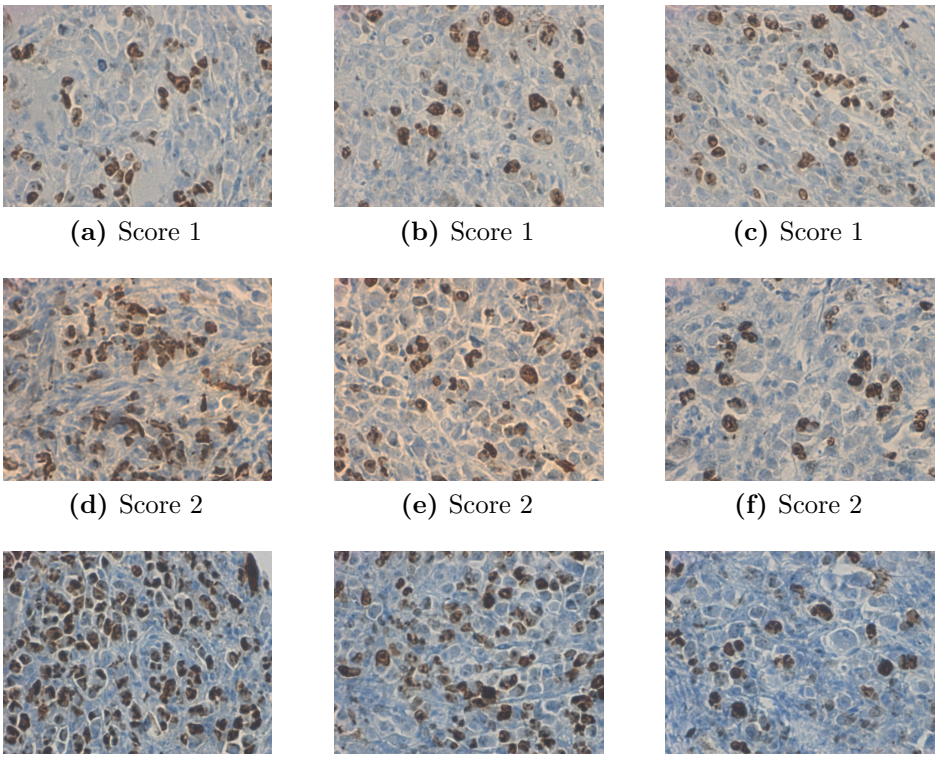

(a) Score 1 **(b)** Score 1 **(c)** Score 1

(d) Score 2 **(e)** Score 2 **(f)** Score 2

(g) Score 3 **(h)** Score 3 **(i)** Score 3

Fig. 51: Examples for Ki-67 expression rating of the tumour tissue sample after immunohistochemical staining. For each of the assessed tumours three pictures on random positions of the slide with a magnification of 40x were made. The assignment of the score is based on the assessment of all three pictures for each tumour.

be analysed. Intriguingly, no significant difference in Ki-67 expression can be inferred from the available data.

To compare cell cycle progress *in vitro* and *in vivo*, four tumours of the control and of the DAB-Am16 group were dissociated into a single-cell suspension. The cell cycle profiles were then measured by DNA staining with propidium iodide. Fig. 52 shows the cell cycle profile of the four control tumours. Clearly, G1 phase is the most prominent phase on the histogram. Interestingly, all control tumours also have a distinct peak within the S phase. This is opposite to the cell cycle profile seen *in vitro*

Table 6: The degree of Ki-67 expression was assessed for each animal. The cumulative relative frequency of each rating within each group was calculated to facilitate comparison between the three treatment groups.

Rating	Absolute frequency			Cumulative relative frequency		
	Control	DAB-Am16	Gemcitabine	Control	DAB-Am16	Gemcitabine
1	4	1	1	0.7	0.3	0.2
2	2	1	3	1.0	0.7	1.0
3	0	1	0	1.0	1.0	1.0

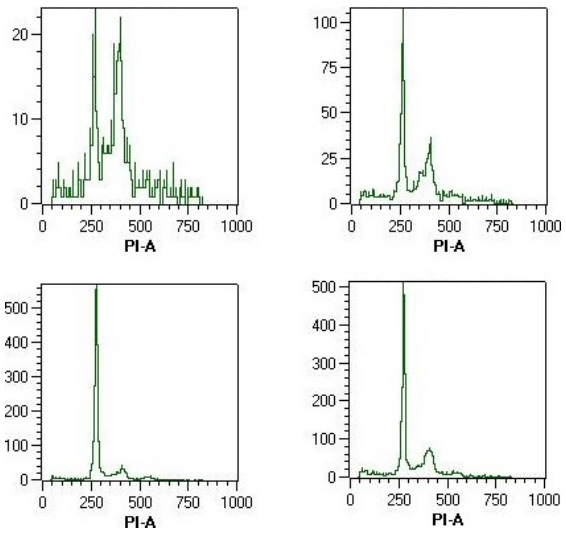

Fig. 52: Cell cycle profile of cells derived from tumours of four randomly selected animals from the control group.

with MiaPaCa-2 cells where the S phase approximates an even plateau below G1 and G2/M peaks. As for the DAB-Am16-treated tumours, 3 out of 4 tested cell samples seem to completely lack S phase cells and have only very small G2/M peaks. It is not known where this striking difference between control and treated tumours is a result of cell cycle phase-selective cell death or of a prevention from further cycling of those cells that reached G1.

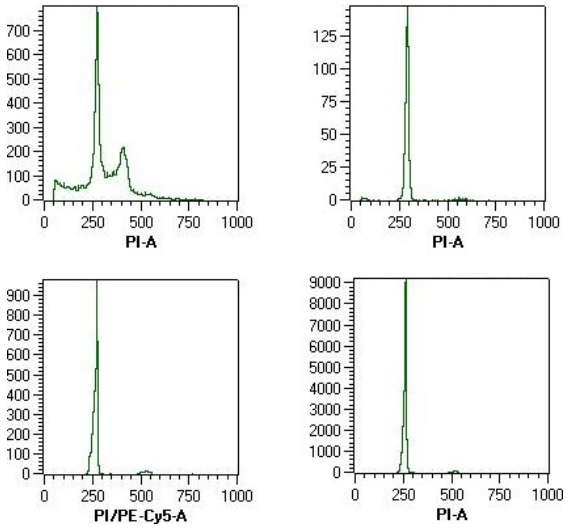

Fig. 53: Cell cycle profile of cells derived from tumours of four randomly selected animals from the dendrimer treated group.

4 Discussion and implications

4.1 Analytical characterisation of DAB-Am16

The identity, purity and stability of the DAB-Am16 dendrimer used for further experiments was confirmed with ^{1}H NMR, ^{13}C NMR and ^{1}H COSY spectroscopy, ESI and MALDI-TOF mass spectrometry and CHN analysis. The dendrimer was found to be highly pure with only a minor fraction of molecules having small defects (absence of one or two 3rd generation branches) and a small unidentified peak at m/z 663.5 in mass spectra that is probably also responsible for an additional peak in the NMR spectrum at approx. 18.5 ppm. The dendrimer did not degrade even after two years of storage within an opened storage container. Formal short term stability test of solutions of dendrimer in water demonstrated the material to be stable for at least 6 days at –20 °C, 4 °C, sroom temperature and at 37 °C.

An important obstacle to the development of new drugs for clinical use is that many potential drug molecules are prone to decomposition over time. For safety reasons, it is crucial that the administered drugs remain stable during long-term storage. The stability issue becomes even more important in outpatients' care as patients might store drugs for a longer time without monitoring the expiry date, and might also store the drugs in a warm environment that promotes decomposition. A lot of effort is put into development of stable drug formulations. The stability of DAB-Am16 over time and temperature range makes it a good drug candidate.

4.2 *In vitro* investigation

4.2.1 Cytotoxicity and drug resistance

The *in vitro* part of the work described in this thesis confirms that the dendrimer DAB-Am16 has cytotoxic and cytostatic effects on a wide range of human cancer cell lines in a time- and concentration-dependent manner. Although the sensitivity to DAB-Am16 varies between cell lines, for all

tested cell lines, the EC50 remains within the same concentration range and drops in an exponential way within the first doubling time. However, longer exposure to DAB-Am16 up to 96 hours does not further decrease viability, indicating that a small subset of the overall cell population remains viable for an extended time frame. Nonetheless, the ability to further divide and build colonies is reduced for these cells even after withdrawal of DAB-Am16 as has been shown in the colony formation assay, indicating a permanent damage caused by DAB-Am16 even within the resistant subpopulation. Thus, within the first doubling time of the cell population DAB-Am16 exerts a cytotoxic effect on the majority of cells, while with further exposure time a cytostatic effect is observed for a small number of surviving cells.

As with each surrogate marker, caution should be exercised when conclusions are drawn from assay results. Although the MTT assay is generally considered to be a viability assay, one must be aware that it measures enzyme activity of the entire cell population, which of course decreases with the number of viable cells, but might also be influenced by the metabolic activity of the cells. A transient effect leading to decreased enzyme activity within viable cells cannot be ruled out. At long incubation times, cell death could also be counteracted by division of the few remaining resistant cells. These two fundamentally different scenarios might both lead to apparently same assay results. Having said that, the MTT assay is a good way to assess drug effect at a range of different concentrations at a high throughput if the experimentator is well aware of the limitations. In the case of the experiments conducted for this thesis, microscopic observations confirmed an enormous change of the morphologic appearance of the cells as well as the dramatic increase of the number of floating (dead) cells at high DAB-Am16 concentrations.

There must be an intracellular, perhaps a genetic difference between the highly sensitive and the long-term surviving cell subpopulations. It is tempting to speculate that the surviving cells might bear stem-cell like properties. The concept of cancer stem cells (CSCs) being the initiators of malignant diseases has been first proposed in mid-90's for acute myeloid

leukemia (Bonnet et al. 1997; Lapidot et al. 1994). Since then, this concept has been extended to a number of other malignancies including pancreatic (Hermann et al. 2007; M. P. Kim et al. 2011; Li et al. 2007), brain (Lathia et al. 2010; Rasper et al. 2010; S. K. Singh et al. 2003) and breast cancer (Ginestier et al. 2007; Al-Hajj et al. 2003; Lorico et al. 2011; Wright et al. 2008). The key characteristics of CSCs are tumorigenicity, self-renewal and multipotency (Lonardo et al. 2010; Tabatabai et al. 2011). Furthermore, CSCs are particularly resistant to chemotherapy due to overexpression of drug efflux pumps and are supposed to be the cause of relapse after tumour treatment (Frank et al. 2010; S. Zhou et al. 2001). Expression of members of the ATP-binding cassette family such as P-glucoprotein (MDR1) and ABCG2 not only causes efflux of cytotoxic drugs, rendering these cells resistant to conventional chemotherapeutics, but also can lead to efflux of lipophilic fluorescent dyes like the DNA-staining dye Hoechst 33342, allowing distinction of cells that express drug efflux pumps and those that don't with flow cytometry. Cells that appear negative for fluorescence of Hoechst 33342 are called "side population" and are supposed to be cancer cells (Takubo et al. 2008). In animal experiments, CSCs are considered to be the tumour-initiating cells (TICs) that are responsible for growth of xenotransplantats in animal models (Lara-Padilla et al. 2012). Apart from their definition as side population, CSCs can be distinguished from the bulk of tumour cells by specific markers, but these markers differ between tumour types. For example, pancreatic cancer stem cells are characterised by $CD44^+CD24^+ESA^+$ marker expression profile (Li et al. 2007) with metastatic CSCs also being CD133-positive (Hermann et al. 2007), while a panel of glioblastoma stem cell markers has been suggested including CD133, integrin $\alpha 6$ and A2B5 expression (Lathia et al. 2010; Ogden et al. 2008; S. K. Singh et al. 2003). Given the fact that a lot is already known about the unique characteristics of CSCs for individual cancer types, it would be interesting to isolate the long-term survivors of *in vitro* DAB-Am16 treatment and to determine if stem-cell like properties can be detected.

However, CSCs/TICs are usually found at an extremely low concentration. Ishizawa et al. (2010) systematically compared TIC frequency in human pancreatic, non-small cell lung, and head and neck carcinomas identified with different mouse models. In all cases, the frequency did not exceed 0.04 %. In contrast, the survival rate in the MTT experiments with DAB-Am16 was at about 10 %. Thus, another mechanism might be responsible for the observed long-term resistance. Similarly, it is unlikely that the resistance occurs in a genetically distinct cell subset that is always present due to genetic heterogeneity of cancer cells, as this again would most probably be true for less than 1 % of the population. Recently, Sharma et al. (2010) showed that cancer cells can switch to a metastable drug-tolerant state upon exposure to high drug concentrations. These drug-tolerant cells (DTCs) give rise to long-term persisters including those that resume normal proliferation despite presence of the drug. This is due to chromatin remodeling associated with insulin-like growth factor 1 (IGF1) receptor signaling and KDM5A histone lysine demethylase activity resulting in reversible epigenetic modifications. Interestingly, in this experiment DTCs were shown to express the stem-cell markers CD133 and CD24. However, while DTPs remained quiescent, they gave rise to a small subset of proliferatively active drug-tolerant cells whose CD133/CD24 expression profile resembled that of the parental drug-sensitive cell population. The authors argue that although there seems to be a relationship between DTCs and CSCs, the nature of this relationship remains to be clarified. In another study, Yan et al. (2011) aimed to mimic the chronic drug exposure pattern of metronomic chemotherapy in prostate cancer cells. Yan et al. also observed the occurrence of a reversible drug-tolerant state within a distinct cell subset associated with chromatin remodeling. Strikingly, these DTCs showed a severe downregulation of CD44 that is a known marker of CSCs in prostate cancer. The CD44 downregulation is accompanied by a decreased or even abrogated tumour-initiating capacity and clonogenicity. However, after 3 months incubation of DTCs in drug-free medium, they almost completely regain the parental tumorigenicity. It

remains to be clarified if similar reversible DTCs are responsible for the appearance of a DAB-Am16-tolerant/resistant cell subset. In accordance with the observations of Yan et al., the DAB-Am16-tolerant cells show a diminished clonogenic potential. An analysis of the expression of CSC marker panels for the individual cell lines used for this study would help to understand the nature of the DAB-Am16-tolerant cell subset.

All in all, two hypotheses arise concerning the tolerant/resistant cell populations:

i) The persisters are CSCs. These cells often exhibit multidrug resistance conferred either by efflux pumps that efficiently transport drugs out of the cell, or by their quiescence that renders them elusive to drugs which predominantly affect cycling cells.

ii) The DAB-Am16-tolerant cells acquire epigenetic modifications that provide a reversible state of insensitivity to the drug. These are not necessarily CSCs. Similar to what Yan et al. (2011) suggest for their studies with paclitaxel and other chemotherapeutics, DAB-Am16 might even preferentially eliminate CSCs as the clonogenicity of the DTCs is lower than that of the parental cell population.

Clearly, these hypotheses need to be tested in order to better understand possible resistance mechanisms that could occur upon DAB-Am16-treatment in clinical context.

4.2.2 Cell cycle changes

With regard to the original hypothesis that DAB-Am16 might be cytotoxic due to interaction with DNA, it was found in this study that DAB-Am16 causes cell cycle delay with accumulation of cells with S phase DNA content on the DNA content histogram. Fig. 27 on page 88 allows an insight into how S phase cells progress over time. The cell cycle distribution of tagged original S phase cells and their progeny can be inferred from this figure. If the cells are not disturbed by cytotoxic or cytostatic compounds, they

leave the S phase and are mostly found either within G2/M oder G1 phase around 24 h later. Given that the average doubling time of MiaPaCa-2 cells is 18 h (Fig. 18), one can conclude that after 24 h, the previous S phase cells have divided into daughter cells. These daughter cells then have passed the S phase a second time to continue with the cell division cycle. The vast majority of the overall cell population (88 %) is BrdU-positive (first plot in Fig. 27 while at any given time point within 30 min only about 45 % of cells are capable of incorporating BrdU into DNA (first plot in Fig. 28 on page 89). As BrdU is stably incorporated into DNA, dividing cells will "inherit" BrdU to daughter cells and thus the progeny of BrdU-tagged cells also carries BrdU.

When a doubling time of a cell line is specified, the particular value does not mean that each cell (and its progeny) requires that particular period of time to pass the cell cycle, but rather the doubling time is an average value for the whole cell sample. Within each cell population that is not completely homogeneous, there will be cells that divide slower and cells that divide faster than the average doubling time. Cancer cell lines are prone to mutations due to the natural genetic instability of tumours, so a cancer cell line will be genetically heterogeneous due to accumulation of mutations over time. One can assume that most of those cells that are found synthesizing DNA within an arbitrarily selected time period of 30 min belong to the fast dividing subpopulation. Thus, within 24 h they will have grown faster than most of the non-labelled cells (from a slower growing subpopulation) and will produce more progeny (some of those that were at the end of the S phase at the labelling time point might have even divided twice). Furthermore, a certain part of the non-labelled cells might have been senescent and thus would not be found among the viable cells 24 h later, but rather be gated out as disintegrated cells and debris during data analysis. These two facts explain the great increase of the proportion of labelled cells 24 h after labelling with BrdU occurred. When the cells are treated with the inhibitor of DNA replication hydroxyurea, almost all of them incorporate BrdU but the cells do not proceed to further DNA

synthesis. This is consistent with the mechanism of action of hydroxyurea that acts upon dNTP pool depletion. So hydroxyurea-treated cells are capable of and ready for DNA synthesis but do not have the building blocks for building up new DNA strands. Once the dNTP-analogue BrdU is added to the surrounding medium, the cells that got stuck at the beginning of the S phase rapidly use up this BrdU for DNA synthesis. When cells are treated with DAB-Am16, a very interesting pattern is observed (Fig. 27). At a low dendrimer concentration, there are three populations with a G1 DNA content: $^{G1}BrdU^{high}$, $^{G1}BrdU^{med}$ and $^{G1}BrdU^{low}$. Furthermore, there is one population with an S phase DNA content and two populations with a G2 DNA content ($^{G2}BrdU^{high}$ and $^{G2}BrdU^{med}$). The $^{G1}BrdU^{med}$ population does not appear within the control sample. These are cells that seem to have taken up BrdU during the labelling process and then to have lost some BrdU along with DNA or having proceeded to G1 and lost BrdU on their way to this point. One possible explanation is that upon exposure to DAB-Am16, some S phase cells became arrested in this phase and started to undergo apoptosis after some time. In late apoptosis, the DNA content of these cells would have started to drop (Darzynkiewicz et al. 1992), which not only would have led to a lower DAPI fluorescence, but also to a decrease of the amount of intracellular BrdU. According to this explanation, the "new" population $^{G1}BrdU^{med}$ (as compared to the untreated control) is derived from labelled cells that did not proceed with cycling but rather started undergoing apoptosis. This idea is supported by the fact that at high DAB-Am16 concentration (last plot in Fig. 27), the whole cell population has shifted to the left compared to the untreated control, indicating a collective loss of DNA by all cells. Looking at the G2 cells, two different levels of BrdU fluorescence are observable, although there is no visible shift in DAPI fluorescence at the lowest concentration. This might well be due to the fact that the BrdU signal is amplified by the use of antibodies for detection and thus accurately reflects even subtle changes in cellular BrdU content, while DAPI fluorescence linearly corresponds to DNA content and thus might not clearly reveal small changes of DNA content. The drop

in BrdU fluorescence for $^{G1}BrdU^{med}$ cells is much more pronounced than hat for $^{G2}BrdU^{med}$ cells, so it might well be that here a mix of apoptotic G1 cells with subtle DNA content change as well as apoptotic S phase cells with a more pronounced decrease of DNA content is seen. Further experiments could help to track the populations by using different DNA synthesis labels at different time points (e.g. BrdU and EdU) and by using additional markers of cell cycle phases, e.g. cell cycle phase specific cyclins.

Interestingly, for both 5 and 15 µg/ml DAB-Am16 concentrations, the vast majority of cells appears to be labelled with BrdU if compared to the positive and negative populations within the untreated control. The previously mentioned suggestion that S phase cells would be preferentially eliminated would predict the opposite outcome: the vast majority of cells would be BrdU-negative. So the approach of cell cycle specific labelling of cells before drug treatment allows a new insight and shows how easily results of simple cell cycle profiling can be misinterpreted if not being combined with additional methods for in-depth investigation. Certainly, intracellular staining of DNA with dyes like propidium iodide or DAPI is a powerful and easy flow cytometric method that enjoys great popularity among researchers, but care should be taken not to overestimate the conclusions that can be drawn solely from this staining.

From Fig. 27 it also becomes obvious that at 50 µg/ml DAB-Am16, not only all the cells are shifted towards a decreased DNA content, but also only two BrdU fluorescence intensities can be detected. The intermediate BrdU population has disappeared. Furthermore, a greater percentage of the cells appears BrdU negative as compared to the control. There are two different scenarios that could lead to this result. The first possibility is that the higher the DAB-Am16 concentration, the faster the cytotoxic processes occur. In this case, leaving cells with lower concentration of DAB-Am16 for a longer time would yield the same result as incubating cells for a short time with a higher DAB-Am16 concentration. The second possibility is that DAB-Am16 exerts different effects depending on its concentration. For example, at a lower dendrimer concentration, S phase cells may benefit and survive

preferentially, applying additional protective mechanisms that allow them to stop cycling for a longer time before committing apoptosis, in particular due to activation of S phase checkpoints. The change to a quiescent state would also explain why there are more RNA^{low} cells with S phase DNA content than with any other DNA content in DAB-Am16-treated samples (while the pattern for non-treated samples is completely opposite) which is illustrated in Fig. 45 on page 108. At a higher concentration, the damage to the cell might be overwhelming so that these protective mechanisms might be insufficient to keep cells alive in such a preferential manner. Assuming that one of the mechanisms of DAB-Am16 action is DNA binding, a low concentration might not lead to a fast collapse of S phase cells while a high concentration might not be efficiently counteracted by the cellular DNA maintenance machinery, so the survival advantage of S phase cells would disappear. Simultaneously, a higher DAB-Am16 concentration would also increase cellular damage by other mechanisms, e.g. nanohole formation within cell membrane (facilitating leakage of intracellular DNA and other cellular content into the surrounding medium), introduction of holes into intracellular organelles (e.g. mitochondria) and so on, leading to a collective decrease of DNA content within all cells.

Fig. 28 introduces another aspect into the considerations about BrdU fluorescence. First of all, there is a tendency to a decrease of the number of DNA synthesizing cells with increasing DAB-Am16 concentration. Secondly, the last plot shows in a particularly clear manner that within the non-DNA synthesizing (BrdU negative) cells, two distinct populations appear. One of them has a slightly lower fluorescence within the BrdU channel along with a slightly lower DAPI fluorescence. As these cells belong to BrdU-negative cells, the reason cannot be a release of BrdU. Rather, it should be kept in mind that fluorescence measurements always record some cellular autofluorescence along with marker-specific fluorescence. It is a known fact that autofluorescence decreases during late apoptosis and can even be used by its own to study kinetics of apoptosis (Wolbers et al. 2004). Along with the slight decrease of DAPI fluorescence, this is another sign of the

appearance of a large apoptotic population after treatment with high doses of DAB-Am16. This factor could additionally have contributed to the drop of fluorecence in the BrdU channel observed in Fig. 27.

Having seen that the percentage of DNA synthesizing cells decreases with increasing DAB-Am16 concentration, another approach was to combine these two markers with a mitosis marker. Histone H3 becomes phosphorylated at serine 10 at the end of G2/beginning of M phase. Figs. 30 and 31 not only confirm once again the severe decrease of DNA synthesis upon DAB-Am16 treatment, but also reveal the depletion of mitosis after a prolonged incubation of cells with a high concentration of DAB-Am16. Thus, cells not only become increasingly unable to replicate their DNA, but also loose the capability to divide into daughter cells if the DNA has already been replicated. This indicates that not only G1/S phase checkpoints are involved into proliferational arrest, but there is another checkpoint at G2 that abrogates cell division. The G2 checkpoint might become activated upon incomplete or erroneous DNA replication or due to DNA damage.

Surprisingly, staining of the marker for DNA damage and stalled replication forks γ-H2A.X yields a negative result (Fig. 25 on page 85). H2A.X becomes phosphorylated far upstream within the DNA damage response pathway (Fig. 8 on page 41) and triggers the repair mechanisms. From the other observations presented within this thesis as well as from the dendrimer structure and its established applications, the assumption that it at least partly acts via DNA interaction appears to be reasonable. However, it is not known much about the nature of this assumed interaction, so it will be subject of future investigation whether DAB-Am16 indeed interacts with nuclear DNA in a way that prevents phosphorylation of histone H2A.X because this interaction/damage might not be sensed by upstream pathway members. Independently from the reasons for this lack of phosphorylation, the absence of γ-H2A.X indicates that most probably DNA repair mechanisms are not initiated upon DAB-Am16 exposure. On the other hand, although Omidi et al. (2005) also could not directly detect DNA damage upon exposure to PPI dendrimers, they saw an upregulation of proteasome

α4 (a DNA double-strand repair facilitator) upon exposure to these dendrimers (section 1.2.7). A more detailed investigation of DNA integrity and of activation of DNA repair pathways caused by PPI dendrimers is required.

Another experiment showed that cell cycle delay was accompanied by a decrease of the cyclin D1 level (Fig. 29 on page 91). The higher the concentration of DAB-Am16, the larger the population of cells with decreased amount of cyclin D1. It is well known that cyclin D1 is quickly degraded upon genotoxic stress (Agami et al. 2000; Pontano et al. 2008). The kinase ATM is activated upon DNA damage, it in turn activats the F-box protein FBXO31 which promotes degradation of cyclin D1 (Santra et al. 2009). If this pathway is also true for DAB-Am16-induced cyclin D1 loss, then it again remains to be clarified why phosphorylation of histone H2A.X which would be part of the DNA damage signaling pathway that involves ATM could not be detected. Strikingly, Jirawatnotai et al. (2011) showed that apart from playing a major role in G1/S transition, cyclin D1 also facilitates homologous recombination-mediated DNA repair by BRCA2-dependent recruitment of RAD51 to DNA damage sites. This does not contradict the notion of DNA damage-induced cyclin D1 degradation, as Jirawatnotai et al. observed that it is the remaining low amount of cyclin D1 that contributes to the repair process. It would be interesting to see if a colocalisation of RAD51 and cyclin D1 can be observed upon DAB-Am16 treatment in order to better understand if DAB-Am16 exerts its cytotoxic effect via genotoxic stress and if DNA repair mechanisms are triggered even bypassing H2A.X phosphorylation.

The effect of DAB-Am16 was also tested *in vivo* with MiaPaCa-2 tumour xenografts in immunodeficient mice. The cell cycle profile of the control tumours differs considerably from the *in vitro* profile. Tumour-derived cells exhibit a distinct S phase peak that has not been observed *in vitro*. In view of this fact, one should be very cautious when trying to transfer conclusions drawn from experiments within a cell culture environment onto living organisms. However, in this case, DAB-Am16 not only affects cell cycle *in vitro*, but also alters the cell cycle profile of the xenograft tumour cells. In

both cases, S phase cells appear to be most sensitive to the dendrimer. Cells from 3 out of 4 DAB-Am16-treated tumours completely lack S phase and have only a very small G2/M peak. Together with the immunohistochemical observation that the proliferation marker Ki-67 is expressed with the same frequency in treated and untreated tumour samples, it appears that in the *in vivo* settings MiaPaCa-2 cells are arrested in G1 (not in the quiescent G0 state), but remain ready for further proliferation once the cause of the cell cycle arrest (the dendrimer) would be withdrawn. It remains to be tested in further experiments if this assumption is true. Furthermore, it would be interesting to know if the disappearance of S phase cells in treated tumours results from selective death of cells that were hit within this phase, or if the cells continued their cell cycle until G1 and became arrested in that phase.

4.2.3 Apoptotic cell death and cell membrane permeabilisation

Much of the implications of the experiments conducted on apoptotic aspects of DAB-Am16 effects have been discussed in section 3.6, so only the key points are to be highlighted in the current section. As described in section 1.3.3, cell death can be the result of different pathways. Within this project, it has been shown that apoptosis is triggered by DAB-Am16 exposure and particular attention was paid to the course of apoptotic events that occur upon DAB-Am16 treatment. Using multicolour flow cytometry, it has become evident that cell membrane permeabilisation, increase of light side scatter and activation of caspase-3 are associated with cellular demise caused by DAB-Am16. This is followed by the loss of mitochondrial membrane potential, decreased forward scatter and finally disintegration of the cell. This is true for all three cell lines tested. The results presented in this thesis suggest that caspase-3 is activated prior to the collapse of $\Delta\Psi_{\mathrm{m}}$. This is in line with the findings of Bossy-Wetzel et al. (1998); Karpinich, Tafani, Rothman et al. (2002); Karpinich, Tafani, Schneider et al. (2006).

Apoptosis is a process that involves a molecular cascade, and cell death itself occurs downstream of this cascade. One of the latest (necrotic)

events is permeabilisation of the plasma membrane. Thus, cell death via apoptosis is not an immediate reaction on the presence of cytotoxic substances. Compromised cell membrane appeared within 20–25 min after addition of DAB-Am16 to the cell culture medium (Fig. 23 on page 81). This time period is too short for the process of reception of apoptotic trigger, apoptotic cascade and final cell disintegration. Thus, this quick cell membrane damage can only be caused either by oncosis/necrosis or by direct membrane damage by the dendrimer. As a number of experiments have shown that cell death occurs via apoptosis in DAB-Am16-treated cells (section 3.6), one can assume that DAB-Am16 directly damages the cell membrane. This is supported by the literature (section 1.2.4). According to the literature, PAMAM and other dendrimers cause lipid bilayer destruction, either by extension of pre-existing membrane defects or by creating new ones. The results presented in this thesis are a first hint that membrane damage is also caused by DAB-Am16. Previous experiments of our group showed that fluorescently labelled DAB-Am16 can be detected within the nucleus 30 min after its addition to the culture medium. This time frame corresponds very well with the data obtained by observation of DAPI entrance. Furthermore, the observation that the percentage of U87MG cells with apoptotic characteristics is increased after 30 min exposure to DAB-Am16 (section 3.6.3) also supports the DAPI entrance data. Additionally, as justified on page 102, there is evidence that while the holes created by DAB-Am16 permit entrance of DAPI into the cell, they are not large enough to allow leakage of large cytosolic ingredients into the surrounding medium. This only happens during late stage apoptosis (designated as secondary necrosis). Thus, although evidence for cell membrane hole formation by DAB-Am16 was found within this study, this process was not identified as the cause of cell death.

Oncotic cell death usually refers to an unspecific and fast cell death. Due to its unspecificity, a molecule that can induce oncosis most probably will do so in a range of different cell types and settings. On the other hand, apoptosis relies on intracellular molecules that might or might not consider

a signal to be apoptotic. A chemical that causes apoptosis in one particular cell type or within one particular tissue will not necessarily also induce apoptosis in other cell types. In fact, this is why cancer treatment fails in many cases: tumour cells often gain resistance to apoptotic signals due to genomic mutations. On the other hand, a compound that drives tumour cells into apoptosis might not be that toxic to non-transformed cells. Thus, the fact that DAB-Am16 triggers apoptosis rather than oncosis gives hope to specificity of its action. However, it also raises concerns that cancer cells with particular mutations within the apoptotic pathway might overcome DAB-Am16 toxicity. For this reason, thorough investigation of how exactly DAB-Am16 activates the apoptotic machinery will help to predict which patients might benefit from its administration.

4.3 *In vivo* evaluation

The significance of *in vitro* work in the field of drug discovery to a large extent depends on whether eventually this drug will be safe enough to be administered in the clinical context while improving the outcome of the patients. In particular, the new drug should have advantages over existing drugs for the disease it is intended to target. Thus, the effect of DAB-Am16 was also tested *in vivo* with MiaPaCa-2 tumour xenografts in immunodeficient mice. The measured outcomes were kinetics of tumour growth, toxicity and *in vivo* effect on the cell cycle profile of tumour cells. Treatment effect was compared with the current chemotherapeutic gold standard in treatment of pancreatic cancer, namely administration of gemcitabine. One should point out that although gemcitabine remains standard treatment for unresectable pancreatic adenocarcinoma, it is not a curative treatment, but rather serves to prolong survival. Even under gemcitabine treatment, the overall survival with chemotherapy alone is 9.2 months (Loehrer et al. 2011). Certainly, tumour xenografts in mice do not reproduce the course of disease of spontaneously occurring tumours

in humans. However, such studies allow a first assessment if a compound should be further evaluated as a potential, promising new drug.

For the *in vivo* assessment, mice with growing MiaPaCa-2 xenografts were divided into three groups: untreated control, DAB-Am16-administered and gemcitabine-administered. Fig. 49 on page 112 shows that at the onset of the treatment, the tumours of control and DAB-Am16-treated groups had the same mean size, while the mean tumour size of the mice in the gemcitabine group was slightly less, although not significantly. For the next four days after the first injection, the DAB-Am16-treated mice exhibited further tumour growth, although it was not as steep as the growth within the control group. However, on day 14 the tumour size decreased to the level of the first treatment day and remained approximately the same with minor fluctuations until day 25 when the animals were sacrificed. From day 19, the difference between the control group and the two treated groups became significant, and a steep tumour growth within the control group was observed. There was no significant difference in tumour size between the DAB-Am16 and the gemcitabine groups, although the tumour size within the gemcitabine group remained slightly lower over the whole time course. However, this might be due to the slightly smaller mean tumour size at treatment onset. Evidently, DAB-Am16 had a beneficial effect on the clinical outcome in this experiment that was similar to that of gemcitabine. This result is in line with the report of Dufes et al. (2005) that A431 epidermoid carcinoma, LS174T colorectal adenocarcinoma and C33a cervix carcinoma xenograft growth is delayed by administration of DAB-Am16, thus corroborating the notion that further exploration of DAB-Am16 as a potential anti-tumour agent is highly desirable.

Safety of DAB-Am16 administration was assessed by measurement of animal weight and observation of animal behaviour. After the first injection of DAB-Am16, a profound weight loss was detected. However, the weight rose to the previous value one day later and remained stable over the whole experimental period. In fact, the mean animal weight was higher than that of control and of gemcitabine animals during the last three measurements.

The behaviour of the animals appeared to be normal within all three groups. There was one animal death within the DAB-Am16 group. However, the reason for the death was unclear as one day before being found dead, this animal behaved normally and showed neither signs of above-average distress or discomfort nor signs of additional physical ailments. The corpse did not allow any conclusions on possible death reasons, and an examination of the organs did not show any abnormalities. Thus, it remains unclear if this death was related to dendrimer toxicity. Overall, the toxicity profile can be appraised as favourable.

Prior to sacrificing the mice, several pictures were taken of each tumour. Later on, the tumours on the pictures were semi-quantitatively assessed for vascularisation of the tumour. Tumour vascularisation is an important target of anti-cancer therapies and a number of anti-angiogenic compounds are used in cancer treatment (Linkous et al. 2012). It has been reported by Al-Jamal et al. (2010) that poly-L-lysine (PLL) dendrimers exert an anti-angiogenic effect in mouse tumour models. With DAB-Am16, a tendency to decreased vascularisation can be concluded from the tumour photos. However, the effect is weak and is likely not to be the main mechanism of action.

As for the molecular investigation, the cell cycle profile of the control tumours differs considerably from the *in vitro* profile. Tumour-derived cells exhibit a distinct S phase peak that has not been observed *in vitro*. In view of this fact, one should be very cautious when trying to transfer conclusions drawn from experiments within a cell culture environment onto living organisms. However, in this case, DAB-Am16 not only affects cell cycle *in vitro*, but also alters the cell cycle profile of the xenograft tumour cells. Interestingly, cells from 3 out of 4 DAB-Am16-treated tumours completely lack S phase and have only a very small G2/M peak. It is not clear whether this is due to selective elimination of S phase cells or if an arrest of the cells within the G1 phase prevails. Further investigations on this issue is necessary, e.g. by BrdU injection a short time before killing the animals and

evaluation of the number of BrdU positive (even though maybe otherwise dead) cells within the tumours.

Additionally to cell cycle analysis, immunohistochemical staining of parts of the tumour for the proliferation marker Ki-67 is performed. Similar expression was found in treated and untreated tumour samples, indicating that the readiness to further proliferate is not affected by DAB-Am16. Taken together these and the cell cycle results, it appears that in the *in vivo* settings MiaPaCa-2 cells are arrested in G1 (not in the quiescent G0 state), but remain ready for further proliferation once the cause of the cell cycle arrest (the dendrimer) would be withdrawn. This is a tremendously important issue that has to be addressed within further experiments. It is a commonly known problem that even after apparent disappearance of the tumour upon chemotherapeutic treatment, a relapse can occur at a later time, indicating that a subset of tumour cells is often able to persist for a longer period of time. Additionally, it is also known that in some cases a tumour rebound occurs after chemotherapeutic treatment associated with remarkably accelerated tumour regrowth (Bourhis et al. 1994; El Sharouni et al. 2003; Shaked et al. 2008). Based on the results of the DAB-Am16 study, it is conceivable that after DAB-Am16 withdrawal the tumour cells that are virtually synchronized within the G1 phase and ready to resume proliferation, would do so within a short time frame leading to a rebound effect. This does not need to be the case, but it is an important issue for future investigations.

The specificity of DAB-Am16 effects in the *in vivo* studies so far has been remarkable. However, the reasons for this specificity remain obscure. While selective targeting of transformed tumour cells on the molecular level is possible, another explanation could be selective accumulation of the dendrimer within the tumour microenvironment. Tumour growth relies on an immense supply of nutrients and oxygen which can only be achieved by the creation of new blood vessels (angiogenesis). The newly built capillaries are fenestrated, i.e., their endothelial cells contain pores, and these pores are larger than the pores of most other capillaries of the body. Thus,

macromolecules can gain access to tumour environment through these pores, while not being able to get into healthy tissue. Once the molecules are within the tumour environment, they are not removed as efficiently as they would be from other organs, as tumour tissue usually lacks efficient lymphatic drainage. Altogether, this is called "enhanced permeability and retention effect" (EPR) and accounts for the selective accumulation of macromolecules, liposomes and nano-scaled drugs within the tumour tissue (Greish 2010; Maeda et al. 2009; Matsumura et al. 1986). However, the EPR effect only leads to preferential drug accumulation in tumour tissue for drugs that escape renal clearance and that cannot cross endothelial tight junctions of normal vasculature, thus setting a molecular cut-off of approximately 20–40 kDa (Greish et al. 2003; Haag et al. 2006) which is well above the size of DAB-Am16 (1.7 kDa). However, preferred accumulation in tumour tissue could be aided by the positive charge of DAB-Am16. This is because tumour vasculature as well as the outer membrane of tumour cells are negatively charged (Ran et al. 2002; Szachowicz-Petelska et al. 2010). Once within the tissue, again, increased retention as stated by the EPR effect would lead to DAB-Am16 accumulation at the tumour site, providing the specificity observed during the *in vivo* studies.

5 Outlook

The work presented in this thesis contributes to the knowledge about the action of DAB-Am16. However, there are still a lot of questions to be answered and a lot of research to be done until the details of this pathway will be unveiled. Furthermore, it remains to be clarified if other dendrimers and in a broader way polymers might have a similar or even stronger anti-cancer effect *in vivo*, and if yes, if the mechanism of action is the same. The following topics constitute a selection of topics worth to be investigated.

5.1 Molecular pathways

A detailed investigation of the molecular players involved into cell cycle disturbance and cellular demise was beyond the scope of this research project. However, without any doubt this will be the next step on the way to unravelling the effect of DAB-Am16 onto cells. In section 1.3.2, I introduced the pathway that leads to S phase arrest in response to DNA damage or stalled replication. Although no γ-H2A.X could be detected after DAB-Am16 exposure of cells, I would not reject the idea of interaction between nuclear DNA and the dendrimer, especially in view of the massive cell cycle disturbance that has been observed predominantly within the S phase. Thus, probing if other members of the pathway in Fig. 8 on page 41 become activated after incubation of cells with DAB-Am16 would be desirable. Furthermore, a more detailed investigation on the possible occurrence of DNA damage with additional tests, e.g. the COMET assay is a highly sensitive and versatile assay for probing a range of different DNA damage modalities on the level of individual cells including those that possibly would not be accompanied by histone H2A.X phosphorylation like DNA crosslinking (N. P. Singh et al. 1988). Central players of DNA damage response machinery like ATM, ATR, CHK1 and CHK2 should be examined, along with a more in-depth investigation of the cell cycle after DAB-Am16 exposure. Cell cycle investigations could include double-labelling with

dNTPs analogues, e.g. labelling S phase cells before addition of DAB-Am16 with BrdU and labelling S phase cells after DAB-Am16 exposure with EdU within one sample. BrdU and EdU can then be detected in different fluorescence channels to track the fate of S phase cells in a precise way. Staining for cell cycle phase specific markers like particular cyclins could help to discern the subtleties that cannot be seen just by DNA staining.

Within the presented work, it was shown that caspase-3 dependent apoptosis is initiated upon DAB-Am16 exposure. However, caspase-3 is situated quite far downstream of the apoptotic pathway. It is not known how apoptosis is initiated upon DAB-Am16 treatment. Different initiator caspases are activated by different apoptotic stimuli, so further dissecting this pathway would help to understand the precise mode of action of DAB-Am16.

Detailed kinetic studies would allow an insight into the speed with which the cells get damaged. In particular, continuous imaging techniques of live cells would allow to create a precise profile of how cells react to DAB-Am16. New technologies like chipcytometry that can record changes of live cells over time including changes in marker fluorescences could aid achieving this aim.

5.2 Resistance mechanisms

As discussed in section 4.2.1, a small population of cells within each tested cell line appears to be resistant to DAB-Am16-induced cell death. It is of tremendous importance to understand which mechanisms contribute to the resistance. This knowledge would help to choose those patients that will most probably benefit from DAB-Am16 in clinical trials, and it might become possible to combine DAB-Am16 with other drugs that would act against additional molecular targets and eliminate the DAB-Am16-resistant cells. Furthermore, the selection of the treatment regimen also depends on this knowledge. For example, metronomic therapy, reviewed in Pasquier et al. (2010), defines a comparatively novel cancer therapy schedule based

on the the observation that anti-angiogenic as well as some other drugs with specific mechanisms of action exert a better anti-cancer effect when being administered almost continuously for a long period of time at low doses instead of following the classical schedule of high dose intermittent chemotherapy blocks. Testing different treatment schedules for DAB-Am16 *in vitro* (continuous vs. intermittent exposure, combination of different treatment and recovery times with different drug concentrations) to find the schedule that eliminates even the currently resistant subpopulation would contribute to the development of a suitable administration schedule in clinical trials. Time-resolved studies of apoptosis and cell cycle disturbance would further help to decide on the best treatment modalities.

5.3 Entry into the cell

At present, there is no clear answer to the question how DAB-Am16 gains access to the interior of the cell. Sections 1.2.4 and 1.2.5 describe that evidence for both nanohole formation in the cell membrane as well as for endocytotic uptake exists. Most probably, the mechanism depends on the polymer/dendrimer tested, on the cell line used for the tests, the polymer/dendrimer concentration and other factors. Most of the studies that have been conducted in this field have looked at PAMAM dendrimers, and only very few studies involved PPI dendrimers. Thus, there is a need for thorough investigation on the cell entrance mechanism of DAB-Am16. Preliminary experiments with scanning ion-conductance microscopy showed that this technique is capable of visualizing cell membrane defects in the nanometer range. As this scanning technique does not involve any contact between the cell surface and the microscope parts, and it furthermore allows recording of the cells within their natural environment for long time periods, it could reveal the existence or lack of holes within the cell membrane, and in case of their existence this technique would allow insight into kinetics of hole occurrence as well as help to determine if these holes are transient or permanent (and thus, if they actually cause the cell death

or not). A range of available endocytosis markers and inhibitors in turn makes it possible to investigate cell entrance from this point of view. Finally, fluorescent labelling of dendrimers, e.g. with dye NHS esters, along with fluorescent labelling of intracellular compartments could help to visualize the intracellular localisation of the dendrimer at particular time points or even over a continuous period of time.

5.4 Comparison with non-tumour cells

The work presented in this thesis was aimed to shed light onto the mechanism of action of DAB-Am16. However, in terms of cancer drug development, it is important that the drug not only triggers death of tumour cells but also spares healthy tissue. A common problem in cancer treatment is that chemotherapeutics cause organ toxicity, and in particular bone marrow toxicity. This hematopoietic toxicity is the cause of immune suppression after treatment with cancer chemotherapeutics and makes the patient particularly susceptible to severe infections that can be fatal. Decreased blood cell count requires frequent blood transfusions that can lead to iron overload and put the patients at risk of getting infected with hepatitis viruses, HIV and similar diseases transferred with infected blood. Furthermore, immune depletion makes it impossible to administer cancer therapeutics continuously. They are rather administered over a short time, followed by a break that allows the patients' organism to recover. However, cancer cells get the opportunity to further divide during this time as well. If the tumour cells recover faster than the healthy tissues, the disease becomes incurable. Research on protection of healthy tissues is under way. Recently, Adair et al. (2012) developed a gene therapy method to make the patient's hematopoietic stem cells less susceptible to chemotherapeutics. In this study, genetic modifications of patients' own hematopoietic stem and progenitor cells and the following autologous bone marrow transplantation with the genetically modified cells allowed the physicians to administer high doses of the alkylating agent temozolamide together with the inhibitor of methyl-

guanine methyltransferase (MGMT) O^6-benzylguanine (O^6BG). MGMT was overexpressed in the glioblastoma cells of these patients, making the tumour resistant against temozolamide by increased repair of DNA damage caused by this drug. However, administration of O^6BG to deplete this resistance would have resulted in severe bone marrow toxicity. Successful engraftment of O^6BG-resistant hematopoietic cells considerably alleviated bone marrow toxicity of O^6BG. Median survival time of glioblastoma patients since diagnosis is 12 months, with unmethylated MGMT promoter being prognostically unfavourable (Krex et al. 2007). Two participants of this study survived 14 and 20 months, respectively, while the 3rd is still alive without disease progression after 34 months. If these results can be repeated in large-scale studies, this could be considered as a break-through in glioblastoma therapy.

This example illustrates the importance of drug selectivity for treatment success. Thus, it does not suffice to develop a drug that effectively eliminates cancer cells but it is crucial to ensure that this drug lacks organ toxicity. The mice in the *in vivo* experiments with DAB-Am16 did not exhibit apparent toxicity. One death was observed, but the relation to treatment remains doubtful. Importantly, this observation gives hope that DAB-Am16 might exert selective toxicity against tumour cells. If this will be the case in clinical trials, development of concomitant organ-protective therapy would become obsolete. Further investigations of this issue in *in vitro* settings are necessary. In fact, preliminary experiments have been conducted with WI-38 human embryonic lung fibroblasts in our group which revealed a higher EC50 value and thus lower sensitivity of these non-cancer cells to DAB-Am16. However, although this cell line is not derived from a tumour, it has the capability of long-term division (approx. 50 population doublings) in tissue culture. In general, unlimited cell division is a feature of cancer cells, while untransformed cells have a very limited divisional capability. Thus, one can assume that WI-38 cells are not a typical representative of healthy cells. To examine the effect of DAB-Am16 on healthy tissue, primary untransformed cells from different tissues should be used. Comparative cytotoxicity assays

should be performed on cancer cells and on healthy primary cells from different tissues as well as blood cells (hemolysis assays). However, one should keep in mind that toxicity against healthy tissue might be decreased *in vivo* compared to *in vitro* due to selective accumulation of DAB-Am16 within the tumour environment and thus spatial sparing of healthy organs. Approaches to examine this issue are described in section 5.6.

5.5 Effectivity and safety of structurally related macromolecules

DAB-Am16 is a PPI dendrimer, and as we have seen that DAB-Am16 exerts an anti-cancer effect in xenografts, one may reasonably expect that other dendrimers might have a similar effect. In general, the toxicity of dendrimers increases with generation number, as described in section 1.2.3. However, Moroson (1971) showed that increasing cationic charge also means increasing effectivity against tumours. By comparison of different types of structurally related macromolecules (PAMAM dendrimers, PLL dendrimers, linear and branched polymers) it might be possible to find a compound that outmatches DAB-Am16 when it comes to the balance of effectivity and safety. Thus, systematic *in vitro* comparison with subsequent *in vivo* tests of promising drug candidates should be performed.

5.6 Further *in vivo* studies

The *in vivo* investigation of DAB-Am16 has just begun. Cancer is a general term for a very heterogeneous set of diseases. Tumours can be derived from almost each cell type, and combinations of many different mutations can lead to the same result: uncontrolled cell division and tumour growth. Selection of suitable treatment modalities depends on the tumour origin, on the mutations that led to tumour formation, on the stage of disease and on the individual situation of the patient. No single drug is conceivable that would be effective against all tumour types. To account at least for a

part of the disease varieties, DAB-Am16 should be tested against a large selection of xenografts. This would help to decide upon tumour types that respond best to this compound and that one should focus on when aiming for application in humans. Another aspect that the xenograft used for the present study was injected subcutaneously. Orthotopic xenografts that are grown within same tissue environment that the tumour cells originate from would mimic the clinical settings better than subcutaneous tumours. Inclusion of metastatic disease models will show if DAB-Am16 can prevent metastasis or if it can act effectively against existing metastatic lesions. It is important to follow up animals where DAB-Am16 led to disappearance of the tumour, as a relapse might occur later. Also, a comparison of growth kinetics of non-treated tumours with tumours that previously had been treated with DAB-Am16 for a limited time would help to understand if an accelerated tumour cell growth might be an issue in case treatment with DAB-Am16 would have to be discontinued.

Another approach would be to get away from xenograft usage and to apply DAB-Am16 onto tumours derived from the same species as the test animals or even onto naturally occurring tumours. Although animal organisms, cells and thus also tumours differ from humans, the fact that the animals would bear the natural immune system, the tumours would develop within the natural microenvironment including normal tissue vascularisation, and naturally occuring tumours would not be as homogeneous as tumours derived from a single cell line might improve prognostic relevance of these studies. To get even closer to human clinical settings, animals with more similar disease course to humans than mice could be used. In fact, plans exist to further test DAB-Am16 as an anti-cancer agent for canine patients of veterinary clinics. The knowledge derived from such experience would be invaluable for planning clinical studies with human patients.

In section 4.3, the question was raised whether DAB-Am16 impedes tumour growth while sparing healthy tissues due to a modification of the EPR effect. This issue should be addressed in future studies. To investigate if this plays a role in selective tumour targeting by DAB-Am16,

biodistribution of the dendrimer should be investigated. To get to the bottom of the reasons for it, the distribution of the dendrimer among the organs over time needs to be investigated. For thorough investigation of DAB-Am16 specificity, determination of *in vivo* biodistribution of the dendrimer is required. Whole animal bioimaging after administration of fluorescently labelled DAB-Am16 would reveal the distribution between the organs in a time-resolved manner.

Systematic and extensive testing of the responding and not-responding tumours for differences in cell cycle progression, cell proliferation, expression of proliferation as well as apoptotic markers and examination of tumour vascularization will help to understand if the mechanism of action of DAB-Am16 *in vivo* is similar to that *in vitro*. Just as S phase cells can be identified in cell culture by BrdU incorporation, mice can also be injected with BrdU before being sacrificed, so that the proportion of S phase tumour cells can be determined and compared between different tumours and between responders/non-responders.

6 Conclusions

Within the project described in this thesis, the dendrimer DAB-Am16 was characterised from the chemical and the biological point of view. ^{1}H, ^{16}C and COSY NMR, MS/MS, MALDI-TOF, and elemental analysis showed that DAB-Am16 retains its chemical structure after prolonged periods of use as well as within a wide range of storage temperatures.

According to *in vitro* cytotoxicity assays, DAB-Am16 exerts a profound cytotoxic effect on MiaPaCa-2, U87MG, A431, A2780, H1299 and MDAMB231 cancer cell lines. Furthermore, it has a lasting inhibitory effect on cell division as indicated by diminished growth of new cell colonies. The EC50 steeply decreases within the first doubling time of the cell line, while remaining stable during longer exposure of cells to DAB-Am16. Several explanations are conceivable in the face of these results. It remains to be investigated whether the concepts of cancer stem cells or of acquisition of reversible epigenetic modifications are applicable in this case.

Detailed examination of the cell cycle changes after DAB-Am16 exposure revealed severe disturbance of the cell cycle. At low DAB-Am16 concentrations, cell cycle is delayed, while high dendrimer concentrations completely abrogate DNA synthesis and mitosis. Some evidence has been presented for S phase cells being more resistant to death at low DAB-Am16 concentrations by acquiring a quiescent-like state, while these cells are more susceptible to DAB-Am16-induced cell death at high dendrimer concentrations. However, this issue is to be investigated in greater detail.

A number of apoptotic characteristics were observed that together yield strong evidence for apoptotic processes being elicited upon DAB-Am16 exposure of cancer cells. This implies a specific mode of triggering cell death, giving rise to the hope that cancer cells might be more efficiently targeted by DAB-Am16 than non-transformed cells. DNA damage was found not to be involved in the process of cellular demise. Hole formation in the plasma membrane is likely to be the way the dendrimer enters the cells,

but this also does not seem to be the reason for cell death. The precise pathway needs to be examined in further detail.

Finally, *in vivo* testing was undertaken to assess the effect of DAB-Am16 on human pancreatic cancer xenografts in mice. The dendrimer was at least as effective as the gold standard gemcitabine, while showing a good safety profile. The tumour size of dendrimer-treated mice remained stable over time, while the non-treated tumours exhibited fast growth. Due to the relatively small cohort of mice this experiment should be repeated on a larger scale. Modifications of the experimental setup for gaining additional information have been suggested in this thesis. However, this thesis presents strong evidence for a specific anti-tumour effect of DAB-Am16 *in vivo*.

On the whole, the data presented in this thesis implicates the need to continue investigations on dendrimers as a novel class of therapeutic compounds, and specifically on DAB-Am16 as a promising drug candidate in cancer therapy.

References

Adair, Jennifer E et al. (2012). 'Extended Survival of Glioblastoma Patients After Chemoprotective HSC Gene Therapy'. *Sci Transl Med* 4.133, pp. 133–57.

Adhiya, Anuj et al. (2002). 'Poly(propylene imine) dendrimer conformations in the gas phase: a tandem mass spectrometry study'. *Int J Mass Spectrom* 214.1, pp. 75–88.

Agami, Reuven et al. (2000). 'Distinct initiation and maintenance mechanisms cooperate to induce G1 cell cycle arrest in response to DNA damage'. *Cell* 102.1, pp. 55–66.

Ahsen, Oliver von et al. (2000). 'Preservation of mitochondrial structure and function after Bid- or Bax-mediated cytochrome c release.' *J Cell Biol* 150.5, pp. 1027–1036.

Akesson, Anna et al. (2010). 'The effect of PAMAM G6 dendrimers on the structure of lipid vesicles.' *Phys Chem Chem Phys* 12.38, pp. 12267–12272.

Aktories, Klaus et al. (2005). *Allgemeine und spezielle Pharmakologie und Toxikologie*. 9th ed. Urban & Fischer.

Alao, John P (2007). 'The regulation of cyclin D1 degradation: roles in cancer development and the potential for therapeutic invention.' *Mol Cancer* 6, p. 24.

Albertazzi, Lorenzo et al. (2010). 'Dendrimer Internalization and Intracellular Trafficking in Living Cells.' *Mol Pharm* 7.3, pp. 680–688.

Anoopkumar-Dukie, Shailendra et al. (2005). 'Resazurin assay of radiation response in cultured cells'. *Br J Radiol* 78.934, pp. 945–7.

Arnoult, Damien et al. (2002). 'Mitochondrial release of apoptosis-inducing factor occurs downstream of cytochrome c release in response to several proapoptotic stimuli.' *J Cell Biol* 159.6, pp. 923–929.

Barbus, Sebastian et al. (2011). 'Differential retinoic acid signaling in tumors of long- and short-term glioblastoma survivors.' *J Natl Cancer Inst* 103.7, pp. 598–606.

Bartek, Jiri et al. (2004). 'Checking on DNA damage in S phase.' *Nat Rev Mol Cell Biol* 5.10, pp. 792–804.

Bates, Stewart et al. (1995). 'Cyclin D1 as a cellular proto-oncogene.' *Semin Cancer Biol* 6.2, pp. 73–82.

Bernas, Tytus et al. (2002). 'Mitochondrial and nonmitochondrial reduction of MTT: interaction of MTT with TMRE, JC-1, and NAO mitochondrial fluorescent probes.' *Cytometry* 47.4, pp. 236–242.

Berridge, Michael V, Patries M Herst et al. (2005). 'Tetrazolium dyes as tools in cell biology: new insights into their cellular reduction.' *Biotechnol Annu Rev* 11, pp. 127–152.

Berridge, Michael V and An S Tan (1993). 'Characterization of the cellular reduction of 3-(4,5-dimethylthiazol-2-yl)-2,5-diphenyltetrazolium bromide (MTT): subcellular localization, substrate dependence, and involvement of mitochondrial electron transport in MTT reduction.' *Arch Biochem Biophys* 303.2, pp. 474–482.

Berridge, Michael V, An S Tan et al. (1996). 'The biochemical and cellular basis of cell proliferation assays that use tetrazolium salts'. *Biochemica* 4, pp. 14–19.

Bhadra, Dipankar et al. (2005). 'Glycodendrimeric nanoparticulate carriers of primaquine phosphate for liver targeting'. *Int J Pharm* 295.1-2, pp. 221–33.

Bianchi, Vera et al. (1986). 'Changes of deoxyribonucleoside triphosphate pools induced by hydroxyurea and their relation to DNA synthesis.' *J Biol Chem* 261.34, pp. 16037–16042.

Biliran, Hector et al. (2005). 'Overexpression of cyclin D1 promotes tumor cell growth and confers resistance to cisplatin-mediated apoptosis in an elastase-myc transgene-expressing pancreatic tumor cell line.' *Clin Cancer Res* 11.16, pp. 6075–6086.

Bird, Martin C et al. (1987). 'Comparison of in vitro drug sensitivity by the differential staining cytotoxicity (DiSC) and colony-forming assays'. *Br J Cancer* 55.4, pp. 429–31.

Blickwedehl, Jennifer et al. (2012). 'The Proteasome Activator PA200 Regulates Tumor Cell Responsiveness to Glutamine and Resistance to Ionizing Radiation'. *Mol Cancer Res* 10.7, pp. 937–44.

Böck, Günther (2001). 'Current status of flow cytometry in cell and molecular biology'. In: *International Review of Cytology*. Ed. by Kwang W Jeon. Vol. 204, pp. 239–298.

Bonfoco, Emanuela et al. (1995). 'Apoptosis and necrosis: two distinct events induced, respectively, by mild and intense insults with N-methyl-D-aspartate or nitric oxide/superoxide in cortical cell cultures.' *Proc Natl Acad Sci U S A* 92.16, pp. 7162–7166.

Bonnet, Dominique et al. (1997). 'Human acute myeloid leukemia is organized as a hierarchy that originates from a primitive hematopoietic cell'. *Nat Med* 3.7, pp. 730–7.

Borenfreund, Ellen et al. (1985). 'Toxicity determined in vitro by morphological alterations and neutral red absorption'. *Toxicol Lett* 24.2-3, pp. 119–24.

Boris, David et al. (1996). 'A Self-Consistent Mean Field Model of a Starburst Dendrimer: Dense Core vs Dense Shell'. *Macromolecules* 29.22, pp. 7251–7260.

Bossy-Wetzel, Ella et al. (1998). 'Mitochondrial cytochrome c release in apoptosis occurs upstream of DEVD-specific caspase activation and independently of mitochondrial transmembrane depolarization.' *EMBO J* 17.1, pp. 37–49.

Bourhis, Jean et al. (1994). 'Rapid tumor cell proliferation after induction chemotherapy in oropharyngeal cancer'. *Laryngoscope* 104.4, pp. 468–72.

Brydøy, Marianne et al. (2007). 'Gonadal dysfunction and fertility problems in cancer survivors.' *Acta Oncol* 46.4, pp. 480–489.

Buck, Suzanne B et al. (2008). 'Detection of S-phase cell cycle progression using 5-ethynyl-2'-deoxyuridine incorporation with click chemistry, an alternative to using 5-bromo-2'-deoxyuridine antibodies'. *Biotechniques* 44.7, pp. 927–9.

Buhleier, Egon et al. (1978). '"Cascade"- and "Nonskid-Chain-like" Syntheses of Molecular Cavity Topologies'. *Synthesis* 2, pp. 155–158.

Bulavin, Dmitry V et al. (2001). 'Initiation of a G2/M checkpoint after ultraviolet radiation requires p38 kinase.' *Nature* 411.6833, pp. 102–107.

Cavallo, Luigi et al. (1998). 'A Molecular Dynamics Study of the First Five Generations of Poly(Propylene Imine) Dendrimers Modified with N-tBoc-L-Phenylalanine'. *Chemistry - A European Journal* 4.5, pp. 927–934.

Chai, Minghui et al. (2001). 'Structure and conformation of DAB dendrimers in solution via multidimensional NMR techniques.' *J Am Chem Soc* 123.20, pp. 4670–4678.

Chooi, Kar Wai (2007). 'A new class of Polymeric Amphiphile.' PhD thesis.

Chung, Daniel C (2004). 'Cyclin D1 in human neuroendocrine: tumorigenesis.' *Ann N Y Acad Sci* 1014, pp. 209–217.

Coller, Hilary A (2007). 'What's taking so long? S-phase entry from quiescence versus proliferation'. *Nat Rev Mol Cell Biol* 8.8, pp. 667–70.

Crissman, Harry A, David J Orlicky et al. (1979). 'Fluorescent DNA probes for flow cytometry. Considerations and prospects'. *J Histochem Cytochem* 27.12, pp. 1652–4.

Crissman, Harry A and John A Steinkamp (1973). 'Rapid, simultaneous measurement of DNA, protein, and cell volume in single cells from large mammalian cell populations'. *J Cell Biol* 59.3, pp. 766–71.

Danial, Nika N et al. (2003). 'BAD and glucokinase reside in a mitochondrial complex that integrates glycolysis and apoptosis.' *Nature* 424.6951, pp. 952–956.

Darzynkiewicz, Zbigniew et al. (1992). 'Features of apoptotic cells measured by flow cytometry.' *Cytometry* 13.8, pp. 795–808.

Davis, Mark E et al. (2008). 'Nanoparticle therapeutics: an emerging treatment modality for cancer.' *Nat Rev Drug Discov* 7.9, pp. 771–782.

Dean, Phillip N et al. (1984). 'Cell-cycle analysis using a monoclonal antibody to BrdUrd'. *Cell Tissue Kinet* 17.4, pp. 427–36.

Dengler, Wolfgang A et al. (1995). 'Development of a propidium iodide fluorescence assay for proliferation and cytotoxicity assays'. *Anticancer Drugs* 6.4, pp. 522–32.

Dmitrieva, Natalia I et al. (2002). 'Rapid activation of G2/M checkpoint after hypertonic stress in renal inner medullary epithelial (IME) cells is protective and requires p38 kinase.' *Proc Natl Acad Sci U S A* 99.1, pp. 184–189.

Doberstein, Stephen K et al. (1993). 'Inhibition of contractile vacuole function in vivo by antibodies against myosin-I'. *Nature* 365.6449, pp. 841–3.

Dolbeare, Frank et al. (1983). 'Flow cytometric measurement of total DNA content and incorporated bromodeoxyuridine'. *Proc Natl Acad Sci U S A* 80.18, pp. 5573–7.

Donnenberg, Albert D et al. (2007). 'Rare-event analysis in flow cytometry'. *Clin Lab Med* 27.3, pp. 627–52, viii.

Duessmann, Heiko et al. (2003). 'Outer mitochondrial membrane permeabilization during apoptosis triggers caspase-independent mitochondrial and caspase-dependent plasma membrane potential depolarization: a single-cell analysis.' *J Cell Sci* 116.Pt 3, pp. 525–536.

Dufes, Christine et al. (2005). 'Synthetic anticancer gene medicine exploits intrinsic antitumor activity of cationic vector to cure established tumors.' *Cancer Res* 65.18, pp. 8079–8084.

Dutta, Tathagata et al. (2008). 'Toxicological investigation of surface engineered fifth generation poly (propyleneimine) dendrimers in vivo'. *Nanotoxicology* 2.2, pp. 62–70.

El Sharouni, Sherif Y et al. (2003). 'Accelerated regrowth of non-small-cell lung tumours after induction chemotherapy'. *Br J Cancer* 89.12, pp. 2184–9.

Esfand, Roseita et al. (2001). 'Poly(amidoamine) (PAMAM) dendrimers: from biomimicry to drug delivery and biomedical applications'. *Drug Discov Today* 6.8, pp. 427–436.

Ewald, Brett et al. (2007). 'H2AX phosphorylation marks gemcitabine-induced stalled replication forks and their collapse upon S-phase checkpoint abrogation'. *Mol Cancer Ther* 6.4, pp. 1239–48.

Ferlini, Cristiano, Roberto Biselli et al. (1996). 'Probing chromatin structure in the early phases of apoptosis.' *Cell Prolif* 29.7, pp. 427–436.

Ferlini, Cristiano, Sebastian Di Cesare et al. (1996). 'Flow cytometric analysis of the early phases of apoptosis by cellular and nuclear techniques.' *Cytometry* 24.2, pp. 106–115.

Ferraro-Peyret, Carole et al. (2002). 'Caspase-independent phosphatidylserine exposure during apoptosis of primary T lymphocytes.' *J Immunol* 169.9, pp. 4805–4810.

Frank, Natasha Y et al. (2010). 'The therapeutic promise of the cancer stem cell concept'. *J Clin Invest* 120.1, pp. 41–50.

Franken, Nicolaas A et al. (2006). 'Clonogenic assay of cells in vitro'. *Nat Protoc* 1.5, pp. 2315–9.

Fréchet, Jean M (1994). 'Functional polymers and dendrimers: reactivity, molecular architecture, and interfacial energy'. *Science* 263.5154, pp. 1710–1715.

Fried, Jerrold et al. (1976). 'Flow cytofluorometric analysis of cell cycle distributions using propidium iodide. Properties of the method and mathematical analysis of the data'. *J Cell Biol* 71.1, pp. 172–81.

Gautschi, Oliver et al. (2007). 'Cyclin D1 in non-small cell lung cancer: a key driver of malignant transformation.' *Lung Cancer* 55.1, pp. 1–14.

Geno Technology, Inc. *CytoScan™ LDH Cytotoxicity Assay.* `http://www.gbiosciences.com/CytoscanLDHCytotoxicityAssayKit.aspx`, accessed 6th July 2011.

Gillies, Elizabeth R et al. (2005). 'Dendrimers and dendritic polymers in drug delivery'. *Drug Discov Today* 10.1, pp. 35–43.

Ginestier, Christophe et al. (2007). 'ALDH1 is a marker of normal and malignant human mammary stem cells and a predictor of poor clinical outcome'. *Cell Stem Cell* 1.5, pp. 555–67.

Gleeson, Helena K et al. (2004). 'The impact of cancer therapy on the endocrine system in survivors of childhood brain tumours.' *Endocr Relat Cancer* 11.4, pp. 589–602.

Gratzner, Howard G (1982). 'Monoclonal antibody to 5-bromo- and 5-iododeoxyuridine: A new reagent for detection of DNA replication'. *Science* 218.4571, pp. 474–5.

Gratzner, Howard G and Robert C Leif (1981). 'An immunofluorescence method for monitoring DNA synthesis by flow cytometry'. *Cytometry* 1.6, pp. 385–93.

Gratzner, Howard G, Robert C Leif et al. (1975). 'The use of antibody specific for bromodeoxyuridine for the immunofluorescent determination of DNA replication in single cells and chromosomes'. *Exp Cell Res* 95.1, pp. 88–94.

Green, Douglas R (2000). 'Apoptotic pathways: paper wraps stone blunts scissors.' *Cell* 102.1, pp. 1–4.

Greish, Khaled (2010). 'Enhanced permeability and retention (EPR) effect for anticancer nanomedicine drug targeting'. *Methods Mol Biol* 624, pp. 25–37.

Greish, Khaled et al. (2003). 'Macromolecular therapeutics: advantages and prospects with special emphasis on solid tumour targeting'. *Clin Pharmacokinet* 42.13, pp. 1089–105.

Haag, Rainer et al. (2006). 'Polymere Therapeutika: Konzepte und Anwendungen'. *Angew Chem* 118.8, pp. 1218–1237.

Haensler, Jean et al. (1993). 'Polyamidoamine cascade polymers mediate efficient transfection of cells in culture'. *Bioconjug Chem* 4.5, pp. 372–9.

Al-Hajj, Muhammad et al. (2003). 'Prospective identification of tumorigenic breast cancer cells'. *Proc Natl Acad Sci U S A* 100.7, pp. 3983–8.

Hamid, Rachid et al. (2004). 'Comparison of alamar blue and MTT assays for high through-put screening.' *Toxicol In Vitro* 18.5, pp. 703–710.

Hans, Fabienne et al. (2001). 'Histone H3 phosphorylation and cell division'. *Oncogene* 20.24, pp. 3021–7.

Harris, Daniel C (1995). *Quantitative Chemical Analysis*. W. H. Freeman and Company.

Hawker, Craig J et al. (1990). 'Preparation of polymers with controlled molecular architecture. A new convergent approach to dendritic macromolecules'. *Journal of the American Chemical Society* 112.21, pp. 7638–7647.

Heinlein, Christina et al. (2010). 'A rapid and optimization-free procedure allows the in vivo detection of subtle cell cycle and ploidy alterations in tissues by flow cytometry.' *Cell Cycle* 9.17, pp. 3584–3590.

Hendricks, Stephen P et al. (1998). 'Differential effects of hydroxyurea upon deoxyribonucleoside triphosphate pools, analyzed with vaccinia virus ribonucleotide reductase.' *J Biol Chem* 273.45, pp. 29519–29523.

Hendzel, Michael J et al. (1997). 'Mitosis-specific phosphorylation of histone H3 initiates primarily within pericentromeric heterochromatin during G2 and spreads in an ordered fashion coincident with mitotic chromosome condensation'. *Chromosoma* 106.6, pp. 348–60.

Hengartner, Michael O (2000). 'The biochemistry of apoptosis.' *Nature* 407.6805, pp. 770–776.

Hermann, Patrick C et al. (2007). 'Distinct populations of cancer stem cells determine tumor growth and metastatic activity in human pancreatic cancer'. *Cell Stem Cell* 1.3, pp. 313–23.

Hirsch, Tamara et al. (1997). 'The apoptosis-necrosis paradox. Apoptogenic proteases activated after mitochondrial permeability transition determine the mode of cell death.' *Oncogene* 15.13, pp. 1573–1581.

Hitomi, Masahiro et al. (1999). 'Cyclin D1 production in cycling cells depends on ras in a cell-cycle-specific manner.' *Curr Biol* 9.19, pp. 1075–1084.

Hollins, Andrew J et al. (2004). 'Evaluation of generation 2 and 3 poly-(propylenimine) dendrimers for the potential cellular delivery of antisense oligonucleotides targeting the epidermal growth factor receptor'. *Pharm Res* 21.3, pp. 458–66.

Hong, Seungpyo, Anna U Bielinska et al. (2004). 'Interaction of poly(amidoamine) dendrimers with supported lipid bilayers and cells: hole formation and the relation to transport.' *Bioconjug Chem* 15.4, pp. 774–782.

Hong, Seungpyo, Pascale R Leroueil et al. (2006). 'Interaction of polycationic polymers with supported lipid bilayers and cells: nanoscale hole formation and enhanced membrane permeability.' *Bioconjug Chem* 17.3, pp. 728–734.

Huang, Melinda et al. (2000). 'Constitutive activation of stat 3 oncogene product in human ovarian carcinoma cells.' *Gynecol Oncol* 79.1, pp. 67–73.

Huang, William C (2008). 'Book Review'. *New England Journal of Medicine* 358.23, pp. 2527–2527.

Hudson, Bruce et al. (1969). 'The use of an ethidium analogue in the dye-buoyant density procedure for the isolation of closed circular DNA: the variation of the superhelix density of mitochondrial DNA'. *Proc Natl Acad Sci U S A* 62.3, pp. 813–20.

Hummelen, Jan C et al. (1997). 'Electrospray Mass Spectrometry of Poly-(propylene imine) Dendrimers - The Issue of Dendritic Purity or Polydispersity'. *Chemistry - A European Journal* 3.9, pp. 1489–1493.

Ishizawa, Kota et al. (2010). 'Tumor-initiating cells are rare in many human tumors'. *Cell Stem Cell* 7.3, pp. 279–82.

Jain, Kewal K (2008). 'Recent advances in nanooncology.' *Technol Cancer Res Treat* 7.1, pp. 1–13.

Jain, Sanjay et al. (2004). 'Prevention of head and neck cancer: current status and future prospects.' *Curr Probl Cancer* 28.5, pp. 265–286.

Al-Jamal, Khuloud T et al. (2010). 'Systemic antiangiogenic activity of cationic poly-L-lysine dendrimer delays tumor growth'. *Proc Natl Acad Sci U S A* 107.9, pp. 3966–71.

Jirawatnotai, Siwanon et al. (2011). 'A function for cyclin D1 in DNA repair uncovered by protein interactome analyses in human cancers'. *Nature* 474.7350, pp. 230–4.

Kallos, George J et al. (1991). 'Molecular weight determination of a poly-amidoamine Starburst polymer by electrospray ionization mass spectrometry'. *Rapid Communications in Mass Spectrometry* 5.9, pp. 383–386.

Karpinich, Natalie O, Marco Tafani, Ronald J Rothman et al. (2002). 'The course of etoposide-induced apoptosis from damage to DNA and p53 activation to mitochondrial release of cytochrome c.' *J Biol Chem* 277.19, pp. 16547–16552.

Karpinich, Natalie O, Marco Tafani, Timothy Schneider et al. (2006). 'The course of etoposide-induced apoptosis in Jurkat cells lacking p53 and Bax.' *J Cell Physiol* 208.1, pp. 55–63.

Kim, Edward S et al. (2011). 'Cotargeting cyclin d1 starts a new chapter in lung cancer prevention and therapy.' *Cancer Prev Res (Phila)* 4.6, pp. 779–782.

Kim, Michael P et al. (2011). 'ALDH activity selectively defines an enhanced tumor-initiating cell population relative to CD133 expression in human pancreatic adenocarcinoma'. *PLoS One* 6.6, e20636.

Kitchens, Kelly M, Amy B Foraker et al. (2007). 'Endocytosis and interaction of poly (amidoamine) dendrimers with Caco-2 cells.' *Pharm Res* 24.11, pp. 2138–2145.

Kitchens, Kelly M, Rohit B Kolhatkar et al. (2008). 'Endocytosis inhibitors prevent poly(amidoamine) dendrimer internalization and permeability across Caco-2 cells.' *Mol Pharm* 5.2, pp. 364–369.

Koç, Ahmet et al. (2004). 'Hydroxyurea arrests DNA replication by a mechanism that preserves basal dNTP pools.' *J Biol Chem* 279.1, pp. 223–230.

Korzeniewski, Carol et al. (1983). 'An enzyme-release assay for natural cytotoxicity.' *J Immunol Methods* 64.3, pp. 313–320.

Krex, Dietmar et al. (2007). 'Long-term survival with glioblastoma multiforme.' *Brain* 130.Pt 10, pp. 2596–2606.

Krishan, Awtar (1975). 'Rapid flow cytofluorometric analysis of mammalian cell cycle by propidium iodide staining'. *J Cell Biol* 66.1, pp. 188–93.

Kumar, Sharad (1998). *Apoptosis: mechanisms and role in disease*. Springer.

Kuo, Jung-hua Steven et al. (2007). 'Interactions between U-937 human macrophages and poly(propyleneimine) dendrimers.' *J Control Release* 120.1-2, pp. 51–59.

Lakhani, Saquib A et al. (2006). 'Caspases 3 and 7: key mediators of mitochondrial events of apoptosis.' *Science* 311.5762, pp. 847–851.

Lapidot, Tsvee et al. (1994). 'A cell initiating human acute myeloid leukaemia after transplantation into SCID mice'. *Nature* 367.6464, pp. 645–8.

Lara-Padilla, Eleazar et al. (2012). 'On the nature of the tumor-initiating cell'. *Curr Stem Cell Res Ther* 7.1, pp. 26–35.

Lathia, Justin D et al. (2010). 'Integrin alpha 6 regulates glioblastoma stem cells'. *Cell Stem Cell* 6.5, pp. 421–32.

Lee, Jong-Ho et al. (2009). 'Nanosized polyamidoamine (PAMAM) dendrimer-induced apoptosis mediated by mitochondrial dysfunction.' *Toxicol Lett*.

Lescanec, Robert L et al. (1990). 'Configurational characteristics and scaling behavior of starburst molecules: a computational study'. *Macromolecules* 23.8, pp. 2280–2288.

Li, Chenwei et al. (2007). 'Identification of pancreatic cancer stem cells'. *Cancer Res* 67.3, pp. 1030–7.

Life Technologies Corporation. *Product Spectra - Propidium iodide/DNA*. `http://www.invitrogen.com/site/us/en/home/support/Product-Technical-Resources/Product-Spectra.1304dna.html`, accessed 5th September 2011.

Linkous, Amanda G et al. (2012). 'Novel therapeutic approaches for targeting tumor angiogenesis'. *Anticancer Res* 32.1, pp. 1–12.

Lockman, Paul R et al. (2004). 'Nanoparticle surface charges alter blood-brain barrier integrity and permeability.' *J Drug Target* 12.9-10, pp. 635–641.

Loehrer, Patrick J Sr et al. (2011). 'Gemcitabine alone versus gemcitabine plus radiotherapy in patients with locally advanced pancreatic cancer: an

Eastern Cooperative Oncology Group trial'. *J Clin Oncol* 29.31, pp. 4105–12.

Lonardo, Enzo et al. (2010). 'Pancreatic cancer stem cells - update and future perspectives'. *Mol Oncol* 4.5, pp. 431–42.

Lorico, Aurelio et al. (2011). 'Phenotypic heterogeneity of breast cancer stem cells'. *J Oncol* 2011, p. 135039.

Lowndes, Noel F et al. (2005). 'DNA repair: the importance of phosphorylating histone H2AX'. *Curr Biol* 15.3, R99–R102.

Ly, Jennifer D et al. (2003). 'The mitochondrial membrane potential (deltapsi(m)) in apoptosis; an update.' *Apoptosis* 8.2, pp. 115–128.

Maeda, Hiroshi et al. (2009). 'Polymeric drugs for efficient tumor-targeted drug delivery based on EPR-effect'. *Eur J Pharm Biopharm* 71.3, pp. 409–19.

Malik, Noeen et al. (2000). 'Dendrimers: relationship between structure and biocompatibility in vitro, and preliminary studies on the biodistribution of 125I-labelled polyamidoamine dendrimers in vivo.' *J Control Release* 65.1-2, pp. 133–148.

Malumbres, Marcos and Mariano Barbacid (2005). 'Mammalian cyclin-dependent kinases.' *Trends Biochem Sci* 30.11, pp. 630–641.

Malumbres, Marcos, Edward Harlow et al. (2009). 'Cyclin-dependent kinases: a family portrait.' *Nat Cell Biol* 11.11, pp. 1275–1276.

Mansfield, Marc L et al. (1993). 'Monte Carlo studies of dendrimer macromolecules'. *Macromolecules* 26.16, pp. 4262–4268.

Manunta, Maria, Benjamin J Nichols et al. (2006). 'Gene delivery by dendrimers operates via different pathways in different cells, but is enhanced by the presence of caveolin.' *J Immunol Methods* 314.1-2, pp. 134–146.

Manunta, Maria, Peng Hong Tan et al. (2004). 'Gene delivery by dendrimers operates via a cholesterol dependent pathway.' *Nucleic Acids Res* 32.9, pp. 2730–2739.

Martin, Seamus J et al. (1996). 'Phosphatidylserine externalization during CD95-induced apoptosis of cells and cytoplasts requires ICE/CED-3 protease activity.' *J Biol Chem* 271.46, pp. 28753–28756.

Marzo, Isabel et al. (2001). 'Cladribine induces apoptosis in human leukaemia cells by caspase-dependent and -independent pathways acting on mitochondria.' *Biochem J* 359.Pt 3, pp. 537–546.

Matsumura, Yasuhiro et al. (1986). 'Mechanism of Tumoritropic Accumulation of Proteins and the Antitumor Agent Smancs'. *Cancer Res* 46, pp. 6387–6392.

Mazzini, Giuliano et al. (1983). 'A flow cytometric study of the propidium iodide staining kinetics of human leukocytes and its relationship with chromatin structure'. *Cytometry* 3.6, pp. 443–8.

McLuckey, Scott A et al. (2000). 'Ion trap collisional activation of protonated poly(propylene imine) dendrimers: generations 1-5'. *Int J Mass Spectrom* 195-196, pp. 419–437.

Mecke, Almut, István J Majoros et al. (2005). 'Lipid bilayer disruption by polycationic polymers: the roles of size and chemical functional group.' *Langmuir* 21.23, pp. 10348–10354.

Mecke, Almut, Srinivas Uppuluri et al. (2004). 'Direct observation of lipid bilayer disruption by poly(amidoamine) dendrimers.' *Chem Phys Lipids* 132.1, pp. 3–14.

Merdan, Thomas et al. (2002). 'Prospects for cationic polymers in gene and oligonucleotide therapy against cancer'. *Adv Drug Deliv Rev* 54.5, pp. 715–58.

Merkel, Olivia M (2009). 'Non-Viral Delivery of Nucleic Acids and Image-Guided Assessment of in vivo Performance of Multifunctional Nanomedicines'. PhD thesis.

Moroson, Harold (1971). 'Polycation- treated tumor cells in vivo and in vitro.' *Cancer Res* 31.3, pp. 373–380.

Mosmann, Tim (1983). 'Rapid colorimetric assay for cellular growth and survival: application to proliferation and cytotoxicity assays.' *J Immunol Methods* 65.1-2, pp. 55–63.

Mourey, Thomas H et al. (1992). 'Unique behavior of dendritic macromolecules: intrinsic viscosity of polyether dendrimers'. *Macromolecules* 25.9, pp. 2401–2406.

Mukherjee, Sourav Prasanna and Hugh J Byrne (2012). 'Polyamidoamine dendrimer nanoparticle cytotoxicity, oxidative stress, caspase activation and inflammatory response: experimental observation and numerical simulation'. *Nanomedicine*.

Mukherjee, Sourav Prasanna, Maria Davoren et al. (2010). 'In vitro mammalian cytotoxicological study of PAMAM dendrimers - towards quantitative structure activity relationships.' *Toxicol In Vitro* 24.1, pp. 169–177.

Mukherjee, Sourav Prasanna, Fiona M Lyng et al. (2010). 'Mechanistic studies of in vitro cytotoxicity of poly(amidoamine) dendrimers in mammalian cells.' *Toxicol Appl Pharmacol* 248.3, pp. 259–268.

Munshi, Anupama et al. (2005). *Chemosensitivity: In vitro assays*. Vol. 1. Methods in Molecular Medicine. Humana Press.

Murat, Michael et al. (1996). 'Molecular Dynamics Study of Dendrimer Molecules in Solvents of Varying Quality'. *Macromolecules* 29.4, pp. 1278–1285.

Namiki, Yoshihisa et al. (2011). 'Nanomedicine for Cancer: Lipid-Based Nanostructures for Drug Delivery and Monitoring.' *Acc Chem Res*.

National Cancer Institute (2012). *What is Cancer?*

Navarro, Gemma et al. (2009). 'Activated and non-activated PAMAM dendrimers for gene delivery in vitro and in vivo'. *Nanomedicine* 5.3, pp. 287–97.

Naylor, Adel M et al. (1989). 'Starburst dendrimers. 5. Molecular shape control'. *J. Am. Chem. Soc.* 111.6, pp. 2339–2341.

Nie, Shuming et al. (2007). 'Nanotechnology applications in cancer.' *Annu Rev Biomed Eng* 9, pp. 257–288.

Oeffinger, Kevin C et al. (2010). 'Challenges after curative treatment for childhood cancer and long-term follow up of survivors.' *Hematol Oncol Clin North Am* 24.1, pp. 129–149.

Ogden, Alfred T et al. (2008). 'Identification of A2B5+CD133- tumor-initiating cells in adult human gliomas'. *Neurosurgery* 62.2, pp. 505–14, 505–14.

Omidi, Yadollah et al. (2005). 'Polypropylenimine dendrimer-induced gene expression changes: the effect of complexation with DNA, dendrimer generation and cell type.' *J Drug Target* 13.7, pp. 431–443.

Ormerod, Michael G (2009). *Flow Cytometry: A Basic Introduction*.

Parimi, Srinivas et al. (2008). 'PAMAM Dendrimer Interactions with Supported Lipid Bilayers: A Kinetic and Mechanistic Investigation.' *Langmuir*.

Pasquier, Eddy et al. (2010). 'Metronomic chemotherapy: new rationale for new directions'. *Nat Rev Clin Oncol* 7.8, pp. 455–65.

Paull, Tanya T et al. (2000). 'A critical role for histone H2AX in recruitment of repair factors to nuclear foci after DNA damage'. *Curr Biol* 10.15, pp. 886–95.

Perumal, Omathanu P et al. (2008). 'The effect of surface functionality on cellular trafficking of dendrimers.' *Biomaterials* 29.24-25, pp. 3469–3476.

Pontano, Laura L et al. (2008). 'Genotoxic stress-induced cyclin D1 phosphorylation and proteolysis are required for genomic stability'. *Mol Cell Biol* 28.23, pp. 7245–58.

Prosperi, Ennio et al. (1991). 'Nuclease-induced DNA structural changes assessed by flow cytometry with the intercalating dye propidium iodide.' *Cytometry* 12.4, pp. 323–329.

Puck, Theodore T et al. (1955). 'A Rapid Method for Viable Cell Titration and Clone Production with Hela Cells in Tissue Culture: The Use of X-Irradiated Cells to Supply Conditioning Factors'. *Proc Natl Acad Sci U S A* 41.7, pp. 432–7.

Ran, Sophia et al. (2002). 'Increased exposure of anionic phospholipids on the surface of tumor blood vessels'. *Cancer Res* 62.21, pp. 6132–40.

Rasper, Michael et al. (2010). 'Aldehyde dehydrogenase 1 positive glioblastoma cells show brain tumor stem cell capacity'. *Neuro Oncol* 12.10, pp. 1024–33.

Rawat, Manju et al. (2006). 'Nanocarriers: promising vehicle for bioactive drugs.' *Biol Pharm Bull* 29.9, pp. 1790–1798.

Roberts, Jess C et al. (1996). 'Preliminary biological evaluation of polyamidoamine (PAMAM) Starburst dendrimers.' *J Biomed Mater Res* 30.1, pp. 53–65.

Rogakou, Emmy P et al. (1998). 'DNA double-stranded breaks induce histone H2AX phosphorylation on serine 139'. *J Biol Chem* 273.10, pp. 5858–68.

Roper, Pamela R et al. (1976). 'Comparison of in vitro methods to determine drug-induced cell lethality'. *Cancer Res* 36.7 PT 1, pp. 2182–8.

Sánchez, Irma et al. (2005). 'New insights into cyclins, CDKs, and cell cycle control.' *Semin Cell Dev Biol* 16.3, pp. 311–321.

Santra, Manas K et al. (2009). 'F-box protein FBXO31 mediates cyclin D1 degradation to induce G1 arrest after DNA damage'. *Nature* 459.7247, pp. 722–5.

Saovapakhiran, Angkana et al. (2009). 'Surface modification of PAMAM dendrimers modulates the mechanism of cellular internalization.' *Bioconjug Chem* 20.4, pp. 693–701.

Scaduto Russell C., Jr. et al. (1999). 'Measurement of mitochondrial membrane potential using fluorescent rhodamine derivatives'. *Biophys J* 76.1 Pt 1, pp. 469–77.

Scherrenberg, Rolf et al. (1998). 'The Molecular Characteristics of Poly-(prop-yleneimine) Dendrimers As Studied with Small-Angle Neutron Scattering, Viscosimetry, and Molecular Dynamics'. *Macromolecules* 31.2, pp. 456–461.

Scholzen, Thomas et al. (2000). 'The Ki-67 protein: from the known and the unknown'. *J Cell Physiol* 182.3, pp. 311–22.

Seib, F Philipp et al. (2007). 'Comparison of the endocytic properties of linear and branched PEIs, and cationic PAMAM dendrimers in B16f10 melanoma cells.' *J Control Release* 117.3, pp. 291–300.

Semrock. Inc. *Filters for Flow Cytometry*. `http://www.semrock.com/flow-cytometry.aspx`, accessed 19th May 2012.

Shaked, Yuval et al. (2008). 'Rapid chemotherapy-induced acute endothelial progenitor cell mobilization: implications for antiangiogenic drugs as chemosensitizing agents'. *Cancer Cell* 14.3, pp. 263–73.

Shapiro, Howard M (2003). *Practical flow cytometry*. 4th. New York: Wiley-Liss.

Sharma, Sreenath V et al. (2010). 'A chromatin-mediated reversible drug-tolerant state in cancer cell subpopulations'. *Cell* 141.1, pp. 69–80.

Shipway, Andrew N (1997). *Dendrimers - Technical Terms, A Review, Diagrams, and Links*.

Singh, Narendra P et al. (1988). 'A simple technique for quantitation of low levels of DNA damage in individual cells'. *Exp Cell Res* 175.1, pp. 184–91.

Singh, Sheila K et al. (2003). 'Identification of a cancer stem cell in human brain tumors'. *Cancer Res* 63.18, pp. 5821–8.

Soerensen, Claus Storgaard et al. (2003). 'Chk1 regulates the S phase checkpoint by coupling the physiological turnover and ionizing radiation-induced accelerated proteolysis of Cdc25A.' *Cancer Cell* 3.3, pp. 247–258.

Stupp, Roger et al. (2009). 'Effects of radiotherapy with concomitant and adjuvant temozolomide versus radiotherapy alone on survival in glioblastoma in a randomised phase III study: 5-year analysis of the EORTC-NCIC trial.' *Lancet Oncol* 10.5, pp. 459–466.

Szachowicz-Petelska, Barbara et al. (2010). 'Characterization of the cell membrane during cancer transformation'. *J Environ Biol* 31.5, pp. 845–850.

Tabatabai, Ghazaleh et al. (2011). 'Glioblastoma stem cells'. *Cell Tissue Res* 343.3, pp. 459–65.

Takubo, Keiyo et al. (2008). 'Stem cell defects in ATM-deficient undifferentiated spermatogonia through DNA damage-induced cell-cycle arrest'. *Cell Stem Cell* 2.2, pp. 170–82.

Taylor, Rebecca C et al. (2008). 'Apoptosis: controlled demolition at the cellular level'. *Nat Rev Mol Cell Biol* 9.3, pp. 231–41.

Telford, William G et al. (2004). 'Multiparametric analysis of apoptosis by flow and image cytometry'. *Methods Mol Biol* 263, pp. 141–60.

Tomalia, Donald A et al. (1985). 'A New Class of Polymers: Starburst-Dendritic Macromolecules'. *Polymer Journal* 17.1, pp. 117–132.

Travis, Lois B et al. (2010). 'Testicular cancer survivorship: research strategies and recommendations.' *J Natl Cancer Inst* 102.15, pp. 1114–1130.

Tsujimoto, Yoshihide et al. (2005). 'Another way to die: autophagic programmed cell death'. *Cell Death Differ* 12 Suppl 2, pp. 1528–34.

Twentyman, Peter R et al. (1984). 'The response of tumour cells to radiation and cytotoxic drugs–a comparison of clonogenic and isotope uptake assays'. *Br J Cancer* 50.5, pp. 625–31.

Ustrell, Vicença et al. (2002). 'PA200, a nuclear proteasome activator involved in DNA repair'. *EMBO J* 21.13, pp. 3516–25.

Uzunoglu, Selim et al. (2010). 'Comparison of XTT and Alamar blue assays in the assessment of the viability of various human cancer cell lines by AT-101 (-/- gossypol).' *Toxicol Mech Methods* 20.8, pp. 482–486.

Vanags, Daina M et al. (1996). 'Protease involvement in fodrin cleavage and phosphatidylserine exposure in apoptosis.' *J Biol Chem* 271.49, pp. 31075–31085.

Voegtle, Fritz (2000). *Dendrimers III: Design, Dimension, Function*. Vol. 3. Springer.

Waring, Michael (1970). 'Variation of the supercoils in closed circular DNA by binding of antibiotics and drugs: evidence for molecular models involving intercalation'. *J Mol Biol* 54.2, pp. 247–79.

Watson, James V (1992). *Flow cytometry data analysis: basic concepts and statistics*. Cambridge: Cambridge University Press.

Welch, Paul M et al. (1998). 'Tuning the Density Profile of Dendritic Polyelectrolytes'. *Macromolecules* 31.17, pp. 5892–5897.

Weyermann, Jörg et al. (2005). 'A practical note on the use of cytotoxicity assays.' *Int J Pharm* 288.2, pp. 369–376.

Wlodkowic, Donald et al. (2011). 'Apoptosis and beyond: cytometry in studies of programmed cell death'. *Methods Cell Biol* 103, pp. 55–98.

Wlodkowic, D. et al. (2010). 'Cytometry in cell necrobiology revisited. Recent advances and new vistas'. *Cytometry A* 77.7, pp. 591–606.

Wolbers, Floor et al. (2004). 'Apoptosis induced kinetic changes in autofluorescence of cultured HL60 cells-possible application for single cell analysis on chip'. *Apoptosis* 9.6, pp. 749–55.

World Health Organization (2011).

Wright, Mollie H et al. (2008). 'Brca1 breast tumors contain distinct CD44+/CD24- and CD133+ cells with cancer stem cell characteristics'. *Breast Cancer Res* 10.1, R10.

Yan, Hong et al. (2011). 'Drug-tolerant cancer cells show reduced tumor-initiating capacity: depletion of CD44 cells and evidence for epigenetic mechanisms'. *PLoS One* 6.9, e24397.

Yeung, Tai K et al. (1999). 'The mode of action of taxol: apoptosis at low concentration and necrosis at high concentration.' *Biochem Biophys Res Commun* 263.2, pp. 398–404.

Yoo, Hoon et al. (2000). 'Enhanced delivery of antisense oligonucleotides with fluorophore-conjugated PAMAM dendrimers.' *Nucleic Acids Res* 28.21, pp. 4225–4231.

Zhang, Lisha et al. (2008). 'Nanoparticles in medicine: therapeutic applications and developments.' *Clin Pharmacol Ther* 83.5, pp. 761–769.

Zhou, Sheng et al. (2001). 'The ABC transporter Bcrp1/ABCG2 is expressed in a wide variety of stem cells and is a molecular determinant of the side-population phenotype'. *Nat Med* 7.9, pp. 1028–34.

Zhou, Xiang-Yang et al. (2002). 'An ATM-independent S-phase checkpoint response involves CHK1 pathway.' *Cancer Res* 62.6, pp. 1598–1603.

Zinselmeyer, Bernd H et al. (2002). 'The lower-generation polypropylenimine dendrimers are effective gene-transfer agents'. *Pharm Res* 19.7, pp. 960–7.